2017

Development of an Electrochemical Method to Study Real-Time in Vivo Neurotransmitter Modulation

Srimal Aminda Samaranayake
University of South Carolina

DEVELOPMENT OF AN ELECTROCHEMICAL METHOD TO STUDY REAL-TIME IN VIVO NEUROTRANSMITTER MODULATION

by

Srimal Aminda Samaranayake

Bachelor of Science
University of Peradeniya, 2010

Submitted in Partial Fulfillment of the Requirements

For the Degree of Doctor of Philosophy in

Chemistry

College of Arts and Sciences

University of South Carolina

2017

Accepted by:

Parastoo Hashemi, Major Professor

Timothy J. Shaw, Committee Member

Thomas M. Makris, Committee Member

Rosemarie M. Booze, Committee Member

Cheryl L. Addy, Vice Provost and Dean of the Graduate School

DEDICATION

I would like to dedicate this dissertation to my loving parents, my brother, and my loving wife, for the all the commitments they have made to make my dreams a reality, and for being my editorial board.

I would also like to dedicate this work to all the animals, who have sacrificed their lives for science in the past, present, and future.

ACKNOWLEDGEMENTS

After an intense five years, today is the day I was waiting for: writing this note of acknowledgments in my dissertation. It has been a wonderful, challenging, exciting and unforgettable period for me, not only in the research arena but also in my personal life. I would love to reflect my gratitude to the wonderful people who have helped me throughout this exciting period.

First and foremost, I would like to express my sincere appreciation to my mentor, Dr. Parastoo Hashemi. She was a great advisor, and her guidance led me through the peaks and valleys of my graduate school career. Her passion toward science has been the key to discovering my abilities and becoming an independent motivated scientist. Thank you very much, Parry, for your support, motivation, and guidance in helping me to become who I am today.

In addition to my advisor, I am very grateful to my dissertation committee, Dr. T.J. Shaw, Dr. T. M. Makris and Dr. R. M. Booze for their advice, insightful comments, and encouragement, which broadened my knowledge from various standpoints. I would also like to thank my past committee members at Wayne State University, Dr. Rigby, and Dr. Trimpin for their invaluable comments and intellectual ideas.

Next, I would like to thank all of our collaborators, Prof. R.M. Booze, Dr. P. Ortinski, Prof. J. Best, Prof. M. Reed, Prof. H. Fred Nijhout, and Prof. M. Heien, for their valuable ideas and encouragements.

I would also like to thank the Hashemi lab members for the kindness, friendship, and support you have all shown me. Even though I'm not a talkative person, I enjoyed all the discussions that I had with all of you. My sincere gratitude goes to Pavithra, Shirley, Rachel, Thushani, Kevin, Aya, Shane, Jordan, Alyssa, Rhiannon, Anna Marie, Matt, Megan, Audrey and Bruce for their true kindness and friendship. A special thank you goes to Pavithra, Shirley and Aya for teaching me everything about our lab and our research; I appreciate all the professional and non-professional topics we have discussed during this time. Also, I would like to thank Aya, Shane, Melinda, Jordan, Alyssa, and Rhiannon for helping me with my English. Thank you very much for everything that you have done for me.

I have a very special appreciation for all the Sri Lankan friends and families both at Wayne State University and University of South Carolina who helped me during this invaluable journey. Also, I want to thank all the technical and administrative staff at both universities, for all the assistance they have provided to make this graduate school journey more comfortable.

I would like to thank my life-coaches: My ever-loving father and mother who have been inspiring me during every step and turn that I have made in my life so far. Additionally, I am privileged to have a great brother and sister-in-law who continuously motivated and encouraged me. Thank you for all that you have done for me because I owe it all to you.

Lastly, but by no means least, I would love to thank my eternal cheerleader, my loving wife, soon to be a mom, who inspired me during every moment in this journey,

and was there conquering every challenge with me. You have offered me more than I could ever have wished for in my life. Thank you, Nadeesha, for everything.

Once again, thank you all for giving me the motivation to rise higher through the valleys and stay humble through the peaks of this unforgettable journey.

ABSTRACT

Histamine and serotonin are important biogenic amines that regulate vital brain functions. These two transmitters are thoughts to be involved in neurodegenerative diseases such as Parkinson's and Alzheimer's and affective disorders including depression. Histamine and serotonin are believed to regulate each other but their fundamental neuromodulation mechanisms are not well understood. This lack of understanding makes brain disorders implicating these two transmitters difficult to diagnose and treat. Our lab extensively investigates the serotonergic system to understand serotonin's neurochemistry in the brain. However, histamine is relatively understudied with respect to other biogenic amines because of an absence of suitable analytical tools. This work introduces a strategic approach to overcome this analytical challenge and investigates the real-time neuromodulation of *in vivo* histamine and serotonin to understand physiological functions in healthy and disease states using fast-scan cyclic voltammetry (FSCV). First, we perform a proof-of-principle study of Copper (Cu(II)) analysis to characterize the adsorption driven FSCV response. Next, we employ FSCV to develop a novel voltammetric method to selectively and sensitively monitor real-time *in vivo* histamine and serotonin neurotransmissions in the posterior hypothalamus (PH). This study reveals that histamine inhibits serotonin *via* an H_3 receptor mediated process, highlighting histamine's roles in regulating serotonin release in the brain. Following that, we examine histamine's reuptake mechanisms *via* monoamine transporter proteins and demonstrate that histamine uptake mechanism is mediated by organic cation transporters.

Finally, we use our novel FSCV method to monitor histamine and serotonin neurotransmissions in HIV- 1 Tg rats, which exhibit neuroinflammation, to understand impaired neurochemical mechanisms in the disease state. Collectively, this dissertation showcases a novel and robust electroanalytical strategy to simultaneously monitor *in vivo* histamine and serotonin neuromodulation in real time. Innovative discoveries in this systematic investigation of the histaminergic regulation of serotonin in diverse neurochemical and pathophysiological processes will pave the way towards more efficient therapies for histamine and serotonin related brain disorders.

PREFACE

This dissertation is based closely on the following refereed publications:

Chapter 2: Pathirathna P, **Samaranayake S**, Atcherley CW, Parent KL, Heien ML, McElmurry SP, Hashemi P (2014) Fast voltammetry of metals at carbon-fiber microelectrodes: copper adsorption onto activated carbon aids rapid electrochemical analysis. *Analyst* 139:4673-4680.

Chapter 3: **Samaranayake S**, Abdalla A, Robke R, Wood KM, Zeqja A, Hashemi P (2015) In vivo histamine voltammetry in the mouse premammillary nucleus. *Analyst* 140:3759-3765.

Chapter 4: **Samaranayake S**, Abdalla A, Robke R, Nijhout HF, Reed MC, Best J, Hashemi P (2016) A voltammetric and mathematical analysis of histaminergic modulation of serotonin in the mouse hypothalamus. *J Neurochem* 138:374-383.

TABLE OF CONTENTS

LIST OF FIGURES

LIST OF ABBREVIATIONS

5-HT ..... Serotonin

CFM ..... Carbon Fiber Microelectrode

CV ..... Cyclic Voltammogram

DAT ..... Dopamine Transporter

FIA ..... Flow Injection Analysis

FSCAV ..... Fast Scan Controlled-Adsorption Voltammetry

FSCV ..... Fast Scan Cyclic Voltammetry

HA ..... Histamine

HIV ..... Human Immunodeficiency Virus

HNMT ..... Histamine *N*-methyl Transferase Enzyme

MFB ..... Medial Forebrain Bundle

NET ..... Norepinephrine Transporter

OCT ..... Organic Cation Transporter

PH ..... Posterior Hypothalamus

PM ..... Premammillary Nucleus

SERT ..... Serotonin Transporter

SNr ..... Substantia Nigra Pars Reticulate

Tg ..... Transgenic

TMN ..... Tuberomammillary Nucleus

CHAPTER 1

INTRODUCTION

1.1 Neuromodulation of Histamine and Serotonin

Histamine is an important biogenic amine which modulates vital brain functions[1-3] by regulating other neurotransmitters, in particular serotonin[4,5]. These two chemical messengers co-exist in multiple brain regions[6,7] and are implicated in many brain dysfunctions such as Parkinson's[8-10] and Alzheimer's diseases[11,12] and mood disorders[13,14]. Lack of knowledge regarding histamine and serotonin neuromodulation mechanisms makes such brain disorders hard to diagnose and cure. Our lab widely investigates the serotonergic system to understand the complex neurochemistry of this molecule using electroanalytical tools[15,16]. However, histamine neurochemistry has been relatively understudied with respect to serotonin. It is desirable, therefore, to study *in vivo* neuromodulation of these two neurotransmitters to understand their functions in healthy and disease states. To date, this topic has been challenging due to the absence of appropriate analytical tools. This dissertation illustrates the development of a novel voltammetric method to monitor, in real-time, the modulatory profile of these two messengers. The serotonergic and histaminergic systems are discussed in the first part of this chapter. The second portion describes existing electroanalytical techniques to monitor *in vivo* neurotransmissions, while the latter part of the chapter focuses on method development toward *in vivo* histamine-serotonin detection.

1.1.1 The Serotonergic System

Serotonin is a vital neurotransmitter that is implicated in mood and emotional brain functions[17]. Dysregulation of this chemical messenger in the brain causes several neurological disorders such as anxiety and depression[13,14]. Therefore, serotonin has been the main focus of depression and antidepressant drug related studies[13]. However, the tight regulation of *in vivo* serotonin in the brain creates limitations for analytical tools to monitor rapid serotonin neurotransmissions. Despite limited selectivity, differential pulse voltammetry and chronoamperometry studies have brought forth noteworthy information about *in vivo* serotonin dynamics[18,19]. In 2009 Hashemi *et al.* employed fast-scan cyclic voltammetry (FSCV) to detect *in vivo* stimulated serotonin release in the rat substantia nigra pars reticulate (SNr) as a more selective and robust method[20].

With this method, our lab primarily concentrates on *in vivo* serotonin neurotransmission in depression and autism spectrum disorder. The Hashemi lab has been studying endogenous serotonin release and reuptake mechanisms using FSCV. For instance, our lab confirmed that the serotonin system consists of two distinct reuptake mechanisms and found a prolonged inhibitory role for serotonin autoreceptors[16]. Histamine has been previously thought to modulate serotonin[4]. Therefore, I became interested in investigating histamine and serotonin neuromodulation. More details about the histaminergic system are presented in the next section.

1.1.2 The Histaminergic System

Histamine is a monoamine neurotransmitter which regulates important brain functions such as circadian rhythm and inflammation[3]. Histamine is synthesized from the

amino acid histidine via decarboxylation by the histidine decarboxylase enzyme[21]. Neuronal histamine is stored in cell somas and neuroeffector junctions[22,23]. Like other biogenic amines, this transmitter is packaged into vesicles by vesicular monoamine transporters and released upon the action potential activation[24]. However unlike other biogenic amines, there is no known active transport mechanism for histamine[25,26]. Therefore, enzymatic degradation is thoughts to be the primary means of histamine inactivation via the *N*-methyltransferase enzyme[27,28]. Tele-methylhistamine, the product of the histamine degradation, undergoes further degradation to t-methyl-imidazoleacetic acid via monoamine oxidase[29].

Past studies have identified four histamine receptors, namely the H_1, H_2, H_3, and H_4 receptors. All receptors are rhodopsin-like G-protein coupled receptors[3]. Histamine neurons are excited through H_1 receptor activation and H_1 receptor dysfunction leads to immunological and behavioral abnormalities[30]. H_1 receptor antihistaminergic agents inactivate the H_1 receptors and break signal propagation[31]. Distribution of the H_2 receptors is more consistent and widespread in the rodent brain[32]. Dysregulation of this receptor is associated with cognitive impairments[33]. Activation of the H_3 autoreceptor, which is an inhibitory feedback receptor on the presynaptic histamine neuron, inhibits histamine release and synthesis[34,35]. Additionally, this presynaptic receptor controls the release of other neurotransmitters, including glutamate, acetylcholine, and serotonin[3,25]. Loss of H_3 receptor function is related to abnormalities in locomotion, behavior, and weight[36,37]. H_4 receptors exhibit properties similar to the H_3 receptors but are expressed in the peripheral system[38].

Recent studies have shown that irregularities of the histaminergic system cause abnormalities in neuroendocrine and higher brain functions. Histamine levels are significantly increased in the brains of Parkinson's patients[8,10]. The degeneration of histaminergic fibers in the tuberomammillary nucleus (TMN), as well as globally lowered neuronal histamine levels, are well-documented in Alzheimer's disease[11]. Moreover, histamine is a key biomarker of inflammation which is comorbid with many brain disorders[39,40]. Also, a recent study has illustrated that histamine may promote anxiety, while lesions of the TMN reduce symptoms[41]. Interestingly, histamine neurons in TMN are related to neuroendocrine signals concerned with mood disorders like depression[33,42]. This relationship between histamine and depression is appealing to our lab since we primarily concentrate on serotonin, which is the transmitter most highly implicated in depression and anxiety.

Therefore, I find it of great significance to direct my efforts to study *in vivo* histamine and serotonin modulation. However, studying this neuromodulation mechanism has been challenging due to the absence of suitable analytical techniques, which can simultaneously monitor these two chemical messengers *in vivo*. An ideal method should encompass: sensitivity for low neurotransmitter concentrations, selectivity for different neurotransmitters, adequate speed for monitoring sub-second neurotransmission and appropriate probes for real-time *in vivo* measurements. Electroanalytical techniques and how they address these challenges are described in the next section.

1.1.3 Detection and Quantification of Neurotransmitters

Monitoring the brain's chemicals and neurotransmitters necessitates specific requirements. First, brain signaling events occur on a sub-second time scale. Thus, the temporal resolution of the method should be sufficient to monitor these events. Secondly, the brain is physically delicate thus the technique should be minimally invasive. Third, neurotransmitters and their metabolites are chemically similar, which means the tool must have a high degree of selectivity to distinguish between species. Lastly, neurotransmitters are present at very low concentrations in the synapse. Accordingly, an ideal detection method must display excellent sensitivity.

Carbon fiber microelectrodes (CFMs) are biocompatible, robust, stable, and cause minimal damage to the brain tissue. They also have favorable and fast surface kinetics for sensitive measurements[43]. Moreover, the large surface area due to the rough exterior of the carbon surface allows for more adsorption as shown in **Figure 1.1**. Undoubtedly, combining CFMs with electroanalytical techniques permits the quantification of electroactive neurotransmitters in the brain, in real time.

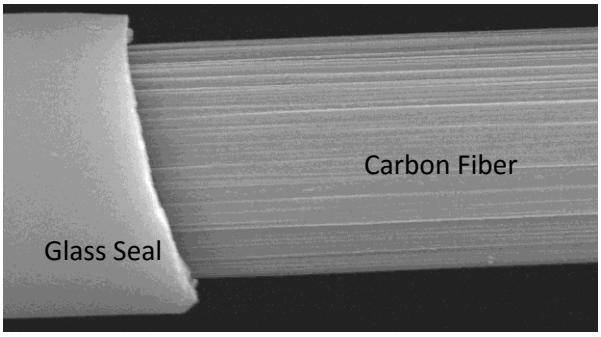

Figure 1.1. SEM image of a carbon-fiber microelectrode

1.1.4 CFMs and Electroanalytical Techniques

Some monoamine, like dopamine, serotonin, histamine and adenosine, are electroactive. Therefore, the dynamics of these electroactive messengers can be studied using electroanalytical techniques *in vivo* as described below.

Amperometry works by holding the CFM at a potential that is more positive than the analyte's oxidation potential. The resulting continuous oxidation produces a current which is used to quantify the neurotransmitters around the electrode. This method has been developed to monitor exocytosis in a single cell[44]. Moreover, the flexibility of CFMs makes it feasible to build microelectrode arrays. For instance, the Ewing group has been using a 16-electrode array to monitor exocytosis from a single cell[45]. Amperometry is a sophisticated technique to measure chemical messengers. However, selectivity is inadequate for monitoring neurotransmission in complex media, because the constant potential oxidizes all electroactive analytes below the applied potential.

Chronoamperometry has been developed to overcome the selectivity problem with amperometry. This method uses a square wave (between defined potential limits) to CFMs at 5-25 Hz. The square wave generates a large capacitative current at the step functions, which decays exponentially over time. Chronoamperometry can provide the selectivity required, to some degree, by taking a ratio of oxidative and reductive currents. This method has been using to study Parkinson's disease[46], depression[47], addiction[48], and transporter kinetics[49]. Collectively, chronoamperometry can successfully monitor neurotransmitter clearance, although more selectivity is required to monitor various

neurotransmissions *in vivo*. The next section describes FSCV as a robust and selective electrochemical technique to monitor real-time *in vivo* neurotransmission.

1.2 Fast-Scan Cyclic Voltammetry (FSCV)

Julian Milar and colleagues first presented FSCV to detect electroactive neurotransmitters in the mid-20th century[50]. Over several decades, FSCV has been emerging as an electroanalytical technique on diverse frontiers. Primarily, FSCV has been utilized to monitor real-time dopamine dynamics[51,52]. Our lab has pioneered the application of FSCV to serotonin, histamine[53], Cu(II)[54] and Pb(II)[55]. FSCV employs high scan rates (100 Vs^{-1} to 1500 Vs^{-1}) at a frequency of 10 Hz, whereas traditional cyclic voltammetry uses mVs^{-1} scan rates. Therefore, with the higher scan rates employed in FSCV, a single data set is collected within milliseconds, which raises the temporal resolution to the sub-second scale. However, high scan rates also produce large non-faradaic currents at the electrode surface, which mask the faradaic signal. Therefore, FSCV is modified to integrate background subtraction to remove this non-faradaic signal. As a result of background subtraction, FSCV can only detect changes. Therefore, stimulation is used to evoke neurotransmitter release *in vivo*.

In FSCV, the CFM is held at a resting potential between cycles, allowing neurotransmitters to adsorb onto the carbon surface. During the anodic wave, which ramps up from the resting potential to a positive potential limit, adsorbed analytes will be oxidized on the electrode surface; likewise, during the cathodic wave analytes will be reduced. This potential vs. time instruction is known as a FSCV waveform and the resulting faradaic events generate electron flow through the electrode, measurable as a

current. After background subtraction, FSCV generates an analyte specific cyclic voltammogram (CV), that can be used for qualitative and quantitative analysis. For data interpretation purposes, a 2D plot, also known as color-plot, is digitally constructed by stacking a set of CVs collected at 10 Hz for a limited time of period. Quantitative data along the time axis is provided by extracting horizontal data points along the event.

Serotonin detection is challenging with FSCV because serotonin's metabolites foul the electrode surface. However, a thin coating of Nafion, a cation exchange polymer, overcomes this fouling issue[20]. **Figure 1.2** illustrates the stimulated release of serotonin in the CA2 region of the hippocampus medial forebrain bundle (MFB) stimulation. **Figure 1.2A** shows a representative data color plot. The discrete green event around 0.7 V demonstrates serotonin oxidation. A typical serotonin CV is presented inset in the color plot. **Figure 1.2B** represents [serotonin] vs. time event upon stimulation.

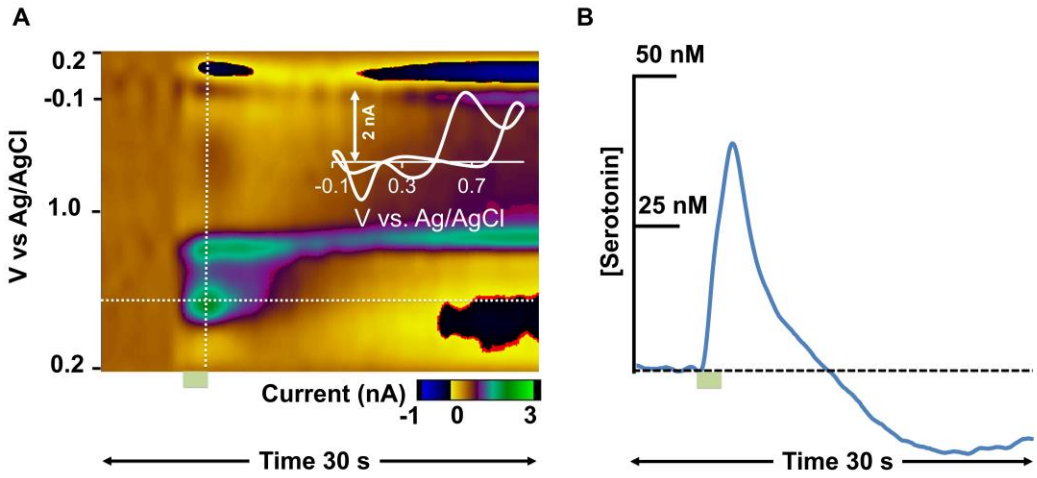

Figure 1.2. The stimulated release of serotonin in mouse hippocampus CA2. (A) representative color plot. Inset shows a classic serotonin CV extracted from the vertical white dashed line. (B) illustrates a [serotonin] vs. time response obtained from the horizontal dashed line along the peak serotonin oxidation event.

1.2.1 Expanding the Scope of FSCV

Histamine[56], adenosine[57] and H_2O_2[58] have similar CVs because their oxidation peaks appear on the cathodic wave. Thus, their identities have only been tested via pharmacological approaches. Modification of the FSCV waveform can permit these neurotransmitters to be monitored more selectively without pharmacological verification. Developing a FSCV method to monitor several neurotransmitters simultaneously is challenging but would provide critical information about their modulatory mechanisms in the brain.

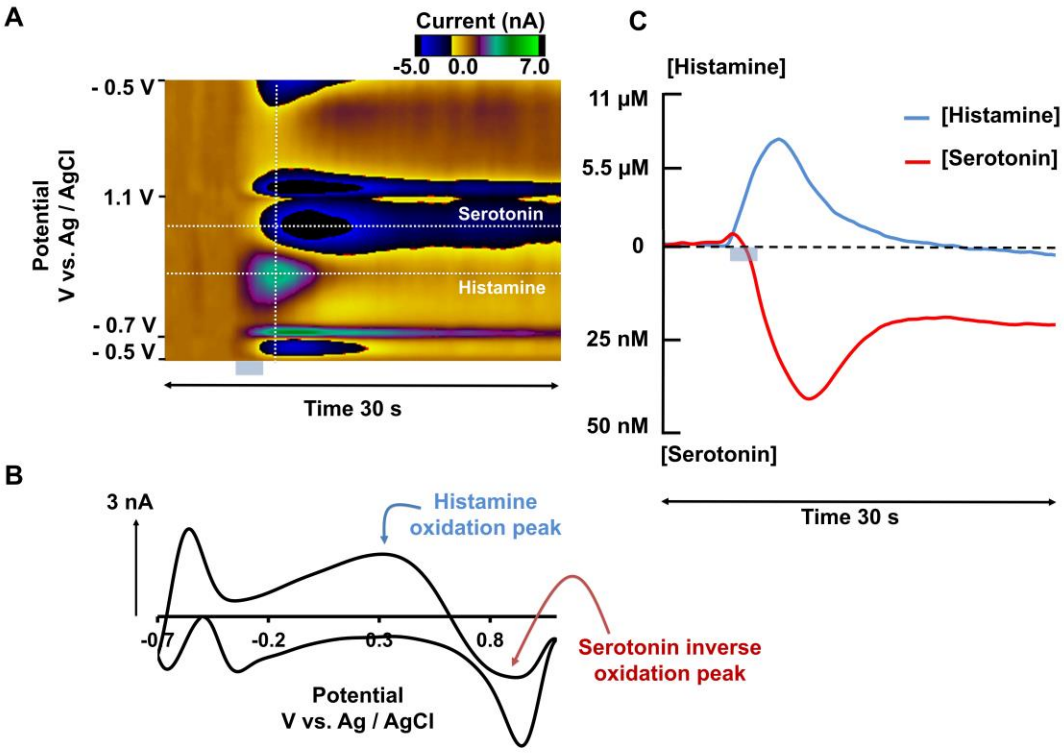

Figure 1.3. (A) Representative color plot for simultaneous detection of histamine and serotonin in mouse posterior hypothalamus. (B) CV extracted from the vertical white dashed line at the histamine event. (C) [histamine] and [serotonin] vs. time obtained from horizontal dashed line along both events. The blue bar right underneath the color plot and in (C) represents the stimulation.

Figure 1.3A illustrates a representative color plot for simultaneous detection of histamine and serotonin in mouse posterior hypothalamus (PH). I developed this novel FSCV waveform that detects both the oxidation of histamine and serotonin simultaneously[53,59]. FSCV recognizes histamine releases (green event), which is denoted by white horizontal dashed line labeled "histamine", in PH upon stimulation of the MFB as shown in the **Figure 1.2A**. A subsequent serotonin event appears (blue event right above histamine event) with a slight delay as denoted by a white dashed line labeled "serotonin" in the color plot. **Figure 1.2B** represents the unique CV that is extracted from the vertical dashed line along the events, and histamine oxidation appears around 0.3 V whereas inverse serotonin oxidation occurs around 0.8 V. This inverse oxidation (negative event) illustrates the reduction of ambient serotonin concentration after the stimulation. **Figure 1.1C** shows [histamine] and [serotonin] vs. time responses obtained from the horizontal dashed lines along both events in the color plot and these traces demonstrate real-time histaminergic modulation of serotonin. This novel method can be used to investigate *in vivo* histamine and serotonin to define their roles in healthy and pathophysiological states.

This dissertation presents a systemic approach to developing a novel electrochemical tool for simultaneous detection of *in vivo* histamine and serotonin, as described below.

1.3 Scope of the Dissertation

In this dissertation, I first used Cu(II) metal analysis to understand the adsorption driven FSCV response (Chapter 2). Using that knowledge, I then developed a novel

FSCV method to selectively and sensitively monitor histamine neurotransmission in the mouse posterior hypothalamus (Chapter 3). This work was extended to simultaneously monitor histamine and serotonin in real time to study their neuromodulation in the brain (Chapter 4). Since an active reuptake mechanism for histamine has not been identified, I then utilized our novel method to study histamine reuptake mechanisms via monoamine transporter proteins (Chapter 5). Finally, I used our novel FSCV method to investigate histaminergic regulation of serotonin during disease using HIV-1 Tg rats which exhibit neuroinflammation (Chapter 7). The outline of this dissertation is described below.

Chapter 1: Introduction

Chapter 2: This chapter describes the underlying fundamental mechanism of adsorption driven FSCV responses. We demonstrated the progression of the FSCV response from the classical cyclic voltammetry response using the Cu(II) analysis. Finally, we proved that adsorption of Cu(II) onto the CFM surface follows a Langmuir adsorption isotherm.

Chapter 3: In this chapter, we optimized an electrochemical waveform that provided a stimulation-locked and unique electrochemical signal for histamine. Then, we described *in vitro* waveform optimization and *in vivo* detection of the stimulated release of histamine in the mouse PH via electrical stimulation in the MFB. Finally, this chapter demonstrated that a robust signal can be used to describe histamine's *in vivo* dynamics.

Chapter 4: This chapter describes a voltammetric approach to simultaneous monitoring of histamine and serotonin in real time. We found that serotonin was rapidly and potently inhibited by histamine release in a concentration-dependent manner. Lastly, we

developed mathematical models and performed pharmacological experiments to verify that this serotonin inhibition was mediated by H_3 receptors.

Chapter 5: In this section, we employed a previously described FSCV method (chapter 4) to investigate histamine reuptake kinetics pharmacologically. Moreover, this section provides evidence for organic cation transporter mediated histamine uptake. We also found that histamine reuptake mechanism were inhibited by commercially available antidepressant drugs: escitalopram, citalopram, and desipramine.

Chapter 6: This chapter illustrates fundamental neurochemical changes in serotonin and histamine in HIV-1 Tg rats, which display neuroinflammation. We employed FSCV to interpret impaired neurotransmissions and found that histamine release was elevated in HIV-1 Tg rats which in turn inhibited more serotonin compared to the control animals.

Chapter 7: The final chapter summarizes the conclusions of this research work and highlights the future directions.

1.4 References

(1) Panula, P.; Yang, H. Y.; Costa, E. *Proceedings of the National Academy of Sciences of the United States of America* **1984**, *81*, 2572.

(2) Panula, P.; Nuutinen, S. *Nature reviews. Neuroscience* **2013**, *14*, 472.

(3) Haas, H. L.; Sergeeva, O. A.; Selbach, O. *Physiological reviews* **2008**, *88*, 1183.

(4) Threlfell, S.; Cragg, S. J.; Kallo, I.; Turi, G. F.; Coen, C. W.; Greenfield, S. A. *The Journal of neuroscience : the official journal of the Society for Neuroscience* **2004**, *24*, 8704.

(5) Schlicker, E.; Betz, R.; Gothert, M. *Naunyn Schmiedebergs Arch Pharmacol* **1988**, *337*, 588.

(6) Russell, W. L.; Henry, D. P.; Phebus, L. A.; Clemens, J. A. *Brain research* **1990**, *512*, 95.

(7) Moore, R. Y.; Halaris, A. E.; Jones, B. E. *The Journal of comparative neurology* **1978**, *180*, 417.

(8) Rinne, J. O.; Anichtchik, O. V.; Eriksson, K. S.; Kaslin, J.; Tuomisto, L.; Kalimo, H.; Röyttä, M.; Panula, P. *Journal of Neurochemistry* **2002**, *81*, 954.

(9) Ionov, I. D. *The International journal of neuroscience* **2008**, *118*, 1763.

(10) Nowak, P.; Noras, Ł.; Jochem, J.; Szkilnik, R.; Brus, H.; Körőssy, E.; Drab, J.; Kostrzewa, R. M.; Brus, R. *Neurotoxicity Research* **2009**, *15*, 246.

(11) Nakamura, S.; Takemura, M.; Ohnishi, K.; Suenaga, T.; Nishimura, M.; Akiguchi, I.; Kimura, J.; Kimura, T. *Neuroscience letters* **1993**, *151*, 196.

(12) Panula, P.; Rinne, J.; Kuokkanen, K.; Eriksson, K. S.; Sallmen, T.; Kalimo, H.; Relja, M. *Neuroscience* **1998**, *82*, 993.

(13) Delgado, P. L.; Charney, D. S.; Price, L. H.; Aghajanian, G. K.; Landis, H.; Heninger, G. R. *Archives of general psychiatry* **1990**, *47*, 411.

(14) Gardner, A.; Boles, R. G. *Progress in neuro-psychopharmacology & biological psychiatry* **2011**, *35*, 730.

(15) Wood, K. M.; Hashemi, P. *ACS Chemical Neuroscience* **2013**, *4*, 715.

(16) Wood, K. M.; Zeqja, A.; Nijhout, H. F.; Reed, M. C.; Best, J.; Hashemi, P. *Journal of Neurochemistry* **2014**, *130*, 351.

(17) Mann, J. J. *Neuropsychopharmacology* **1999**, *21*, 99S.

(18) Daws, L. C.; Toney, G. M.; Gerhardt, G. A.; Frazer, A. *The Journal of pharmacology and experimental therapeutics* **1998**, *286*, 967.

(19) Crespi, F.; Martin, K. F.; Marsden, C. A. *Neuroscience* **1988**, *27*, 885.

(20) Hashemi, P.; Dankoski, E. C.; Petrovic, J.; Keithley, R. B.; Wightman, R. M. *Analytical Chemistry* **2009**, *81*, 9462.

(21) Pipkorn, U.; Granerus, G.; Proud, D.; Kagey-Sobotka, A.; Norman, P. S.; Lichtenstein, L. M.; Naclerio, R. M. *Allergy* **1987**, *42*, 496.

(22) Diewald, L.; Heimrich, B.; Busselberg, D.; Watanabe, T.; Haas, H. L. *The European journal of neuroscience* **1997**, *9*, 2406.

(23) Hayashi, H.; Takagi, H.; Takeda, N.; Kubota, Y.; Tohyama, M.; Watanabe, T.; Wada, H. *The Journal of comparative neurology* **1984**, *229*, 233.

(24) Merickel, A.; Edwards, R. H. *Neuropharmacology* **1995**, *34*, 1543.

(25) Brown, R. E.; Stevens, D. R.; Haas, H. L. *Progress in neurobiology* **2001**, *63*, 637.

(26) Bolam, J. P.; Ellender, T. J. *Neuropharmacology* **2016**, *106*, 74.

(27) Barnes, W. G.; Hough, L. B. *J Neurochem* **2002**, *82*, 1262.

(28) Bowsher, R. R.; Verburg, K. M.; Henry, D. P. *The Journal of biological chemistry* **1983**, *258*, 12215.

(29) Lin, J. S.; Kitahama, K.; Fort, P.; Panula, P.; Denney, R. M.; Jouvet, M. *The Journal of comparative neurology* **1993**, *330*, 405.

(30) Parmentier, R.; Ohtsu, H.; Djebbara-Hannas, Z.; Valatx, J. L.; Watanabe, T.; Lin, J. S. *The Journal of neuroscience : the official journal of the Society for Neuroscience* **2002**, *22*, 7695.

(31) Simons, F. E. *The New England journal of medicine* **2004**, *351*, 2203.

(32) Ruat, M.; Traiffort, E.; Bouthenet, M. L.; Schwartz, J. C.; Hirschfeld, J.; Buschauer, A.; Schunack, W. *Proceedings of the National Academy of Sciences of the United States of America* **1990**, *87*, 1658.

(33) Dai, H.; Kaneko, K.; Kato, H.; Fujii, S.; Jing, Y.; Xu, A.; Sakurai, E.; Kato, M.; Okamura, N.; Kuramasu, A.; Yanai, K. *Neuroscience Research* **2007**, *57*, 306.

(34) Stevens, D. R.; Eriksson, K. S.; Brown, R. E.; Haas, H. L. *Behavioural brain research* **2001**, *124*, 105.

(35) Arrang, J.-M.; Garbarg, M.; Schwartz, J.-C. *Nature* **1983**, *302*, 832.

(36) Tokita, S.; Takahashi, K.; Kotani, H. *Journal of pharmacological sciences* **2006**, *101*, 12.

(37) Toyota, H.; Dugovic, C.; Koehl, M.; Laposky, A. D.; Weber, C.; Ngo, K.; Wu, Y.; Lee, D. H.; Yanai, K.; Sakurai, E.; Watanabe, T.; Liu, C.; Chen, J.; Barbier, A. J.; Turek, F. W.; Fung-Leung, W. P.; Lovenberg, T. W. *Molecular pharmacology* **2002**, *62*, 389.

(38) Morgan, R. K.; McAllister, B.; Cross, L.; Green, D. S.; Kornfeld, H.; Center, D. M.; Cruikshank, W. W. *The Journal of Immunology* **2007**, *178*, 8081.

(39) Najjar, S.; Pearlman, D. M.; Alper, K.; Najjar, A.; Devinsky, O. *Journal of Neuroinflammation* **2013**, *10*, 43.

(40) Passani, M. B.; Ballerini, C. *Frontiers in Systems Neuroscience* **2012**, *6*, 32.

(41) Frisch, C.; Hasenohrl, R. U.; Krauth, J.; Huston, J. P. *Experimental brain research* **1998**, *119*, 260.

(42) Ito, C.; Shen, H.; Toyota, H.; Kubota, Y.; Sakurai, E.; Watanabe, T.; Sato, M. *Neuroscience letters* **1999**, *262*, 143.

(43) Lama, R. D.; Charlson, K.; Anantharam, A.; Hashemi, P. *Analytical Chemistry* **2012**, *84*, 8096.

(44) Zhang, B.; Heien, M. L. A. V.; Santillo, M. F.; Mellander, L.; Ewing, A. G. *Analytical chemistry* **2011**, *83*, 571.

(45) Wigström, J.; Dunevall, J.; Najafinobar, N.; Lovrić, J.; Wang, J.; Ewing, A. G.; Cans, A.-S. *Analytical Chemistry* **2016**, *88*, 2080.

(46) Nevalainen, N.; af Bjerkén, S.; Lundblad, M.; Gerhardt, G. A.; Strömberg, I. *Journal of Neurochemistry* **2011**, *118*, 12.

(47) Gould, G. G.; Hensler, J. G.; Burke, T. F.; Benno, R. H.; Onaivi, E. S.; Daws, L. C. *J Neurochem* **2011**, *116*, 291.

(48) Callaghan, P. D.; Owens, W. A.; Javors, M. A.; Sanchez, T. A.; Jones, D. J.; Irvine, R. J.; Daws, L. C. *Journal of Neurochemistry* **2007**, *100*, 617.

(49) Toney, G.; Daws, L. In *Electrochemical Methods for Neuroscience*; CRC Press: 2006, p 63.

(50) Stamford, J. A.; Kruk, Z. L.; Millar, J. *Journal of neuroscience methods* **1984**, *10*, 107.

(51) Hermans, A.; Keithley, R. B.; Kita, J. M.; Sombers, L. A.; Wightman, R. M. *Analytical Chemistry* **2008**, *80*, 4040.

(52) Robinson, D. L.; Venton, B. J.; Heien, M. L. A. V.; Wightman, R. M. *Clinical chemistry* **2003**, *49*, 1763.

(53) Samaranayake, S.; Abdalla, A.; Robke, R.; Wood, K. M.; Zeqja, A.; Hashemi, P. *Analyst* **2015**, *140*, 3759.

(54) Pathirathna, P.; Yang, Y.; Forzley, K.; McElmurry, S. P.; Hashemi, P. *Analytical Chemistry* **2012**, *84*, 6298.

(55) Yang, Y.; Pathirathna, P.; Siriwardhane, T.; McElmurry, S. P.; Hashemi, P. *Analytical Chemistry* **2013**, *85*, 7535.

(56) Hashemi, P.; Dankoski, E. C.; Wood, K. M.; Ambrose, R. E.; Wightman, R. M. *Journal of Neurochemistry* **2011**, *118*, 749.

(57) Nguyen, M. D.; Venton, B. J. *Computational and Structural Biotechnology Journal* **2015**, *13*, 47.

(58) Sanford, A. L.; Morton, S. W.; Whitehouse, K. L.; Oara, H. M.; Lugo-Morales, L. Z.; Roberts, J. G.; Sombers, L. A. *Analytical chemistry* **2010**, *82*, 5205.

(59) Samaranayake, S.; Abdalla, A.; Robke, R.; Nijhout, H. F.; Reed, M. C.; Best, J.; Hashemi, P. *J Neurochem* **2016**, *138*, 374.

CHAPTER 2

FAST VOLTAMMETRY OF METALS AT CARBON-FIBER MICROELECTRODES: COPPER ADSORPTION ONTO ACTIVATED CARBON AIDS RAPID ELECTROCHEMICAL ANALYSIS

Reprinted with permission from Royal Society of Chemistry.

Pathirathna P, **Samaranayake S**, Atcherley CW, Parent KL, Heien ML, McElmurry SP, Hashemi P (2014) Fast voltammetry of metals at carbon-fiber microelectrodes: copper adsorption onto activated carbon aids rapid electrochemical analysis. *Analyst* 139:4673-4680. *I contributed both experimentally and intellectually and the results of this project directed me to my next project.*

2.1 Abstract

Rapid, *in situ* trace metal analysis is essential for understanding many biological and environmental processes. For example, trace metals are thought to act as chemical messengers in the brain. In the environment, some of the most damaging pollution occurs when metals are rapidly mobilized and transported during hydrologic events (storms). Electrochemistry is attractive for *in situ* analysis, primarily because electrodes are compact, cheap and portable. Electrochemical techniques, however, do not traditionally report trace metals in real-time. In this work, we investigated the fundamental mechanisms of a novel method, based on fast-scan cyclic voltammetry (FSCV), that reports trace metals with sub-second temporal resolution at carbon-fiber microelectrodes (CFMs). Electrochemical methods and geochemical models were employed to find that activated CFMs rapidly adsorb copper, a phenomenon that greatly advances the temporal capabilities of electrochemistry. We established the thermodynamics of surface copper adsorption and the electrochemical nature of copper deposition onto CFMs and hence identified a unique adsorption-controlled electrochemical mechanism for ultra-fast trace metal analysis. This knowledge can be exploited in the future to increase the sensitivity and selectivity of CFMs for fast voltammetry of trace metals in a variety of biological and environmental models.

2.2 Introduction

Trace metal analysis in real-time is essential for understanding many biological and environmental processes. For example, trace metals have important functions in biology and are garnering new attention for their roles as neurotransmitters[1,2]. In

Alzheimer's disease for example, copper accumulates in β-amyloid plaques[3]. It is thought that this copper build-up comes at the expense of its normal roles as a neurotransmitter, accounting for some of the disease's neurological deficits[3,4]. It has been impossible to chemically monitor endogenously acting copper to verify this hypothesis, primarily because chemical transmission occurs so quickly (< seconds).

Rapid metal analysis is also important in the environment, particularly in natural water systems where trace metal contamination is extremely hazardous[5]. The well-documented health consequences of trace metal exposure[6-9] are exacerbated because metals bioaccumulate in plants and animals[10-13], providing numerous exposure paradigms for humans. Anthropogenic sources of trace metals are commonly mobilized and transported during hydraulic events (storms)[14]. It is critical to characterize aquatic trace metals in real-time because their interactions with organic ligands and soils are fast (< seconds)[15]. Such rapid metal detection would provide the most efficient implementation of existing metal mitigation systems [16-21] via a diagnostic approach.

Most analytical techniques cannot monitor metals rapidly (< seconds). Spectroscopic techniques are sensitive and selective[22], however sample collection and preparation can alter metal speciation and make dynamic measurements difficult[23,24]. Electrochemical methods are attractive because the chemistry occurs at a submersible or integrated surface that minimally impacts its surroundings. Ion-selective electrodes have a temporal resolution of seconds;[25,26] however it is typically challenging to make measurements in dynamically changing matrices. Stripping voltammetries (such as anodic stripping and adsorptive stripping voltammetry) have extremely high sensitivities[27]. This high sensitivity is largely due to a lengthy pre-concentration step

(minutes) that decreases temporal resolution[28-30]. Moreover, anodic stripping voltammetry is most commonly performed at Hg electrodes[31] which have limited portability and pose their own toxicity concerns.

We recently described the use of carbon-fiber microelectrodes (CFMs) to detect copper (II) (Cu^{2+}) and lead (II) (Pb^{2+}) with fast scan cyclic voltammetry (FSCV) at scan rates of 300 – 600 Vs^{-1} [32,33]. Our ultra-fast, Hg-free method can quantify Cu^{2+} and Pb^{2+} concentration changes every 100 ms with parts per billion and parts per million sensitivity, respectively[32,33]. Our method is highly applicable for studying metals in real time. However it is essential to describe the fundamental mechanisms of this fast voltammetric method before it can be developed into a routine analytical tool for biological and environmental applications. In this paper therefore, we take a multi-faceted approach and establish the underlying mechanisms of fast voltammetry of Cu^{2+} on CFMs in established laboratory test solutions.

We analyzed Cu^{2+}, a biologically relevant[2] and environmentally problematic metal ion[34] with well-known redox chemistry[35,36]. Besides classical nucleation, growth and stripping features[36], we observed new, additional peaks in Cu^{2+} slow scan cyclic voltammograms. These additional peaks were not diminished, as the classical features were, when the scan-rate was increased. In fact, with increasing scan rate, the new features were augmented, as seen previously with neurotransmitters adsorbed to CFM surfaces[37]. We therefore investigated surface adsorption as a fundamental mechanism of the Cu^{2+} FSCV signal. We utilized electrochemical, geochemical, and microscopic tools to describe CFM's surface and thermodynamic mechanisms towards Cu^{2+}. This study provides valuable insight into the adsorption chemistry that governs the FSCV response

to metals. Our findings are critical to the future development of the method, namely increases in sensitivity and selectivity, in application to real samples.

2.3 Experimental Section

2.3.1 Solutions

Cu^{2+} solutions were prepared by dissolving $Cu(NO_3)_2$ in NaCl (0.01 M) and in tris buffer (15 mM tris(hydroxymethyl)aminomethane), 140 mM NaCl, 3.25 mM KCl, 1.2 mM $CaCl_2$, 1.25 mM NaH_2PO_4, 1.2 mM $MgCl_2$ and 2.0 mM Na_2SO_4). All chemicals were purchased from Sigma-Aldrich (St. Louis, MO). At room temperature and pressure, the pH of Cu^{2+} in NaCl and tris buffer solutions was ~5.5 and 7.4 respectively.

2.3.2 Microelectrodes

CFMs were prepared by vacuum aspirating a single carbon fiber of 5 µm radius (T-650, Cytec Industries, NJ) into a glass capillary (0.6 mm external diameter, 0.4 mm internal diameter, A-M Systems, Inc., Sequim, WA). The capillary was pulled under gravity with a micropipette puller (Narishige, Tokyo, Japan) leaving a tapered end to form a carbon-glass seal. The exposed end of the carbon fiber was cut to approximately 150 µm under a microscope. Gold microelectrodes (AuMs) were prepared as described above but with a gold microwire of 10 µm radius (Goodfellow Co, PA), cut to approximately 150-200 µm.

2.3.3 Cyclic Voltammetry

All voltammetry employed a 2-electrode system. Cyclic voltammograms were collected on 5 different electrodes and representative examples are displayed. For slow scan cyclic voltammetry (scan rates $\leq$ 100 mVs^{-1}), microelectrodes were placed into a

constantly stirred solution of $Cu(NO_3)_2$ and a triangular wave form (+1 V to –1 V) was applied using custom software, Wildcat CV, written in LAB-VIEW 2012 (National Instruments, Austin, TX). Only solutions for slow scan cyclic voltammetry were nitrogen-purged prior to experimentation. The reference electrode was fabricated by electroplating Cl^- on a Ag wire (A-M systems, WA). For scan rates above 1 Vs^{-1}, in-house software, WCCV 2.0, written in LABVIEW 2012 collected background-subtracted voltammograms in a flow-injection analysis system.

2.3.4 Electrochemical Pre-treatment

For most experiments microelectrodes were electrochemically pre-treated with a Cu^{2+} sensitive triangular waveform as previously described.[33] For experiments comparing electrochemical and chemical pretreatments, the anodic potential/rest potential of the CFMs was varied from +0.4 V to +1.3 V at a constant cathodic potential of -1.0 V at a scan rate of 300 Vs^{-1}. Electrodes were treated with each waveform for 10 minutes at 60 Hz and then 10 minutes at 10 Hz.

2.3.5 Chemical Pre-treatment

CFMs were chemically pretreated with a mixture of H_2SO_4 (0.25 M) and HNO_3 (0.25 M) in a 3:1 ratio[38] and washed with DI water prior to analysis.

2.3.6 Solution Geochemistry

Solution chemistry of Cu^{2+} in tris buffer and NaCl was modeled using PHREEQCi, a geochemical modeling software capable of determining speciation based on thermodynamic equilibrium. Stability constants during modeling were based on the MINTEQ.v4 database developed by the U.S. Environmental Protection Agency while

additional constants for complexation with solutions were modeled in equilibrium with $CO_{2(g)}$ ($10^{-4.8}$ atm.) and $O_{2(g)}$ ($10^{-0.67}$ atm.).[39] The pH values predicted by PHREEQCi models were found to match the pH observed in experimental solutions.

2.3.7 Fast Scan Controlled-Adsorption Voltammetry (FSCAV)

A CFM was placed into a constantly stirred $Cu(NO_3)_2$ solution and a waveform (-1.0 V – +1.3 V, resting potential of 0 V, at 600 Vs^{-1}) was applied. An electronic relay (ADG-419, Analog Devices) was used to switch between the applied waveform and a constant potential of 0 V for 10 seconds to allow copper adsorption at the electrode surface reach equilibrium. After 10 seconds, the waveform was reapplied, and the first background-subtracted cyclic voltammogram was collected and analyzed for total adsorbed copper. In house LabVIEW 2012 software integrated the reduction peak from the background subtracted cyclic voltammogram of Cu^{2+} and Faraday's law was used to convert this to a surface concentration (Γ_{Cu}). Measured data was fit to the linearized Langmuir isotherm (eq. 1) where C is the $[Cu^{2+}]$ in bulk solution, Γ_{max} is the maximum monolayer surface coverage, and K is the equilibrium constant for adsorption. This experiment was performed in NaCl (10 mM) and tris buffer (15 mM).

$$c/\Gamma_{Cu} = \frac{1}{\Gamma_{Max}}c + \frac{1}{\Gamma_{Max}K} \qquad (1)$$

2.3.8 Atomic Force Microscopy (AFM)

CFMs were prepared as described above and electrochemically activated. During slow scan cyclic voltammograms of $Cu(NO_3)_2$ (100 µM) (from +1 V to -1 V , back to +1 V), electrodes were temporarily disconnected for groups of electrodes at 6 different points. Those were 0.2, -0.6 and -1 V on the forward scan and -0.6, -0.3 and 0.2 V on the

reverse scan, all vs. Ag/AgCl. These electrodes had been exposed only to a partial section of the waveform. Electrodes were stored in a closed container and transported to the AFM. AFM images were taken using a Park Systems XE-NSOM instrument with a non-contact tip.

2.4 Results and Discussion

2.4.1 Slow Scan Cu^{2+} Cyclic Voltammetry at CFMs

During slow-scan Cu^{2+} cyclic voltammetry, a cathodic potential sweep is applied to the electrode at 1 – 10 mVs^{-1}, followed by an anodic sweep that brings the potential back to rest[36]. During the cathodic scan, copper is deposited on the electrode surface following a nucleation and growth mechanism. Copper nucleates over a broad potential range. These nuclei allow more Cu to deposit during a growth phase at any potential sufficient for deposition. Therefore, there are often two broad 'loop' reduction peaks, between the same voltages, on both cathodic and anodic scans[36]. The differences between the nature of the electrode surface and the Cu surface make this nucleation/growth deposition occur at a more negative voltage than the standard Cu^{2+} reduction potential[40,41]. Indeed when holding a CFM at a constant potential of 0.34 V (Cu^{2+} $2e^{-}\rightarrow$ $Cu_{(s)}$ standard reduction potential), addition of $Cu(NO_3)_2$ induced no change in current. This behavior is true for holding potentials down to -0.1 V (data not shown). During the anodic scan, the deposited $Cu_{(s)}$ is stripped off the electrode surface. Because this happens from a $Cu_{(s)}$ rich surface (a single phase), the stripping or oxidation peak is sharp and its voltage is much closer to the standard equilibrium potential[40,41]. Metal deposition can also occur via other mechanisms, for example, adsorption, charge transfer, and under

potential deposition (UPD)[42-44]. UPD is a process by which a metal deposits onto another metal at a more positive electrode potential than the Nernst potential for bulk deposition[42].

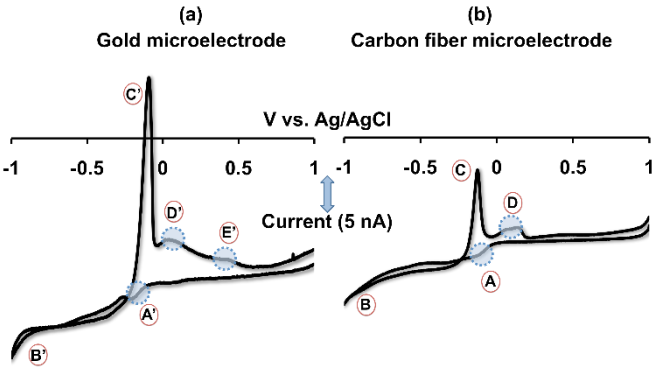

Figure 2.1. Slow scan cyclic voltammograms of $Cu(NO_3)_2$ on (a) AuM and (b) CFM at a scan rate of 10 mVs^{-1} in NaCl. Peaks A' – E' appear on the AuM, whereas peaks A – D appear on the CFM.

CFM slow scan cyclic voltammetry of Cu^{2+} was probed here by comparisons to AuMs. **Figure 2.1** shows representative cyclic voltammograms of $Cu(NO_3)_2$ (100 µM) on a Au Microelectrode (AuM) **(a)** and a CFM **(b)** at 10 mVs^{-1} in NaCl. These two voltammograms share common features. For example, Cu^{2+} reduction to metallic Cu begins at -0.1 V (peaks A', A) and continues via a loop formation between -0.4 V and -1.0 V on the cathodic scans (peaks B', B). This loop formation is an indication of nucleation and growth processes and is similar to previous observations.[43] On both AuMs and CFMs, sharp stripping peaks (C', C) and shoulder peaks (D', D) are present between -0.1 to 0.2 V on the anodic scans. Shoulders accompanying stripping peaks have previously been reported on glassy carbon electrodes[44] and highly oriented pyrolytic graphite electrodes[43]. The presence of complexing agents such as chloride and ammonia strongly affect copper redox processes and lead to the observation of shoulder peaks at

potentials higher than stripping peaks[41,43-47]. Shoulder peaks have not been found to be associated with stripping peaks in media containing no complexing agents[40,48-51].

A mechanism for shoulder peak formation in the presence of Cl^- has been speculated previously[44,47,52]. First, deposited Cu oxidizes to Cu^+, creating a stripping peak (C', C) and forming a barely conductive, passive layer of CuCl according to reaction (2).

$$Cu + Cl^- \rightarrow CuCl + e^- \text{ ----------(2)}$$

The CuCl layer shields underlying metallic copper thereby momentarily arresting further oxidation. Dissolution of this passive layer occurs either via direct diffusion or diffusion of a more soluble complex (such as $CuCl_2^-$). Dissolution exposes the remaining underlying metal allowing the electro-oxidation of Cu to continue as shown in reactions (3) and (4):

$$CuCl + Cl^- \rightarrow CuCl_2^- \text{ ----------(3)}$$

$$CuCl_2^- \rightarrow Cu^{2+} + 2Cl^- + e^- \text{ ----------(4)}$$

We determined whether these processes are responsible for shoulder peaks D' and D by systematically increasing the scan rate as described in the next section. There is an additional peak on the AuM that is not present on the CFM (peak E'). UPD plays a significant role in copper deposition on gold surfaces[42] whereas on carbon materials, metallic copper follows bulk deposition with no evidence for UPD[41,43,44,46,48,53]. Peak E' on the AuM is likely a consequence of anodic processes associated with UPD on gold[42].

2.4.2 Scan Rate Dependence

The shoulder peak mechanism proposed above was tested on CFMs by progressively increasing scan rate. The rationale here is that by increasing scan rate, nucleation/growth and hence stripping become limited because these processes are mass-

transport dependent.[41] Because reactions (3) and (4) rely on the stripping peak, any limitations in stripping should manifest proportionally on the shoulder peak.

In this experiment cyclic voltammograms of $Cu(NO_3)_2$ were collected at CFMs at increasing scan rates. From 10 – 100 mVs^{-1}, raw traces were analyzed; however at higher scan rates, the charging current due to double layer capacitance dominates the Faradaic component of the voltammetric signal. Therefore, cyclic voltammograms at 1 Vs^{-1} and above were collected in a flow injection system (FIA) using background subtraction.

Figure 2.2 shows cyclic voltammograms collected at 10, 30, 50 and 100 mVs^{-1} (left, blue panel) and at 1, 50, 100 and 300 Vs^{-1} (right, green panel). This experiment illustrates the evolution of a slow scan $Cu(NO_3)_2$ cyclic voltammogram in a typical FSCV signal[33]. Increased peak separation at high FSCV scan rates is due to slow electron transfer kinetics. All peaks are labeled as in **Figure 2.1**. From 10 – 100 mVs^{-1}, the magnitude of peaks (B) and (C) are greatly reduced such that they are almost absent at 100 mVs^{-1}. This is consistent with the notion that nucleation and growth are mass-transport limited and therefore can be 'outrun' at high scan rates. The magnitude of peaks (A) and (D) however are not subject to the same behavior. Peaks (A) and (D) are present and well defined at 100 mVs^{-1} implying that these features are neither mass-transport limited nor dependent on peaks (B) and (C). The results of these experiments indicate that mechanisms other than those described by Reactions (3) and (4) are responsible for peak (D).

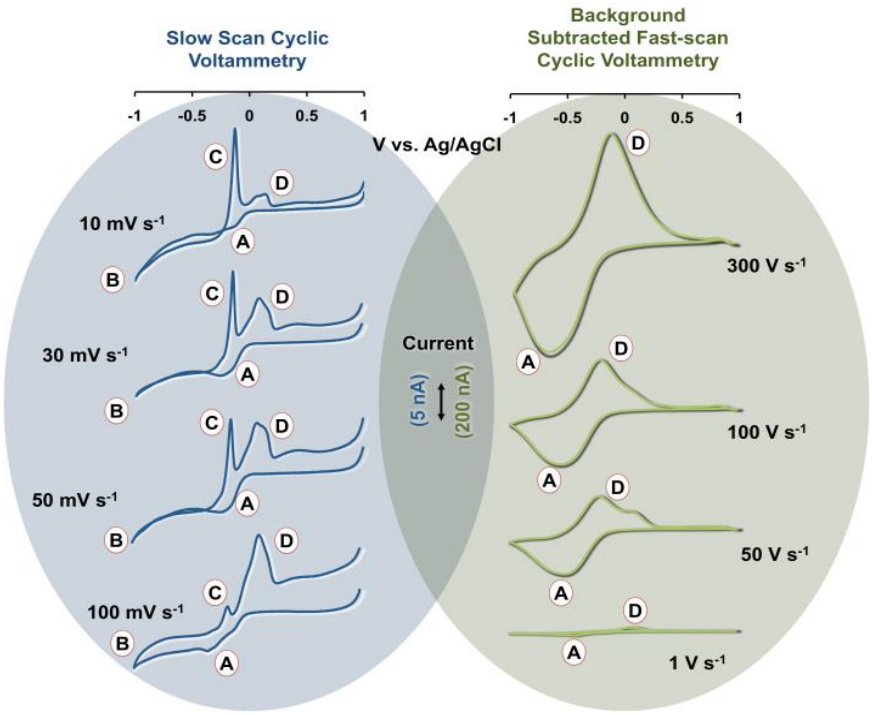

Figure 2.2. Left: Slow scan cyclic voltammograms of $Cu(NO_3)_2$ on CFMs at scan rates of 10, 30, 50 and 100 mVs^{-1}. Right: Fast scan background-subtracted cyclic voltammograms of $Cu(NO_3)_2$ at scan rates of 1, 50, 100 and 300 Vs^{-1}.

For adsorbed species, the peak current is proportional to scan rate[51] and we indeed found that from 1 – 300 Vs^{-1}, peak amplitudes increased. Furthermore, the slope of a plot of the log current vs. log scan rate for $Cu(NO_3)_2$ was previously reported to be approximately 1 at high scan rates[33]. Taken together, these findings strongly support a hypothesis that peaks (A) and (D) stem from an adsorption controlled process. Adsorption is explored in the following sections.

2.4.3 CFM Over-oxidation Leads to Enhanced Sensitivity

Activated carbon is widely used in wastewater treatment and is the primary purification component of domestic water filters[54,55]. When carbon is activated (e.g. via heat in the presence of air, or with chemical or electrochemical pretreatments) a wide

array of oxygen functionalities are created on its surface[54]. These oxygen moieties adsorb and complex trace metals, removing them from solution[56,57].

CFMs are typically electrochemically pre-treated prior to use[56]. Therefore, in analogy to metal adsorption by activated carbon, the oxygen functionalities on the CFM surface may rapidly complex trace metals in solution, pre-concentrating them on the surface. In this experiment, we tested the hypothesis that enhanced surface oxidation is responsible for increased FSCV sensitivity towards Cu^{2+}, presumably due to an increased number of adsorption sites.

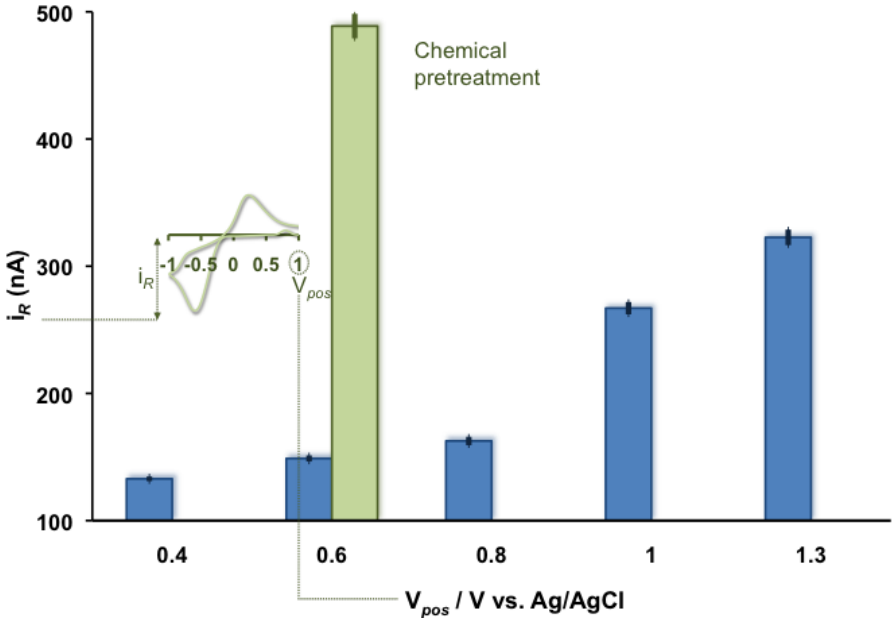

Figure 2.3. Maximum cathodic current of $Cu(NO_3)_2$ (10 µM) fast scan cyclic voltammograms as a function of anodic potential limit (blue series) at 300 Vs^{-1} and as a function of acid pretreatment (green).

Using flow injection analysis, we collected background subtracted cyclic voltammograms of CFMs exposed to a bolus of $Cu(NO_3)_2$ (10 µM) with different FSCV waveforms. We systematically increased the anodic potential limit of the waveform at a constant cathodic limit, -1.0 V.

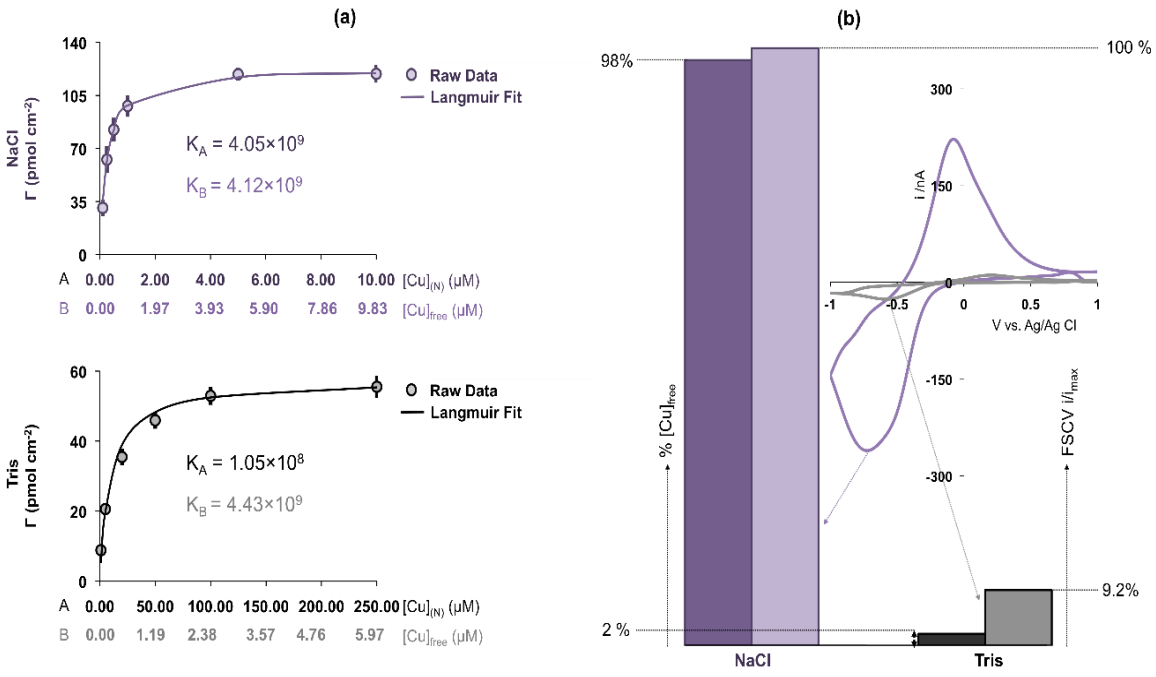

Figure 2.4. (a) Langmuir adsorption isotherms for $Cu(NO_3)_2$ on CFMs in NaCl (top) and in tris buffer (bottom). (b) Histogram showing % $[Cu^{2+}]_{free}$ in solution and % cathodic current of $Cu(NO_3)_2$ (10 µM) in NaCl (purple series) and in tris buffer (black series) at 300 Vs^{-1} (% cathodic current is shown by setting the maximum cathodic current with tris buffer to 100% and expressing the cathodic current with NaCl as a percentage of this). The inset background-subtracted cyclic voltammograms are representative examples taken in NaCl (purple) and tris buffer (black)

Figure 2.3 shows the magnitude of cathodic current (demonstrated by the inset cyclic voltammogram) as a function of the anodic potential limit. The cathodic current showed exponential increases with increasing anodic potential. This exact behavior was previously reported with neurotransmitters and attributed to surface 'activation' or over-oxidation[56]. To confirm that the enhanced sensitivity was due to over-oxidation, an alternative method to over-oxidize the CFM surface was employed. An acid pretreatment [38] was applied to the electrode surface prior to use (H_2SO_4 (0.25 M) and HNO_3 (0.25 M) in a 3:1 ratio). An anodic potential limit of +0.6 V was used where we previously found negligible effects of electrochemical over-oxidation. The resultant cathodic current is

plotted in green on the 0.6 V series. The current here is substantially higher than the non-acid treated CFM confirming that surface activation, by two separate means, begets similar outcomes.

2.4.4 Cu^{2+} Adsorption to CFMs drives the FSCV Signal

We sought to verify that the enhanced FSCV sensitivity towards Cu^{2+} as a consequence of activation is an adsorption-driven mechanism. This was successfully confirmed by construction of adsorption isotherms using fast scan controlled-adsorption voltammetry (FSCAV) on CFMs[57]. Adsorption isotherms describe the thermodynamic equilibrium of Cu^{2+} onto the CFM, providing an index of the amount of Cu^{2+} on the CFM surface with respect to bulk solution via the equilibrium constant, K.

In all experiments described above, we used a simple matrix, NaCl, for characterizations. The adsorption isotherm of Cu^{2+} on CFMs in NaCl is shown in **Figure 2.4a (top panel)** and follows a Langmuir fit. Authentic biological and environmental matrices are more complicated than NaCl and contain copper binding components. Therefore, we studied whether a complex matrix would affect Cu^{2+} adsorption. We previously characterized copper in tris buffer[33] which has considerable metal binding capacity[58,59]. Additionally Tris acts as a model biological medium because it contains amines that mimic proteins. The other salts in the buffer are at a ratio and concentration designed to mimic artificial cerebrospinal fluid (ACSF). Many neurotransmitters and other biologically relevant molecules have been characterized in tris *in vitro*[60-62] therefore adsorption isotherms were additionally constructed in tris buffer, (**Figure 2.4a bottom)** also following a Langmuir fit.

We previously used a geochemical model to calculate the equilibrium concentrations of free Pb^{2+} in test solutions[32]. We employed the same model here to calculate free Cu^{2+} concentration ($[Cu^{2+}]_{free}$) in NaCl and tris solutions. Our isotherms therefore have two x-axes, (A) denotes the concentration of Cu^{2+} added ($[Cu^{2+}]_{(N)}$) to the test solutions and (B) denotes the free Cu^{2+} concentration $[Cu^{2+}]_{free}$ in solution. For NaCl, the two x-axes values are similar because NaCl has little Cu^{2+} binding capacity. Therefore when calculating K, there is little difference between the values calculated with $[Cu^{2+}]_{(N)}$ vs. $[Cu^{2+}]_{free}$ (K_A and K_B). For tris the values of axes (A) and (B) are dramatically different because tris has Cu^{2+} binding capacity with K ~ 10^4 [59]. It is interesting however, that when $[Cu^{2+}]_{free}$ is taken into consideration in the calculation, K (K_B) is similar to the K values in NaCl. Therefore, this complex matrix does not affect the monolayer characteristics of Cu^{2+} adsorption onto CFMs. This experiment further shows that solution complexes and other species do not significantly adsorb to the CFM surface and alter K.

The interactions of the Cu^{2+}- CFM and Cu^{2+} - tris equilibria are complicated. **Figure 2.4b** is a histogram that compares % $[Cu^{2+}]_{free}$ in solution to the cathodic current of background subtracted cyclic voltammograms of $Cu(NO_3)_2$ in NaCl (purple series) and tris buffer (black series). Shown in the inset are representative examples of cyclic voltammograms of $Cu(NO_3)_2$ in NaCl and tris buffer. In the histogram, we compared the two FSCV signals thus: the maximum cathodic current with tris buffer was normalized to 100% and the current with NaCl was expressed as a percentage of this. It is seen that despite only 2% $[Cu^{2+}]_{free}$ in tris buffer, that the Cu^{2+} signal is 9.2% of the Cu^{2+} signal in NaCl (with 98% $[Cu^{2+}]_{free}$). This discrepancy implies that the two equilibria compete. The

equilibrium of Cu^{2+}- CFM complexation is more favorable than Cu^{2+} - tris complexation, and a serendipitous outcome of this effect is high FSCV sensitivity, even in Cu^{2+} complexing matrices.

Given the confirmation that our Cu^{2+} FSCV signal is highly adsorption driven, the nucleation characteristics of the cyclic voltammetry peaks on CFMs were next studied.

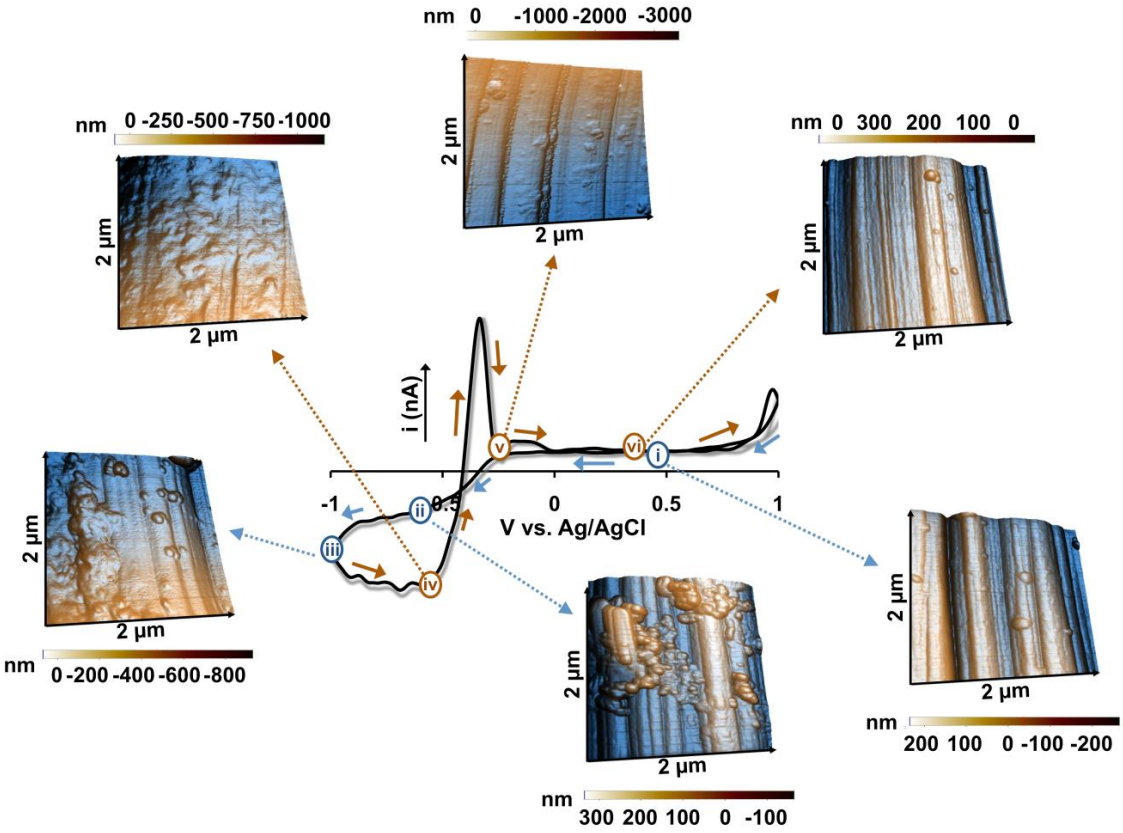

Figure 2.5. AFM images of a slow scan (10 mVs^{-1}) cyclic voltammogram of $Cu(NO_3)_2$ (100 µM) in tris buffer taken at six different points along the scan. On the forward scan, images were recorded at 0.2 V (i), -0.6 V (ii) and -1 V (iii) and on the backward scan at 0.6 V (iv), -0.3 V (v) and 0.2 V (vi). AFM images are 2 µM x 2 µM.

2.4.5 AFM Characterization of Cu Nucleation and Oxidation

Changes in the morphology of the CFM surface can be visualized with AFM. AFM is a sensitive surface imaging technique, which employs a cantilevered tip to convert surface contours into images. AFM is routinely used to establish and characterize the formation of metallic copper on electrode surfaces[40,41]. In **Figure 2.5**, AFM images were recorded at six different points along a slow scan cyclic voltammogram of $Cu(NO_3)_2$ in a complex matrix, tris buffer. Shortly after the start of the scan (i) the striations of the bare CFM surface are well defined. The small round features on the surface are likely solid contaminants. At (ii), metallic copper clusters are present on the CFM surface showing that the eventual cathodic FSCV peak (which evolves from this peak at high scan rates) involves deposition of $Cu_{(s)}$. $Cu_{(s)}$ is more elaborate during nucleation (iii) and after growth (iv) where striations are no longer visible under metallic Cu. After stripping (v), striations are again visible and due to the removal of metallic Cu. During the stripping process, $Cu_{(s)}$ may either be oxidized to Cu^+ (as discussed above) or directly to Cu^{2+}. The presence of clear carbon striations and the scan rate dependent data provide little evidence for the formation of CuCl. However, the nature of the peak directly proceeding the stripping peak (the eventual anodic FSCV anodic peak) is yet to be determined. One explanation is that this $Cu_{(s)}$ is deposited on specific CFM adsorption sites that have their own discrete oxidation potentials. The remaining clusters are no longer present at point (vi), confirming that $Cu_{(s)}$ is completely oxidized at the end of the scan.

These surface morphology data confirm the nucleation and oxidation of metallic Cu associated with the cathodic and anodic FSCV peaks, i.e., peaks A and B in the FSCV segment of **Figure 2.2** are due to $Cu^{2+} + 2\ e^- \rightarrow Cu_{(s)}$ and the reverse reaction.

2.5 Conclusion

FSCV at CFMs is an excellent tool for fast metal analysis with essential applications in biology and the environment. In this work, we described the fundamental mechanisms of fast scan voltammetry of Cu^{2+} on CFMs. In analogy to metal remediation by activated carbon, we showed that adsorption on CFMs underlies rapid FSCV responses. We ascertained the thermodynamic and physical characteristics of the CFM adsorption mechanism. This study has allowed us to understand the fundamentals of Cu^{2+} FSCV, enabling future improvements in the sensitivity and selectivity of fast metal voltammetry for real-time biological and environmental analysis.

2.6 References

(1) Gaier, E. D.; Eipper, B. A.; Mains, R. E. *J Neurosci Res* **2013**, *91*, 2.

(2) Que, E. L.; Domaille, D. W.; Chang, C. J. *Chem Rev* **2008**, *108*, 1517.

(3) Hung, Y. H.; Bush, A. I.; Cherny, R. A. *J Biol Inorg Chem* **2010**, *15*, 61.

(4) Macreadie, I. G. *Eur Biophys J* **2008**, *37*, 295.

(5) Haarstad, K.; Bavor, H. J.; Maehlum, T. *Water Sci Technol* **2012**, *65*, 76.

(6) Vaiopoulou, E.; Gikas, P. *Water Res* **2012**, *46*, 549.

(7) Chiodo, L. M.; Jacobson, S. W.; Jacobson, J. L. *Neurotoxicol Teratol* **2004**, *26*, 359.

(8) Charlesworth, S.; De Miguel, E.; Ordonez, A. *Environ Geochem Health* **2011**, *33*, 103.

(9) Brewer, G. J. *Clin Neurophysiol* **2010**, *121*, 459.

(10) Islam, E.; Yang, X. E.; He, Z. L.; Mahmood, Q. *J Zhejiang Univ Sci B* **2007**, *8*, 1.

(11) Peralta-Videa, J. R.; Lopez, M. L.; Narayan, M.; Saupe, G.; Gardea-Torresdey, J. *Int J Biochem Cell Biol* **2009**, *41*, 1665.

(12) Ward, D. M.; Nislow, K. H.; Folt, C. L. *Annals of the New York Academy of Sciences* **2010**, *1195*, 62.

(13) Balshaw, S.; Edwards, J.; Daughtry, B.; Ross, K. *Rev Environ Health* **2007**, *22*, 91.

(14) Dean, C. M.; Sansalone, J. J.; Cartledge, F. K.; Pardue, J. H. *J. Environ. Eng.-ASCE* **2005**, *131*, 632.

(15) Strawn, D. G.; Sparks, D. L. *Soil Science Society of America Journal* **2000**, *64*, 144.

(16) Selin, N. E. *J Environ Monit* **2011**, *13*, 2389.

(17) Ritter, L.; Solomon, K.; Sibley, P.; Hall, K.; Keen, P.; Mattu, G.; Linton, B. *Journal of Toxicology and Environmental Health-Part a-Current Issues* **2002**, *65*, 1.

(18) Peters, R. W. *J Hazard Mater* **1999**, *66*, 151.

(19) Kumpiene, J.; Lagerkvist, A.; Maurice, C. *Waste Manag* **2008**, *28*, 215.

(20) Brix, H. *Water Science and Technology* **1999**, *40*, 45.

(21) Kadlec, R. H.; Wallace, S. D. *Treatment Wetlands*; 2nd ed.; CRC Press: Boca Ranton, 2009.

(22) Butler, O. T.; Cairns, W. R. L.; Cook, J. M.; Davidson, C. M. *Journal of Analytical Atomic Spectrometry* **2012**, *27*, 187.

(23) Anawar, H. M. *Talanta* **2012**, *88*, 30.

(24) Fytianos, K. *J AOAC Int* **2001**, *84*, 1763.

(25) Pretsch, E. *Trac-Trends in Analytical Chemistry* **2007**, *26*, 46.

(26) Bakker, E.; Pretsch, E.; Buhlmann, P. *Anal Chem* **2000**, *72*, 1127.

(27) Dai, X.; Nekrassova, O.; Hyde, M. E.; Compton, R. G. *Anal Chem* **2004**, *76*, 5924.

(28) Tercier-Waeber, M. L.; Buffle, J.; Graziottin, F.; Koudelka-Hep, M. *Abstracts of Papers of the American Chemical Society* **2000**, *220*, U317.

(29) Mota, A. M. A.; Buffle, J.; Kounaves, S. P.; Goncalves, M. L. S. *Analytica Chimica Acta* **1985**, *172*, 13.

(30) Pei, J. H.; Tercier-Waeber, M. L.; Buffle, J. *Analytical Chemistry* **2000**, *72*, 161.

(31) Barek, J.; Fogg, A. G.; Muck, A.; Zima, J. *Critical Reviews in Analytical Chemistry* **2001**, *31*, 291.

(32) Yang, Y.; Pathirathna, P.; Siriwardhane, T.; McElmurry, S. P.; Hashemi, P. *Anal Chem* **2013**.

(33) Pathirathna, P.; Yang, Y.; Forzley, K.; McElmurry, S. P.; Hashemi, P. *Anal Chem* **2012**, *84*, 6298.

(34) Kiaune, L.; Singhasemanon, N. *Rev Environ Contam Toxicol* **2011**, *213*, 1.

(35) Hyde, M. E.; Compton, R. G. *Journal of Electroanalytical Chemistry* **2003**, *549*, 1.

(36) Prado, C.; Wilkins, S. J.; Marken, F.; Compton, R. G. *Electroanalysis* **2002**, *14*, 262.

(37) Keithley, R. B.; Takmakov, P.; Bucher, E. S.; Belle, A. M.; Owesson-White, C. A.; Park, J.; Wightman, R. M. *Anal Chem* **2011**, *83*, 3563.

(38) Parra, E. J.; Blondeau, P.; Crespo, G. A.; Rius, F. X. *Chem Commun* **2011**, *47*, 2438.

(39) Aslamkhan, A. G.; Aslamkhan, A.; Ahearn, G. A. *Journal of Experimental Zoology* **2002**, *292*, 507.

(40) Pesic, B.; Grujicic, D. *Electrochimica Acta* **2002**, *47*, 2901.

(41) Grujicic, D.; Pesic, B. *Electrochimica Acta* **2005**, *50*, 4426.

(42) Krznaric, D.; Goricnik, T. *Langmuir* **2001**, *17*, 4347.

(43) Srinivasan, R.; Gopalan, P. *Surf Sci* **1995**, *338*, 31.

(44) Shi, K.; Hu, K.; Wang, S.; Lau, C. Y.; Shiu, K. K. *Electrochimica Acta* **2007**, *52*, 5907.

(45) Garcia-Rodriguez, D. E.; Mendoza-Huizar, L. H.; Rios-Reyes, C. H.; Alatorre-Ordaz, M. A. *Quimica Nova* **2012**, *35*, 699.

(46) Nila, C.; Gonzalez, I. *Journal of Electroanalytical Chemistry* **1996**, *401*, 171.

(47) Yoo, K.; Miller, B.; Shi, X.; Kalish, R. *Journal of the Electrochemical Society* **2001**, *148*, C95.

(48) Huang, L.; Lee, E. S.; Kim, K. B. *Colloids and Surfaces a-Physicochemical and Engineering Aspects* **2005**, *262*, 125.

(49) Ghodbane, O.; Roue, L.; Belanger, D. *Electrochimica Acta* **2007**, *52*, 5843.

(50) Majidi, M. R.; Asadpour-Zeynali, K.; Hafezi, B. *Electrochimica Acta* **2009**, *54*, 1119.

(51) Grubač, Z.; Metikoš-Huković, M. *Materials Letters* **2007**, *61*, 794.

(52) Lang, G. G.; Ujvari, M.; Horanyi, G. *Journal of Electroanalytical Chemistry* **2002**, *522*, 179.

(53) Lee, J. J.; Miller, B.; Shi, X.; Kalish, R.; Wheeler, K. A. *Journal of the Electrochemical Society* **2001**, *148*, C183.

(54) Corapcioglu, M. O.; Huang, C. P. *Water Research* **1987**, *21*, 1031.

(55) Mohan, D.; Pittman, C. U., Jr. *J Hazard Mater* **2006**, *137*, 762.

(56) Biniak, S.; Pakula, M.; Szymanski, G. S.; Swiatkowski, A. *Langmuir* **1999**, *15*, 6117.

(57) Seredych, M.; Hulicova-Jurcakova, D.; Lu, G. Q.; Bandosz, T. J. *Carbon* **2008**, *46*, 1475.

CHAPTER 3

IN VIVO HISTAMINE VOLTAMMETRY IN THE MOUSE PREMAMMILLARY NUCLEUS

Reproduced with permission from Royal Society of Chemsitry.

Samaranayake S, Abdalla A, Robke R, Wood KM, Zeqja A, Hashemi P (2015) In vivo histamine voltammetry in the mouse premammillary nucleus. *Analyst* 140:3759-3765.

3.1 Abstract

Histamine plays a major role in the mediation of allergic reactions such as peripheral inflammation. This classical monoamine is also a neurotransmitter involved in the central nervous system but its roles in this context are poorly understood. Studying histamine neurotransmission is important due to its implications in many neurological disorders. The sensitivity, selectivity and high temporal resolution of fast scan cyclic voltammetry (FSCV) offer many advantages for studying electroactive neurotransmitters. Histamine has previously been studied with FSCV; however, the lack of a robust Faradaic electrochemical signal makes it difficult to selectively identify histamine in complex media, as found in vivo. In this work, we optimize an electrochemical waveform that provides a stimulation-locked and unique electrochemical signal towards histamine. We describe in vitro waveform optimization and a novel in vivo physiological model for stimulating histamine release in the mouse premamillary nucleus via stimulation of the medial forebrain bundle. We demonstrate that a robust signal can be used to effectively identify histamine and characterize its' in vivo kinetics.

3.2 Introduction

The central nervous system holds four aminergic systems, dopamine, serotonin, norepinephrine and histamine. These messengers are in an intricate chemical interplay with one-another and other neurotransmitters to precisely modulate many aspects of brain function. It is critical to understand the fundamental neurochemistry of these four modulatory systems to better prevent, diagnose and treat brain disorders and diseases. Fast scan cyclic voltammetry (FSCV) at carbon fiber microelectrodes (CFMs) is a

uniquely powerful method for *in vivo* analysis. CFMs are biocompatible, cause negligible damage to brain tissue and, because of their kinetically favorable surface kinetics, provide real-time output of electroactive neurotransmitters.

The dopaminergic system has been extensively studied with FSCV over the previous three decades leading to breakthroughs in understanding dopaminergic mechanisms in the brain[1-3]. More recently, FSCV has been recently developed for the detection of serotonin and norepinephrine[4,5] and many important aspects of the two neurotransmitters are thus being unearthed[6-10]. Histamine is also an electroactive amine, and there have been previous reports of histamine induced FSCV signals in mast cells,[11-13] brain tissue slice preparations[14] and *in vivo*[15], however mechanistic studies on histamine are limited. This is primarily because histamine electrochemistry is complex, and FSCV induced histamine signals are often interpreted via changes in the capacitative current on the electrode surface. This approach is fully quantitative, however many analytes induce a capacitative change at the electrode surface limiting selectivity and rendering *in vivo* studies very difficult.

Faradaic electrochemistry more selectively identifies analytes because of the unique potential position of redox peaks[16]. In this paper, we discuss the relevance of histamine adsorption to capacitative currents at CFMs. We describe a novel FSCV waveform that generates a robust oxidation peak in response to histamine. We show *in vitro*, that histamine can be detected selectively and with high sensitivity. Finally, we report and verify a robust histamine signature in the mouse premamillary nucleus (PM) in response to medial forebrain bundle (MFB) stimulation.

Our novel FSCV waveform for histamine provides a tool that will enable the same level of investigation for histamine as other, more established brain amines. Histamine's roles in the brain, in particular with respect to disorders in which it is implicated (e.g. Alzheimer's disease) can thus be systematically studied.

3.3 Experimental Section

3.3.1 Chemicals and Reagents

Standard solutions were prepared by dissolving histamine dihydrochloride, dopamine hydrochloride, serotonin hydrochloride and adenosine hydrocloride (Sigma-Aldrich, Co., MO, USA) respectively in Tris-buffer. Tris-buffer was constituted thus: 15 mM $H_2NC(CH_2)(OH)_3.HCl$, 140 mM NaCl, 3.25 mM KCl, 1.2 mM $CaCl_2$, 1.25 mM $NaH_2PO_4.H_2O$, 1.2 mM $MgCl_2$ and 2.0 mM Na_2SO_4 at pH=7.4 in deinoized water (EMD Chemicals Inc. NJ, USA).

3.3.2 Carbon-Fiber Microelectrodes (CFMs)

CFMs were fabricated with 7µm diameter carbon-fibers (Goodfellow Corporation, PA, USA) aspirated in to glass capillaries (0.6 mm external diameter, 0.4 mm internal diameter, A-M systems, Inc., Sequim, WA). A carbon-glass seal was formed via a vertical micropipette puller (Narishige Group, Tokyo, Japan). The exposed length of the carbon fiber was trimmed to 150 µm under an optical microscope. Microelectrodes were electroplated with Nafion as described previously[4].

3.3.3 Data Collection/Analysis

Waveform generation was via a PCIe-6341 DAC/ADC card (National Instruments, Austin, TX). Output current was measured by a CHEM-CLAMP potentiostat (Dagan corporation, MN). Custom built software was employed to drive the hardware, collect data and perform analysis including background subtraction, signal averaging and digital filtering (Knowmad Technologies LLC, Tucson, AZ). All potentials are quoted with respect to Ag/AgCl reference electrodes, which were fabricated via electrodeposition of Cl^- by holding a silver wire (A-M systems, WA) at 4.0 V for 5 s in 1 M HCl. All data represented with error bars represent the standard error of the mean (SEM). Statistical differences were determined using one-tailed student's-tests on paired data sets ($p<0.45$ was taken as statistically different).

3.3.4 Langmuir Adsorption Isotherms

A CFM was placed into histamine solution of standard concentration and an optimized histamine waveform was applied. An electronic relay (ADG-419, Analog Devices) was used to switch between the applied waveform and a constant potential (-0.5 V) for 10 seconds to allow histamine adsorption at the electrode surface and reach equilibrium. After 10 seconds, the waveform was reapplied, and the first background-subtracted cyclic voltammogram was collected and analyzed for total adsorbed histamine. In house LabVIEW 2012 software integrated the oxidation peak from the background subtracted cyclic voltammogram and Faraday's law was used to convert this to a surface concentration ($\Gamma_{\text{histamine}}$). Measured data was fit to a linearized Langmuir adsorption

isotherm as previously described[17], and *K* is the equilibrium constant for adsorption. This experiment was performed in tris buffer (15 mM).

3.3.5 Flow Injection Analysis

In vitro analyses were performed with flow injection analysis (FIA). CFMs were inserted into a flangeless short 1/8 nut (PEEK P-335, IDEX, Middleboro, MA) such that around 2 mm of the tip remained exposed outside of the nut. The microelectrode-containing nut was then fastened into a modified HPLC union (Elbow PEEK 3432, IDEX, Middleboro, MA). The other end of the elbow union was fastened into the out-flowing steam of the FIA buffer and two holes were drilled into the union for incorporation of the reference electrode and for a 'waste' flow stream. Flow was maintained with a syringe infusion pump (kd Scientific, model KDS-410, Holliston, MA) at 2 mL min^{-1}. A rectangular pulse of analyte was introduced into the flow steam for 10 s via a six-port HPLC loop injector (Rheodyne model 7010 valve, VICI, Houston, TX). For calibrations and waveform optimization, analytes were injected in random concentrations order to avoid carry-over effects.

3.3.6 Potentiometry

The open circuit potential between CFMs and Ag/AgCl was measured using a potentiostat with an integrated high impedance amplifier (eDAQ Pty Ltd, NSW, Australia). 200 µM of histamine was injected onto the CFM in Tris-buffer using FIA at pH = 7.4. Subsequent injections were after potential recovered to base line.

3.3.7 Animal Surgeries

Handling and surgery on male C57BL/6J mice weighing 20−25 g (Jackson Laboratory, Bar Harbor, ME) were in agreement with The Guide for the Care and Use of Laboratory Animals, approved by the Institutional Animal Care and Use. Urethane (25% dissolved in 0.9% NaCl solution, Hospira, Lake Forest, IL) was administered via intraperitoneal (i.p.) injection, and stereotaxic surgery (David Kopf Instruments, Tujunga, CA) was performed. A heating pad sustained mouse body temperature around 37 °C (Braintree Scientific, Braintree, MA). Stereotaxic coordinates were taken in reference to bregma. A Nafion modified CFM was inserted into the PM (AP: −2.45, ML: +0.50, DV: −5.45 to −5.55.). A stainless steel stimulating electrode (diameter: 0.2 mm, Plastics One, Roanoke, VA) was positioned into the MFB (AP: -1.07, ML: +1.10, DV: −5.00). 120 biphasic pulses were applied through a linear constant current stimulus isolator (NL800A, Neurolog, Medical Systems Corp., Great Neck, NY). The 60 Hz trains were 350 μA each phase, 2 ms in width, and 2 s in length. An Ag/AgCl reference electrode was implanted into the brain's opposite hemisphere.

3.3.8 Drugs

Tacrine hydrochloride (2 mg kg^{-1}) and thioperamide maleate (20 mg kg^{-1}) from TOCRIS bioscience (Bristol, UK) were dissolved in saline respectively and injected i.p. at a volume of 0.6 ml kg^{-1}.

3.4 Results and Discussion

3.4.1 Histamine Adsorption onto CFMs Underlies Capacitative FSCV Current

Histamine has previously been detected in mast cells and neural tissues with FSCV[11-15]. In the majority of these studies, the oxidation peak that appeared at or after the switching potential on the positive wave, as illustrated in **Figure 3.1**, was used for quantification. **Figure 3.1Ai** is an FSCV color plot during flow injection of histamine (20 µM) onto a CFM with a serotonin sensitive waveform[18]. The interpretation of color plots is described in detail elsewhere[19], briefly, potential is displayed on the y-axis, time on the x-axis and current in false color and injection time is denoted by the star.

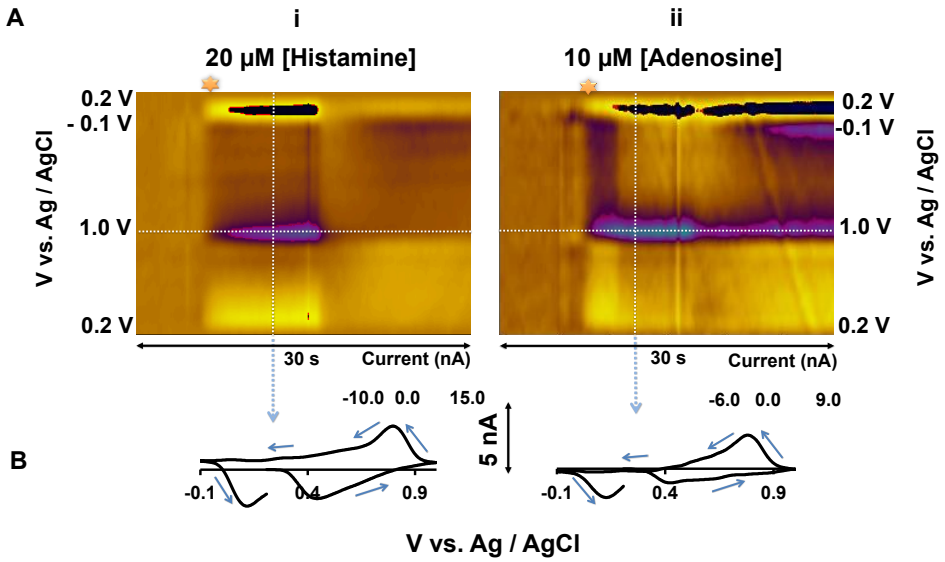

Figure 3.1. A shows color plots for FIA of **(i)** 20 µM histamine **(ii)** 10 µM adenosine. **B** shows CVs extracted from the vertical dashed lines from **(i)** and **(ii)**.

A cyclic voltammogram (CV) taken from the vertical white dashed line of the color plot displays an oxidation peak at around 0.8 V that appears after the switching potential (on the returning positive scan). In previous work, a stimulation-locked signal in the rat substantia nigra (SNr) displayed a similar CV and was pharmacologically determined to be histamine[15]. In the absence of pharmacology however, it is not possible

to selectively verify histamine with this waveform, this is because other electroactive species give identical CVs. **Figure 3.1Aii** is a color plot taken during FIA of adenosine (10 µM). The corresponding CV (**Figure 3.1B**) is almost identical to that of histamine's. In a region containing both adenosine and histamine, therefore, it is not possible to distinguish between these analytes electrochemically. Furthermore, other work has shown similar CVs for H_2O_2 and gonatropin-releasing hormone[20,21], further complicating selective histamine detection.

Histamine electrochemistry is kinetically limited within the oxidation potential window of previously utilized waveforms. In fact the electrochemical oxidation scheme for histamine is not known, presumably because it involves charge transfer. We therefore postulate that the peaks observed in **Figure 3.1** are due to non-Faradaic processes. These processes arise on the CFM surface when spontaneous adsorption of histamine causes changes in the electrical bilayer. The electrical bilayer on electrode surfaces acts as a capacitor, discharging current into the electrode, particularly at switching potentials. Capacitative or charging currents are a well-known phenomenon in FSCV because of the high scan rates employed[16]. FSCV is background-subtracted, specifically to remove such background charging currents which do not reflect Faradaic processes associated with analytes of interest. However, adsorption of histamine changes the background capacitative current which cannot be subtracted out, this effect manifests as the features in the CVs in **Figure 3.1**.

In **Figure 3.2**, FIA was utilized to inject histamine (200 µM) onto CFMs while the open field potential was measured vs. Ag/AgCl (**Figure 3.2A**). **Figure 3.2B** shows that the potential of the CFMs rapidly peaks in response to histamine injections. Because

there is no driving potential, this implies that histamine spontaneously adsorbs to and changes the potential of the CFM. The features on histamine's CV in **Figure 3.1** are likely a consequence of the current that arises from this adsorption. To further verify this histamine adsorption, Langmuir isotherms were constructed for histamine with a previously described method[22] confirming monolayer coverage of the CFM (**Figure 3.2C**).

While charging current peaks can quantify histamine, little selectivity is offered since many analytes adsorb onto CFMs. We therefore designed a novel waveform to capture histamine electrochemistry before the switching potential.

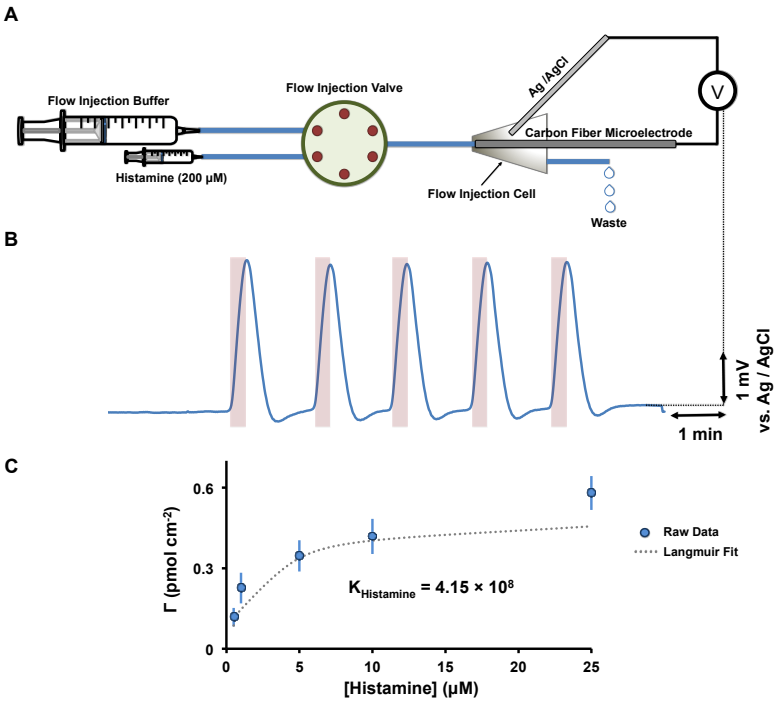

Figure 3.2. A shows the schematic diagram of the experimental setup used for potentiometric experiments. **B** shows the experimental potentiometric data for five consecutive injections of histamine (200 µM) on CFM. **C** Langmuir isotherm for histamine adsorption on CFMs in Tris buffer.

3.4.2 Histamine Selective Waveform (HSW)

Histamine contains an imidazole ring and an aliphatic amine group. This molecule's ability to readily bind metals such as Cu[23,24], because of its electronegative sites, means that it is readily amenable to oxidation. However histamine electro-oxidation differs from serotonin and dopamine in that it likely involves charge transfer. This mechanism introduces kinetic limitations that have not yet enabled stimulation-locked peaks on the positive direction of the wave in FSCV studies. Therefore preliminary we utilized a triangular waveform and expanded the potential window to cover a large range thereby allowing histamine oxidation to occur within a single scan. Through trial and error we determined that, *in vitro*, a waveform scanning from -0.7 to 1.1 V (resting at -0.7 V at 600 Vs^{-1}) provided an oxidation peak during the positive scan. However this waveform was not successful *in vivo*, showing rapid degradation (fouling). By changing the resting potential to -0.5 V, we found that electrode degradation was eliminated and *in vivo* detection was possible. A possible explanation for this phenomenon is that at -0.7 V, fouling species (e.g proteins) may preferentially adsorb onto the electrode surface.

Our optimized waveform, the histamine selective waveform (HSW), therefore is -0.7 V to 1.1 V, resting at -0.5 V, with a scan rate of 600 Vs^{-1}. **Figure 3.3** compares histamine detection with the previously described serotonin waveform[15] to the HSW. **Figure 3.3A** (serotonin waveform) and **C** (HSW) show color plots and CVs during FIA of histamine (20 µM). The HSW detects histamine oxidation at around +0.3 V vs. Ag/AgCl, and in contrast to the serotonin waveform, this peak occurs before the switching potential on the positive wave. Furthermore, current vs. time traces, extracted from horizontal dashed lines from the color plots (**Figure 3.3B)**, show that the HSW

response is a square injection while the serotonin waveform response does not reach steady state. This makes it possible to more accurately describe histamine *in vivo* kinetics (i.e. histamine clearance kinetics) with the HSW. The HSW has a linear dynamic range up to 20 µM of histamine **(Figure 3.3Dii),** a sensitivity of 0.354 ± 0.032 nA/µM and a limit of detection of 1 µM. Finally, histamine measurements with this waveform show good stability, as evidenced by the negligible loss in signal (normalized oxidation current) during 50 successive flow injections of histamine (10 µM) (**Figure 3.3E**).

3.4.3 HSW Selectivity

We sought to develop a waveform to produce a histamine oxidation peak before the switching potential on the positive scan to increase the selectivity of FSCV towards histamine. To assess the selectivity of the waveform *in vitro*, we tested dopamine, serotonin and adenosine, which are electroactive species that are chemically similar to histamine and commonly found in brain regions containing histamine[25,26,27]. **Figure 3.4** shows CVs obtained during FIA of histamine (20 µM), dopamine (100 nM), serotonin (10 nM) and adenosine (1 µM). These concentrations were chosen to mimic previously reported evoked *in vivo* concentrations[11,26,28]. Adenosine's peak still occurs at the switching potential with this waveform and is therefore unlikely to interfere. The oxidation peak for histamine appears at around 0.3 V vs. Ag/AgCl (green dashed line) and is in a different position from dopamine and serotonin oxidation peaks (around 0.5 and 0.6 V vs. Ag/AgCl (red and blue dashed lines), respectively).

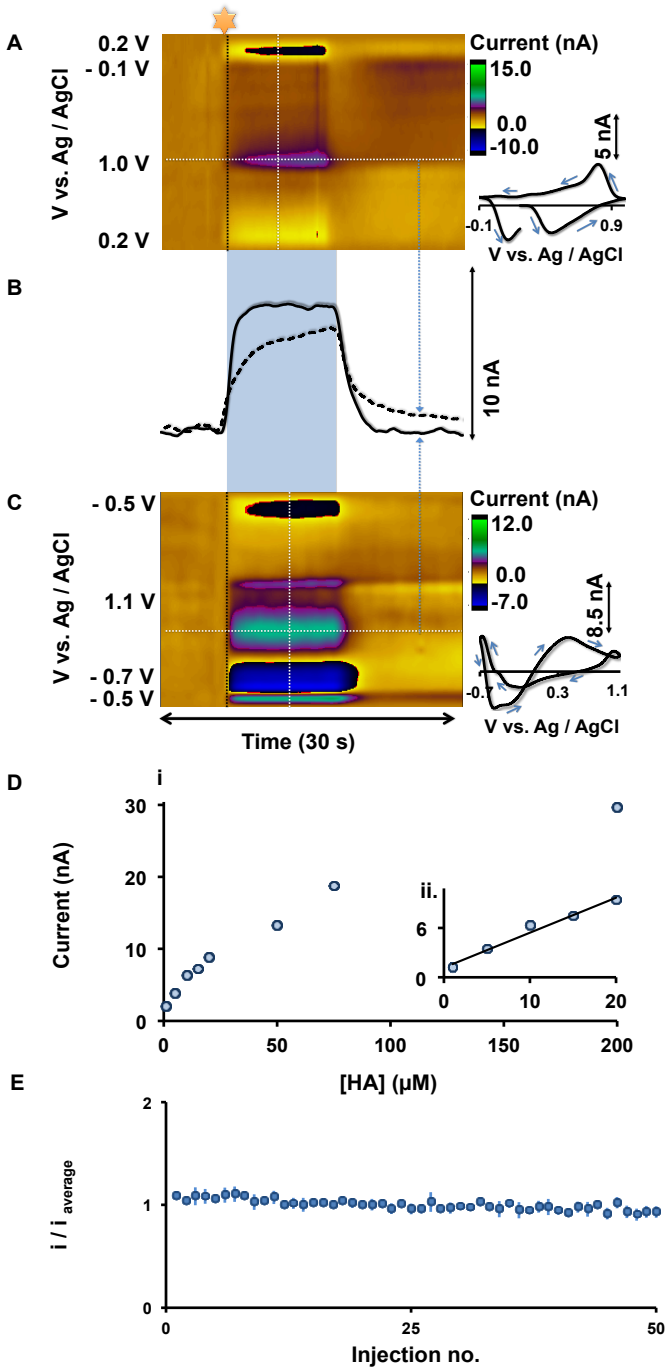

Figure 3.3. A & C show color plots for FIA of 20 μM histamine with the serotonin and HSW waveforms respectively. CVs extracted from vertical dashed lines are shown on the right. **B** shows Current vs. time traces from the horizontal dashed lines from color plots. **D** shows **(i)** Calibration curve, **(ii)** Linear dynamic range (n=4 ± SEM). **E** Stability of CFM over 50 consecutive injections of 10 μM histamine (n=4 ± SEM).

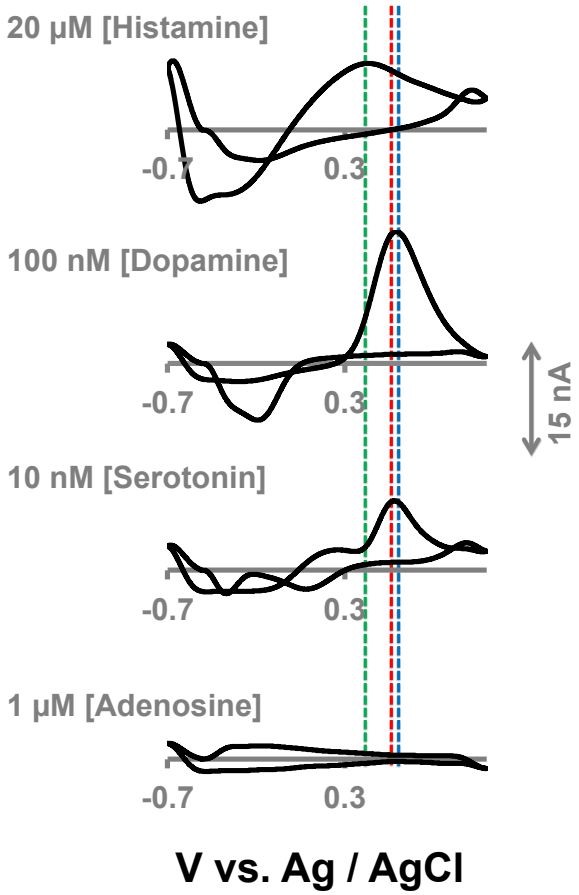

Figure 3.4. CVs for 20 µM histamine, 100 nM dopamine, 10 nM serotonin and 1 µM adenosine with *in vitro* FIA using HSW on CFMs. Vertical dashed lines indicate potential positions of peaks.

The HSW therefore shows good selectivity *in vitro*. However, the *in vivo* matrix is far more complicated than can be reproduced on the bench. We next assessed the ability of our novel waveform to measure histamine *in vivo*.

In Vivo Histamine

Histamine and serotonin were previously found to be co-released in the SNr upon electrical stimulation of the MFB[15]. We were interested in isolating a histamine signal in a novel physiological circuitry involving the histamine cell bodies. Histamine cell bodies are confined to the posterior hypothalamus, the tuberomamillary nucleus (PM), and send

their afferents to the forebrain via the MFB[29,30,31]. By utilizing a retrograde-stimulation[15] of the MFB, we reasoned that we would be able to detect histamine in the PM since histamine has previously been measured in this region with microdialysis[32].

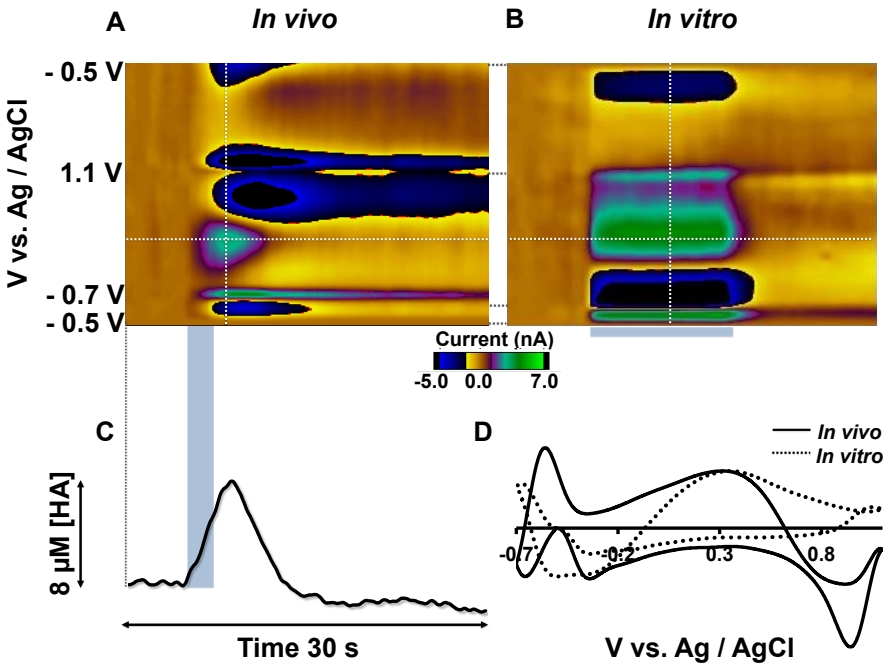

Figure 3.5. **A** shows a representative colors plot of in the PM upon MFB stimulation. **B** shows a representative *in vitro* color plot of histamine (20 µM) using FIA. **C** shows [histamine] vs. time extracted from the horizontal dashed line from color plot **A**. **D** shows normalized CVs of *in vivo* and *in vitro* (5 µM histamine) signals taken from vertical dashed lines.

Figure 3.5A shows a color plot in the mouse PM upon MFB stimulation (at 5-7 seconds indicated with the blue bar). An event at around 0.3 V vs. Ag/AgCl is clearly visible: a vertical dashed line through the maximum amplitude of this event (at 7 s) provides the CV in **Figure 3.5D**. When a CV collected for histamine *in vitro* (**Figure 3.5B**) was normalized and superimposed onto this *in vivo* CV, there was very good agreement between the oxidation peaks at 0.3 V. The additional features of the *in vivo* CV are due to the capacitative changes on the electrodes surface because of changes in the *in vivo* environment (ionic fluxes, pH changes). Where it not for the peak at 0.3V, it

would be impossible to disentangle histamine's electrochemistry from this other electrochemisty occurring at the switching potential.

Figure 3.5C shows how histamine changes with time, determined by extracting current vs. time from the horizontal dashed line of the color plot and the calibration curve in **Figure 3.3D**. Histamine levels elevate in response to electrical stimulation to around 8 μM and then clear after the stimulation, similar in magnitude to histamine release from mast cells[11]. This profile is similar to dopamine and serotonin reuptake[10,33]. This is an important finding since it implies a similar reuptake system for histamine, however a histamine transporter is yet to be identified[34].

Although the electrochemistry is supportive of histamine's identity. It is necessary to perform pharmacological experiments to validate the histamine response. Histamine neuropharmacology is not well explored in voltammetry models and there are very few histamine selective compounds that can cross the blood brain barrier. As a first step, we utilized tacrine, a pharmaceutical therapy for Alzheimer's disease. Tacrine is thought to primarily inhibit acetylcholinesterase, however it also is a potent inhibitor of histamine N-methyltransferase (HNMT) (histamine metabolizing enzyme)[35-37]. **Figure 3.6** shows the effect on the evoked PM signal (schematic of circuitry shown in **Figure 3.6A**) upon i.p. tacrine (2 mg kg^{-1})[38] administration (n=5 animals ± SEM). Consistent with tactrine's pharmacokinetic profile in rodents[39], there was a clear effect 50 minutes after administration, whereby the $t_{1/2}$ of histamine clearance increased significantly from 10.9 ± 1.1 s to 15.44 ± 2.6 s (p=0.01) (**Figure 3.6B**). This is an expected result of inhibition of histamine metabolism: because HNMT is located intracellularly[40,41], inhibition of this

enzyme raises cystolic histamine levels which slows down the reuptake equilibria back into the cell.

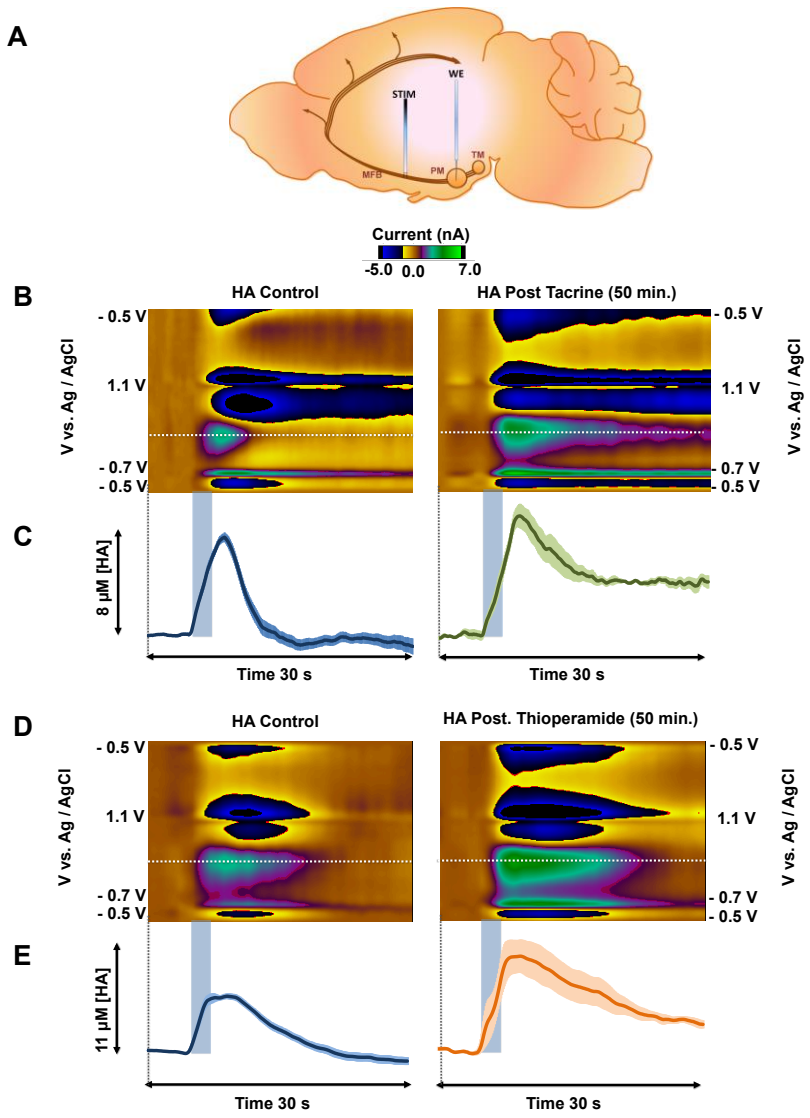

Figure 3.6. A shows the positions of electrodes (stimulation and CFM) in mouse brain. **B & D** show representative color plots of stimulated release of histamine using HSW - before and after tacrine (2 mg Kg^{-1}) and thioperamide (20 mg Kg^{-1}). **C & E** show concentration vs. time traces extracted from horizontal dashed line from **B & D** respectively, (n=5 ± SEM). The 2 s stimulation starting at 5 s is shown by the blue bar.

Because tacrine is non-selective, we performed a further pharmacological experiment to verify the PM signal. Thioperamide is a selective H3 receptor antagonist. We would expect thioperamide administration to affect the kinetics of histamine release and clearance via inhibition of these histamine autoreceptors in the PM[42]. **Figure 3.6C** and **D** show that 50 minutes after thioperamide (20 mg kg^{-1})[43], there was a pronounced increase in histamine release from 7.9 ± 2.1 to 11.8 ± 4.6 μM (p=0.02). Increases in evoked release have previously been seen with dopamine and autoreceptor antagonism[44,45]. A significant increase in the $t_{1/2}$ of histamine clearance was also observed from 13.3 ± 3.4 s to 18.8 ± 3.2 s (p=0.03), which was seen in prior studies with serotonin autoreceptor antagonism[10]. The time course of this experiment is also consistent with thioperamide's pharmacokinetics in rodents[46]. These pharmacological experiments, in addition to the electrochemical characterization allow us to confidently verify the histamine nature of this signal in the PM.

3.5 Conclusion

Histamine has important, but not well studied roles as a neurotransmitter. FSCV is an ideal tool for histamine detection because of its sensitivity, selectivity and high temporal resolution. Previous FSCV studies have not been able to selectively identify histamine because the CV features were due to capacitative processes on the electrode surface that are not selective. Here, we developed the HSW that provides a robust oxidation peak before the switching peak. We described *in vitro* waveform optimization and a novel *in vivo* physiological model for retrograde stimulation of histamine release in the mouse PM. We verified this signal

pharmacologically as histamine. This novel FSCV method will enable detailed *in vivo* characterizations of this important neuromodulator.

3.6 References

(1) Robinson, D. L.; Venton, B. J.; Heien, M. L.; Wightman, R. M. *Clinical chemistry* **2003**, *49*, 1763.

(2) Howe, M. W.; Tierney, P. L.; Sandberg, S. G.; Phillips, P. E.; Graybiel, A. M. *Nature* **2013**, *500*, 575.

(3) Ford, C. P.; Gantz, S. C.; Phillips, P. E.; Williams, J. T. *The Journal of neuroscience : the official journal of the Society for Neuroscience* **2010**, *30*, 6975.

(4) Hashemi, P.; Dankoski, E. C.; Petrovic, J.; Keithley, R. B.; Wightman, R. M. *Analytical Chemistry* **2009**, *81*, 9462.

(5) Park, J.; Kile, B. M.; Wightman, R. M. *Eur J Neurosci* **2009**, *30*, 2121.

(6) Wood, K. M.; Hashemi, P. *ACS Chem Neurosci* **2013**.

(7) Hashemi, P.; Dankoski, E. C.; Lama, R.; Wood, K. M.; Takmakov, P.; Wightman, R. M. *Proc Natl Acad Sci U S A* **2012**, *109*, 11510.

(8) Park, J.; Takmakov, P.; Wightman, R. M. *J Neurochem* **2011**, *119*, 932.

(9) Park, J.; Bucher, E. S.; Fontillas, K.; Owesson-White, C.; Ariansen, J. L.; Carelli, R. M.; Wightman, R. M. *Biol Psychiatry* **2013**.

(10) Wood, K. M.; Zeqja, A.; Nijhout, H. F.; Reed, M. C.; Best, J.; Hashemi, P. *J Neurochem* **2014**.

(11) Pihel, K.; Hsieh, S.; Jorgenson, J. W.; Wightman, R. M. *Anal Chem* **1995**, *67*, 4514.

(12) Pihel, K.; Hsieh, S.; Jorgenson, J. W.; Wightman, R. M. *Biochemistry* **1998**, *37*, 1046.

(13) Travis, E. R.; Wang, Y. M.; Michael, D. J.; Caron, M. G.; Wightman, R. M. *Proc Natl Acad Sci U S A* **2000**, *97*, 162.

(14) Chang, S. Y.; Jay, T.; Munoz, J.; Kim, I.; Lee, K. H. *Analyst* **2012**, *137*, 2158.

(15) Hashemi, P.; Dankoski, E. C.; Wood, K. M.; Ambrose, R. E.; Wightman, R. M. *J Neurochem* **2011**, *118*, 749.

(16) Bard, A.; Faulkner, L. *Electrochemical Methods: Fundamentals and Applications*; John Wiley & Sons, Inc, 2001.

(17) Pathirathna, P.; Samaranayake, S.; Atcherley, C. W.; Parent, K. L.; Heien, M. L.; McElmurry, S. P.; Hashemi, P. *Analyst* **2014**, *139*, 4673.

(18) Jackson, B. P.; Dietz, S. M.; Wightman, R. M. *Anal Chem* **1995**, *67*, 1115.

(19) Michael, D.; Travis, E. R.; Wightman, R. M. *Anal Chem* **1998**, *70*, 586A.

(20) Sanford, A. L.; Morton, S. W.; Whitehouse, K. L.; Oara, H. M.; Lugo-Morales, L. Z.; Roberts, J. G.; Sombers, L. A. *Analytical chemistry* **2010**, *82*, 5205.

(21) Glanowska, K. M.; Venton, B. J.; Moenter, S. M. *The Journal of neuroscience : the official journal of the Society for Neuroscience* **2012**, *32*, 14664.

(22) Pathirathna, P.; Yang, Y.; Forzley, K.; McElmurry, S. P.; Hashemi, P. *Anal Chem* **2012**, *84*, 6298.

(23) Torreggiani, A.; Tamba, M.; Bonora, S.; Fini, G. *Biopolymers* **2003**, *72*, 290.

(24) Xerri, B.; Flament, J.-P.; Petitjean, H.; Berthomieu, C.; Berthomieu, D. *The Journal of Physical Chemistry B* **2009**, *113*, 15119.

(25) RICHELSON, E. *Journal of clinical psychopharmacology* **1996**, *16*, 1S.

(26) Heien, M. L. A. V.; Khan, A. S.; Ariansen, J. L.; Cheer, J. F.; Phillips, P. E. M.; Wassum, K. M.; Wightman, R. M. *Proceedings of the National Academy of Sciences of the United States of America* **2005**, *102*, 10023.

(27) van Dijk, A.; Klompmakers, A. A.; Feenstra, M. G. P.; Denys, D. *Journal of Neurochemistry* **2012**, *123*, 897.

(28) Swamy, B. E.; Venton, B. J. *Anal Chem* **2007**, *79*, 744.

(29) *Histamine in the Nervous System*, 2008; Vol. 88.

(30) Vanhala, A.; Yamatodani, A.; Panula, P. *The Journal of comparative neurology* **1994**, *347*, 101.

(31) Auvinen, S.; Panula, P. *The Journal of comparative neurology* **1988**, *276*, 289.

(32) Russell, W. L.; Henry, D. P.; Phebus, L. A.; Clemens, J. A. *Brain Res* **1990**, *512*, 95.

(33) Wu, Q.; Reith, M. E. A.; Wightman, R. M.; Kawagoe, K. T.; Garris, P. A. *Journal of Neuroscience Methods* **2001**, *112*, 119.

(34) Hough, L. B. *Progress in neurobiology* **1988**, *30*, 469.

(35) Morisset, S.; Traiffort, E.; Schwartz, J. C. *Eur J Pharmacol* **1996**, *315*, R1.

(36) Musial, A.; Bajda, M.; Malawska, B. *Curr Med Chem* **2007**, *14*, 2654.

(37) Taraschenko, O. D.; Barnes, W. G.; Herrick-Davis, K.; Yokoyama, Y.; Boyd, D. L.; Hough, L. B. *Methods Find Exp Clin Pharmacol* **2005**, *27*, 161.

(38) Nishibori, M.; Oishi, R.; Itoh, Y.; Saeki, K. *Japanese journal of pharmacology* **1991**, *55*, 539.

(39) Telting-Diaz, M.; Lunte, C. E. *Pharmaceutical research* **1993**, *10*, 44.

(40) Maintz, L.; Novak, N. *Am J Clin Nutr* **2007**, *85*, 1185.

(41) Pollard, H.; Bischoff, S.; Schwartz, J. C. *J Pharmacol Exp Ther* **1974**, *190*, 88.

(42) Brown, R. E.; Stevens, D. R.; Haas, H. L. *Progress in neurobiology* **2001**, *63*, 637.

(43) Bernaerts, P.; Lamberty, Y.; Tirelli, E. *Behavioural Brain Research* **2004**, *154*, 211.

(44) Kita, J. M.; Parker, L. E.; Phillips, P. E.; Garris, P. A.; Wightman, R. M. *J Neurochem* **2007**, *102*, 1115.

(45) Clark, D.; Exner, M.; Furmidge, L. J.; Svensson, K.; Sonesson, C. *European journal of pharmacology* **1995**, *275*, 67.

(46) Bordi, F.; Mor, M.; Plazzi, P. V.; Silva, C.; Caretta, A.; Morini, G. *Farmaco (Societa chimica italiana : 1989)* **1992**, *47*, 1095.

CHAPTER 4

A VOLTAMMETRIC AND MATHEMATICAL ANALYSIS OF HISTAMINERGIC MODULATION OF SEROTONIN IN THE MOUSE HYPOTHALAMUS

Reprinted with permission from Journal of Neurochemistry and John Wiley and Sons.

Samaranayake S, Abdalla A, Robke R, Nijhout HF, Reed MC, Best J, Hashemi P (2016) A voltammetric and mathematical analysis of histaminergic modulation of serotonin in the mouse hypothalamus. *J Neurochem* 138:374-383.

4.1 Abstract

Histamine and serotonin are neuromodulators which facilitate numerous, diverse neurological functions. Being co-localized in many brain regions, these two neurotransmitters are thought to modulate one another's chemistry and are often implicated in the etiology of disease. Thus, it is desirable to interpret the *in vivo* chemistry underlying neurotransmission of these two molecules to better define their roles in health and disease. In this work, we describe a voltammetric approach to monitoring serotonin and histamine simultaneously in real time. Via electrical stimulation of the axonal bundles in the medial forebrain bundle, histamine was evoked in the mouse premammillary nucleus. We found that histamine release was accompanied by a rapid, potent inhibition of serotonin in a concentration dependent manner. We developed mathematical models to capture the experimental time courses of histamine and serotonin, which necessitated incorporation of an inhibitory receptor on serotonin neurons. We employed pharmacological experiments to verify that this serotonin inhibition was mediated by H_3 receptors. Our novel approach provides fundamental mechanistic insights that can be used to examine the full extent of interconnectivity between histamine and serotonin in brain.

4.2 Introduction

Serotonin and histamine are neuromodulators thought to carry a variety of roles in the brain [1-3]. These two modulators are co-localized in many brain regions [4,5] and are postulated to closely modulate one another [6,7]. However, while there is much focus on serotonin's roles in affective, sleep and cognition processes [8,9], histamine's contribution

to the same processes remains relatively neglected. In recent years, we established fast scan cyclic voltammetry (FSCV) at carbon fiber microelectrodes (CFMs) to investigate *in vivo* serotonin dynamics [10]. We are systematically studying the array of *in vivo* processes that regulate serotonin extracellular levels [11,12] with the ultimate goal of identifying distinct mechanistic abnormalities that underlie different pathophysiological states. Because of histamine's close association with serotonin, in particular the electrophysiological, histological and slice voltammetry studies that imply histamine inhibits serotonin release [6,13-15] we now find it of great importance to direct our efforts to voltammetrically defining histamine and serotonin co-modulation *in vivo*.

In this paper, we extend on recent work where we described the first voltammetrically selective waveform for real time FSCV histamine measurements *in vivo* in the mouse [16], to detail simultaneous *in vivo* measurements of serotonin and histamine. To achieve this, CFMs were implanted in the mouse premammillary nucleus (PM), a hypothalamic region rich in serotonin and histamine [4,5,17]. To assess the effects of histamine release on endogenous serotonin chemistry, we identified a discrete location in the medial forebrain bundle (MFB) that, when electrically stimulated, evoked histamine but not serotonin in the PM. This robust experimental model allowed us to observe histamine release rapidly followed by potent, long lasting serotonin inhibition. We found that both histamine release and serotonin inhibition were dependent on stimulation parameters in a manner that indicated an inversely correlative relationship. We mathematically modeled both responses and found that an inhibitory receptor term was necessary to fit both sets of data. We postulated that this inhibitory receptor was the H_3

receptor and provided pharmacological evidence, in the form of manipulations with thioperamide, an H_3 receptor antagonist, in favor of our hypothesis.

We thus provide not only an important technological advance, but our physiological findings also represent an opportunity to more closely scrutinize histamine's roles in controlling serotonin chemistry in the context of disease.

4.3 Materials and Methods

4.3.1 Chemicals and Reagents

Standard solutions were prepared by dissolving histamine dihydrochloride and serotonin hydrochloride (Sigma-Aldrich, Co., MO, USA) respectively in Tris-buffer. Tris-buffer was constituted thus: 15 mM $H_2NC(CH_2OH)_2$.HCl, 140 mM NaCl, 3.25 mM KCl, 1.2 mM $CaCl_2$, 1.25 mM $NaH_2PO_4.H_2O$, 1.2 mM $MgCl_2$ and 2.0 mM Na_2SO_4 (EMD Chemicals Inc. NJ, USA) in deinoized water at pH=7.4 Thioperamide maleate (2, 20, or 200 mg kg^{-1}) from TOCRIS bioscience (Bristol, UK) was dissolved in sterile saline and administered via intra-peritoneal injection at a volume of 0.6 ml kg^{-1}.

4.3.2 Carbon-Fiber Microelectrodes (CFMs)

CFMs were fabricated employing 7µm diameter carbon-fibers (Goodfellow Corporation, PA, USA) aspirated into glass capillaries (0.6 mm external diameter, 0.4 mm internal diameter, A-M systems, Inc., Sequim, WA). A carbon-glass seal was formed using vertical micropipette puller (Narishige Group, Tokyo, Japan). The exposed length of the carbon fiber was trimmed to 150 µm under an optical microscope. Microelectrodes were electroplated with Nafion as described previously [10].

4.3.3 Data Collection

Waveform generation, data acquisition and signal processing were achieved by a commercial potentiostat (Dagan corp.), custom-built hardware, software written in house using LabVIEW 2009 and interfacing a PCIe-6341 DAC/ADC card (National Instruments, Austin, TX). Custom built software was employed to drive the hardware and perform data analysis including background subtraction, signal averaging and digital filtering (Knowmad Technologies LLC, Tucson, AZ). All potentials are quoted with respect to Ag/AgCl reference electrodes, which were fabricated via electrodeposition of Cl^- by holding a silver wire (A-M systems, WA) at 4.0 V for 5 s in 1 M HCl. All data represented with error bars represent the standard error of the mean (SEM).

4.3.4 Data Analysis

All the Current vs time data were extracted from custom made software. Histamine current was transferred to its concentration using 2.825 µM/nA factor. Conversion factor for serotonin was 11 nM/nA. Statistical differences were obtained using one-tailed Student's *t*-tests on paired data sets. ($p < 0.05$ was taken as significantly different)

4.3.5 Data Modeling

Simulations were carried out in MatLab R2014a (MathWorks, Natick, MA, USA) using ODE solver ode23s, implemented on an iMAC with operating system OS X Version 10.6.8. We modeled our experimental data with two differential equations:

$$\frac{d[eha]}{dt} = A_{H3}(t)\, fire_{ha}(t)[vha] - V_u([eha]) + a_1[cha] - V_{ug}([eha]) - a_2[gha] \text{ --------- (1)}$$

The left hand side is the rate of change of the extracellular histamine [eha]. The first term on the right side multiplies the fractional release, $A_{H3}(t)$, caused by autoreceptor inhibition by the firing rate, $fire_{ha}(t)$, and the vesicular histamine concentration, [vha]. The remaining terms are reuptake into the terminal, $V_u([eha])$, leakage from the terminal, $a_1[cha]$, uptake into glial cells, $V_{ug}([eha])$, and leakage from the glial cells, $a_2[gha]$. There is a similar differential equation for serotonin in the extracellular space:

$$\frac{d[e5ht]}{dt} = A_{H3}^{5ht}(t)\, fire_{5ht}(t)[v5ht] - V_{sert}([e5ht]) + a_3[c5ht] - V_{ug}([e5ht]) - a_4[g5ht] \text{------(2)}$$

The term A_{H3}^{5ht} is the time course of fractional serotonin release caused by the H_3 receptors on serotonin neurons. All other terms in equation 2 are analogous to the terms in equation 1.

4.3.6 Flow Injection Analysis

Flow injection analysis *(FIA)* was used for *in vitro* analyses. CFMs were inserted into a flangeless short 1/8 nut (PEEK P-335, IDEX, Middleboro, MA) in order for 2 mm of the tip to be exposed outside of the nut. The microelectrode-containing nut was then fastened into a modified HPLC union elbow (PEEK 3432, IDEX, Middleboro, MA). The other end of the elbow union was fastened into the out-flowing stream of the FIA buffer and incorporation of the reference electrode and for a 'waste' flow stream by drilling into the union. *In vitro* experiments were carried out at 2 mL min^{-1} flow rate using syringe infusion pump (kd Scientific, model KDS-410, Holliston, MA). Starting at 5s, a rectangular pulse of analyte was introduced into the buffer stream for 10 s via a six-port HPLC loop injector (Rheodyne model 7010 valve, VICI, Houston, TX). In order to avoid carry-over effects, analytes were injected randomly.

4.3.7 Animal Surgeries

Handling and surgery on male C57BL/6J mice weighing 20−25 g (Jackson Laboratory, Bar Harbor, ME) were in agreement with University of South Carolina Guide for the Care and Use of Laboratory Animals, approved by the Institutional Animal Care and Use. Urethane (25% dissolved in 0.9% NaCl solution, Hospira, Lake Forest, IL) was injected intraperitoneally (i.p) and once deep anesthesia was confirmed, animals were secured into a stereotaxic instrument (David Kopf Instruments, Tujunga, CA) and stereotaxic surgery was performed. A heating pad sustained mouse body temperature around 37 °C (Braintree Scientific, Braintree, MA). Stereotaxic coordinates were taken in reference to bregma. A Nafion modified CFM was in the PM (AP: −2.45, ML: +0.50, DV: −5.45 to −5.55.). A stainless steel stimulating electrode (diameter: 0.2 mm, Plastics One, Roanoke, VA) was positioned into the MFB (AP: -1.07, ML: +1.10, DV: −5.00). Biphasic pulse trains applied through a linear constant current stimulus isolator (NL800A, Neurolog, Medical Systems Corp., Great Neck, NY) provoked histamine efflux. The 60 Hz trains were 350 μA each phase, 2 ms in width, and 2 s in length. To determine the effects of different stimulation parameters on histamine and serotonin, stimulation frequency, width and amplitude were systematically altered. The time in between stimulations (2 minutes) was determined sufficient to produce negligible effects on serotonin and histamine in subsequent stimulations. A Ag/AgCl reference electrode (constructed by plating Cl^- ions onto a Ag wire) was implanted into the brain's opposite hemisphere.

4.4 Results

4.4.1 Simultaneous Measurements of Serotonin and Histamine

In this experiment, we implanted a CFM in the PM of an anesthetized mouse and electrically stimulated the MFB. A representation of this experimental model, illustrating the relative positions of the working and stimulations electrodes can be found in **Figure 4.1Ai**. Directly underneath this, in **Figure 4.1Bi,** is a raw data color plot showing the resultant electrochemical signal at the CFM. The interpretation of color plots is described elsewhere in detail [18]. Concisely, background subtracted cyclic voltammograms collected at 10 Hz for 30 seconds are displayed as voltage (y-axis) vs. time (x-axis) and current (false color). The green bar directly under the color plot denotes the occurrence and duration of the electrical stimulation. Upon stimulation there are several events, typical of *in vivo* FSCV measurements whereby other electroactive species, pH changes and ionic fluxes affect the measurement [19,20]. Of interest is the discrete event occurring at 0.3 V which is denoted by the horizontal dashed line and the blue star. A cyclic voltammogram (CV) extracted from the vertical dashed line through this event is displayed in **Figure 4.1Ci** (solid line). The oxidation peak at 0.3 V shows excellent agreement with the oxidation peak extracted from an *in vitro* injection of histamine (dashed) normalized to maximum current and superimposed onto this *in vivo* CV. In our prior work, we showed electrochemically and pharmacologically that this event is histamine release [16]. Histamine's electro-oxidation scheme has not yet been described. It is likely that the peak at 0.3V occurs because of a proton transfer type oxidation between the aliphatic amine group and imidazole amine group in the histamine molecule. Because this is an internal

proton transfer oxidation, it follows that it should occur at a potential lower than observed for classic serotonin and dopamine electrooxidation (i.e. 0.6 - 0.8 V) [21].

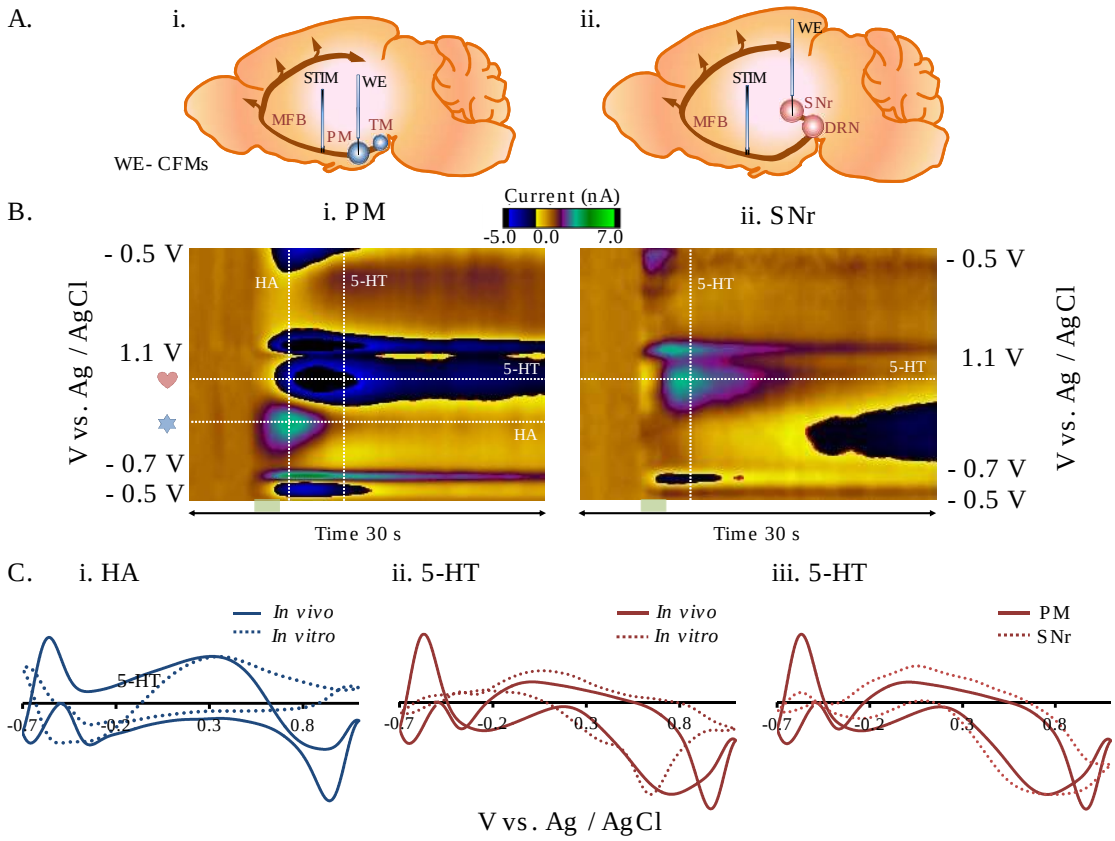

Figure 4.1. (Ai & Aii) The position of electrodes (stimulation and CFM) in mouse brain. (Bi & Bii) Representative color plots of the stimulated release of histamine and serotonin in the premammillary nucleus (PM) and stimulated release of serotonin in the substantia nigra (SNr) respectively. (Ci & ii) Superimposed cyclic voltammograms of *in vivo* and *in vitro* histamine and serotonin signals taken from vertical dashed lines in the PM. (Ciii) Comparison of normalized CVs of *in vivo* serotonin signals taken from vertical dashed lines in both PM and SNr. HA= histamine, 5-HT = serotonin.

An additional event of interest occurs at around 0.7 V and is denoted by the horizontal dashed line and red heart. Because FSCV is background subtracted, ambient levels cannot be determined, thus according to the false color scale, this event signals a decrease in concentration. A CV collected at the vertical dashed line through this event is

presented in **Figure 4.1Cii**. A CV taken from an *in vitro* injection of serotonin was inverted on the current axis (to mimic a decrease in concentration), normalized to maximum current and superimposed (dashed) onto the *in vivo* CV. The good agreement between the peaks at 0.7 V strongly implies that this event is caused by serotonin. To further confirm this notion, we made a measurement of serotonin with this waveform via an experimental model of MFB stimulation and measurement in the substantia nigra pars reticulata (SNr) that we have well established for serotonin FSCV [22]. This experimental model is depicted in **Figure 4.1Aii** and the color plot arising from the *in vivo* experiment is shown in **Figure 4.1Bii.** The stimulated serotonin event occurs at the same horizontal (potential) position on the color plot. The CV extracted from this color plot, inverted, normalized to maximum current and superimposed to the *in vivo* CV collected in the PM shows in excellent agreement in **Figure 4.1Ciii**.

4.4.2 Serotonin Inhibition Following Histamine Release

The event immediately following histamine release proceeds in the negative false color current direction. FSCV cannot determine basal concentrations (*vide supra*) thus one can only determine changes from ambient levels. This result, therefore, is indicative of a reduction in the ambient concentration of serotonin after stimulation. **Figure 4.2A** is a representative color plot showing simultaneous histamine release and serotonin inhibition in the PM upon MFB stimulation. **Figure 4.2C-E** shows serotonin and histamine concentrations with time for different stimulation parameters (dark solid lines = maximum responses and lighter dashed lines = lower responses) extracted from the horizontal dashed lines from the color plot (n=5 animals). The decrease in serotonin concentration is delayed around 2 seconds with respect to histamine release, implying

that serotonin inhibition may be dependent on histamine release. To probe this notion, we systematically altered stimulation parameters to assess whether the profile of histamine release affects serotonin inhibition. The dark solid line shows the maximum responses for the 60 Hz stimulation frequency in **Figure 4.2C**.

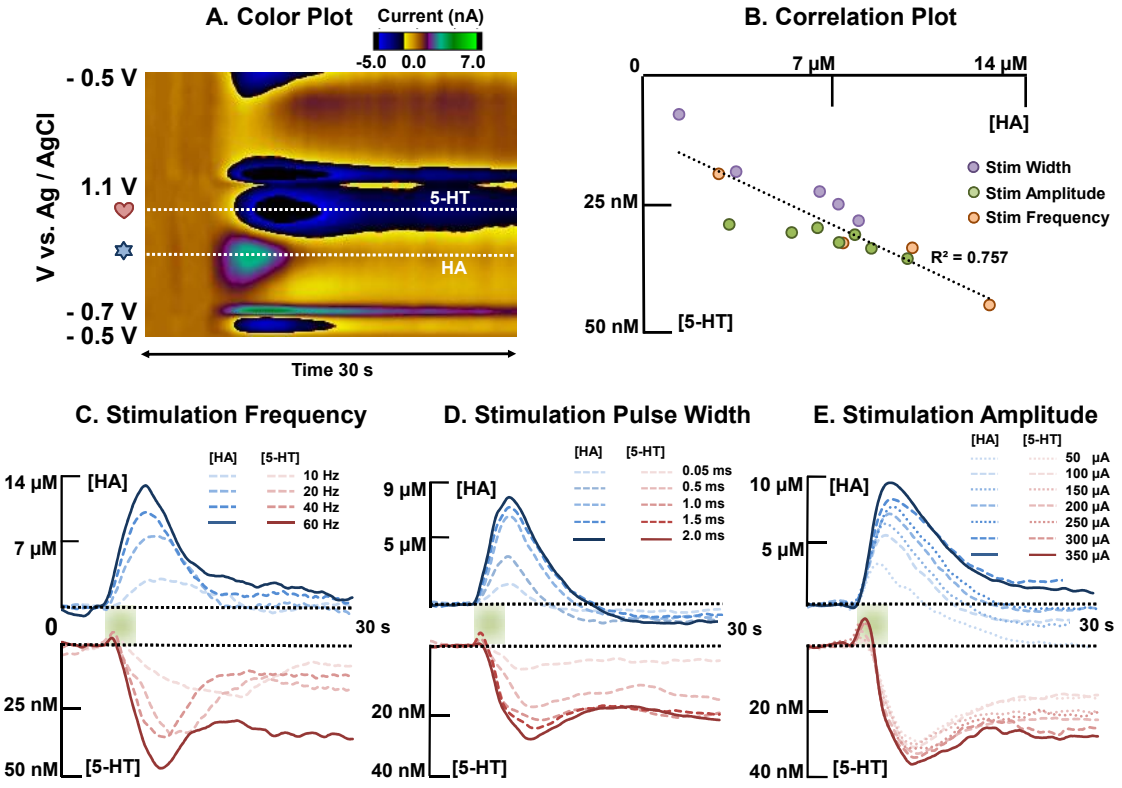

Figure 4.2. (A) Representative color plot of the stimulated release of histamine and serotonin inhibition in the PM. (B) Correlation plot between [histamine] and [serotonin] for all stimulation parameters. (C) Averaged current vs. time traces along the two horizontal dashed lines of histamine and serotonin with respect to different stimulation frequencies (n=5). (D) Averaged current responses to various stimulation pulse widths of histamine and serotonin (n=5). I Averaged current responses to various stimulation amplitudes of histamine and serotonin (n=5). [HA] = [histamine], [5-HT] = [serotonin].

The lighter colored dashed lines in **Figure 4.2C** shows the result of altering the stimulation frequency from 10 - 40 Hz (n=5 animals). There is a clear correlation between histamine release and the serotonin inhibition profiles. This is apparent in terms

of both time course (i.e. 10 Hz stimulation leading to lower, more prolonged histamine release and subsequent serotonin inhibition) and amplitude (higher level of histamine release corresponds to higher level of serotonin inhibition). This pattern holds true for stimulation pulse width and amplitude (**Figure 4.2D and E**) (n=5 animals). In **Figure 4.2B**, the relationship between histamine release and serotonin inhibition was more formally explored by directly plotting amplitude of histamine release vs. amplitude of serotonin inhibition for the three stimulation parameters explored. We found a linear relationship ($R^2 = 0.757$) connecting histamine release to serotonin inhibition for all three parameters explored.

4.4.3 Mathematical Modeling of Serotonin and Histamine Co-regulation

We needed to vary only three functions, $\mathrm{fire_{ha}}(t)$, $A_{H3}(t)$, and $A_{H3}^{5ht}(t)$, from equations 1 and 2 to obtain excellent model fits to our experimental data. **Figures 4.3A** and **B** show the model fits (dotted lines) to the experimental curves (solid lines) for control and 20 mg kg^{-1} thioperamide, respectively. Thioperamide selectively acts as an H_3 receptor (auto and hetero) antagonist on both histamine and serotonin pre synaptic neurons [23]. In our model, the electrical stimulation is mimicked by raising $\mathrm{fire_{ha}}(t)$ above its tonic level of 5 spikes/sec. **Figure 4.3C** shows $\mathrm{fire_{ha}}(t)$ vs. time that best fits the control and thioperamide experiments. $\mathrm{fire_{ha}}(t)$ returns to baseline at 9 seconds and the rates are higher after thioperamide.

To fit the slow decline in histamine after stimulation, it was necessary to incorporate an autoreceptor function as per our previous serotonin model [12] **Figure 4.3D** shows fractional histamine release, $A_{H3}(t)$, as a function of H_3 autoreceptors activation following stimulation before and after thioperamide. In the control experiment, tonic

inhibition was $A_{H3}(t)$= 0.7 up to 9 seconds, then dropped to $A_{H3}(t)$= 0 up to 15 seconds (complete inhibition), and then returned to $A_{H3}(t)$= 0.4 from 15 seconds to 30 seconds. For thioperamide, $A_{H3}(t)$= 0.9, and the smallest fractional release is $A_{H3}(t)$ = 0.5. Our model shows that the H_3 autoreceptor effect is delayed (starting at 9 seconds) and lasts throughout our file collection window (30 seconds).

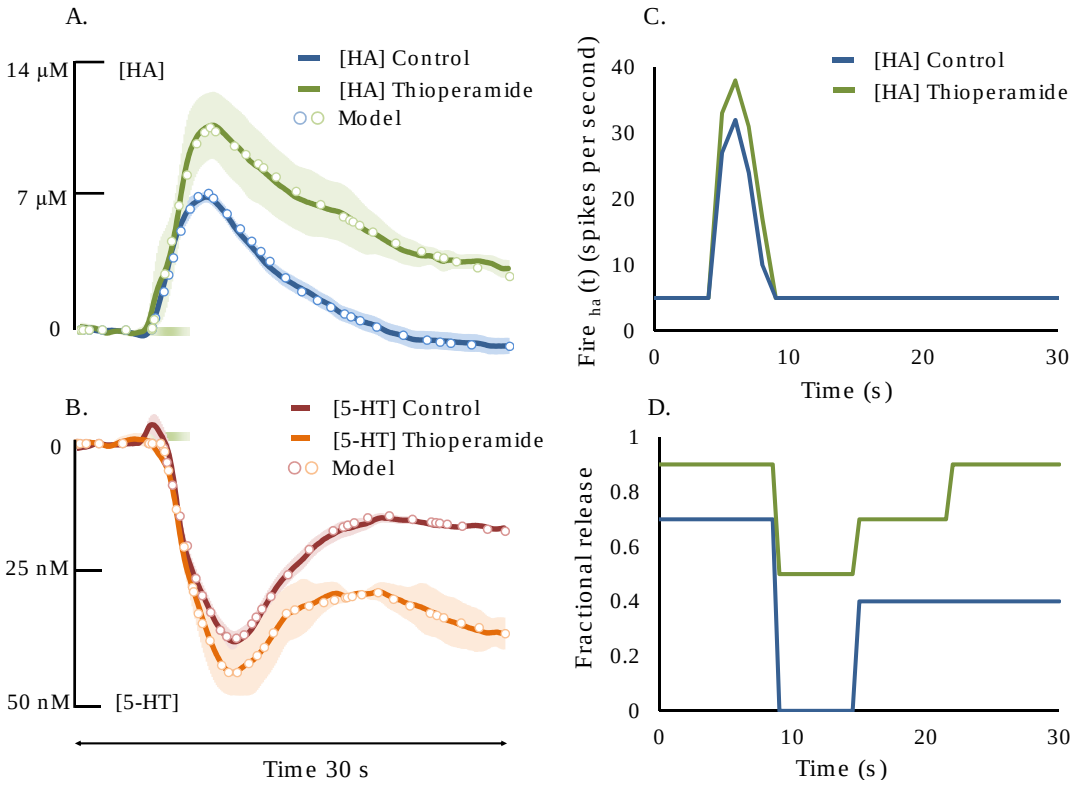

Figure 4.3. (A) [Histamine] vs. time plots comparing *in vivo* (solid traces) and the results of the mathematical model (large dots) in the control case. (B) [Serotonin] vs. time plots comparing *in vivo* (solid traces) and the results of the mathematical model (large dots) in the presence of thioperimide (20 mg kg^{-1}) (C) Firing rate of the histamine neurons as a function of time in the two cases control (blue) and drug (green), respectively. (D) Assumed fractional release of histamine from the histamine neurons as a function of time in the two cases. [HA] = [histamine], [5-HT] = [serotonin].

We next modeled our serotonin curves. Since the serotonin neurons are not stimulated, $\text{fire}_{5\text{ht}}(t)$ remains at a tonic level of 5 spikes/sec. We varied $A_{H3}^{5\text{ht}}(t)$ (fraction of serotonin release permitted by the H_3 receptors on serotonin neurons). For the control experiment, $A_{H3}^{5\text{ht}}(t)$ starts at 0.9, goes down to 0.45, and then returns to 0.9. For thioperamide, $A_{H3}^{5\text{ht}}(t)$ starts at 0.9, goes down to 0.36, and then returns to 0.8 at 30 seconds (graphs not shown). As above, the H_3 receptor effect is prolonged throughout file collection (> 60 seconds).

4.4.4 H_3 Receptor Mediated Inhibition of Serotonin

Three different doses of thioperamide, an H_3 receptor antagonist [23], were administered to different groups of mice. This agent's effects on histamine release and serotonin inhibition was observed 50 minutes after administration, which is a sufficient time period for thioperamide to exert its effects [24,25]. The results are shown in **Figure 4.4**. Here, histamine before drug is displayed in blue and after drug in green, serotonin before drug is red, and after drug is orange. Error bars showing SEM (n=5 ± SEM) are lighter versions of these respective colors.

Thioperamide, administered at 2 mg kg^{-1} caused a significant increase in the amplitude of histamine release from 7.5 ± 1.4 µM to 11.5 ± 1.4 µM (p = 0.004), but not in rate of histamine clearance ($t_{1/2}$ from 11.5 ± 1.5 s to 14.3 ± 2.4 s, p = 0.07). The effects of 2 mg kg^{-1} on the amplitude and time course of serotonin inhibition were negligible. Maximum serotonin inhibition changed from 34.2 ± 7.5 nM to 37.5 ± 11.9 nM (p = 0.55), whereas, inhibition at 30 s enhanced from 15.8 ± 1.5 nM to 22.1 ± 8.9 nM (p = 0.31).

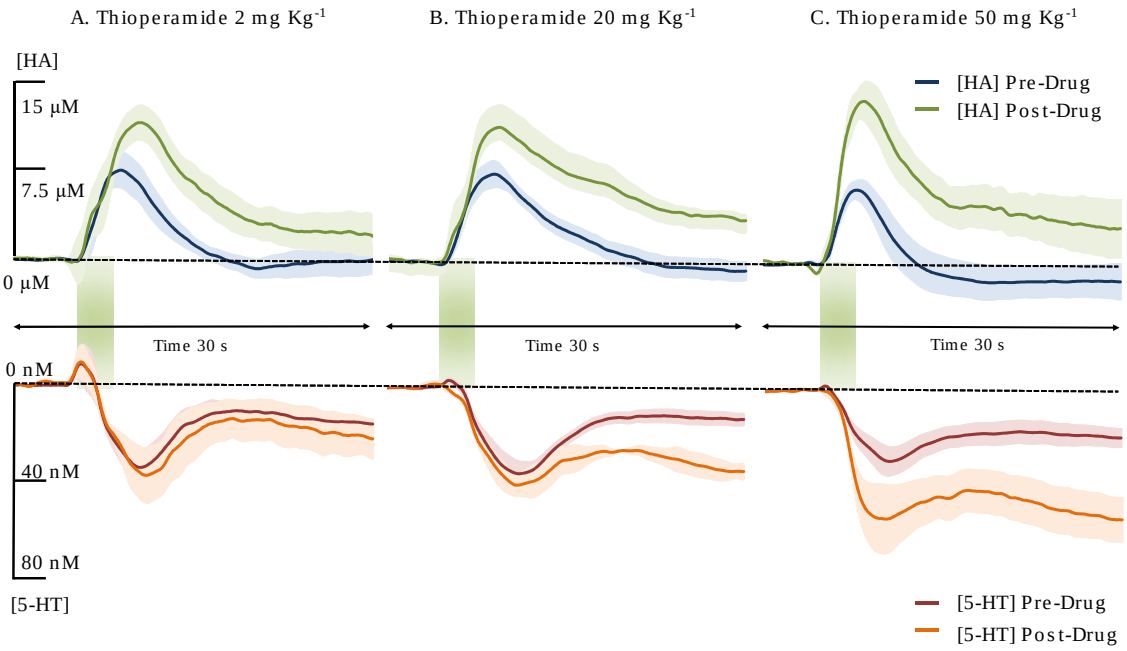

Figure 4.4. [Histamine] vs time traces are shown in blue and green for pre and post drug administration respectively. [Serotonin] vs time traces are shown in red and orange for before and after the drug. Error bars showing SEM (n=5 ± SEM) are lighter versions of these respective colors. (A) thioperamide 2 $mgKg^{-1}$ (B) thioperamide 20 $mgKg^{-1}$ (C) thioperamide 50 $mgKg^{-1}$. [HA] = [histamine], [5-HT] = [serotonin].

Thioperamide administered at 20 mg kg^{-1} dose affected both the amplitude and clearance time of histamine response. Histamine elevated from 7.9 ± 2.1 µM to 11.9 ± 4.2 µM (p = 0.03) and $t_{1/2}$ from 14.7 ± 2.8 s to 19.6 ± 2.3 s (p = 0.02), but only the time course of the serotonin response (maximum inhibition from 38.8 ± 5.01 nM to 44.8 ± 4.5 nM (p = 0.31). Furthermore, serotonin inhibition at 30 s increases from 16.5 ± 5.3 nM to 37.7 ± 9.6 nM, (p = 0.002). At the highest dose, thioperamide greatly affected histamine release from 6.8 ± 1.9 µM to 14.3 ± 4.1 µM (p = 0.006) and reuptake such that histamine does not return to baseline during the 30 second file acquisition window. The effects on serotonin are also highly significant. Maximum inhibition elevated from 37.3 ± 9.6 nM to

68.2 ± 20.0 nM (p = 0.04), whereas, inhibition at 30 s enhanced from 24.4 ± 7.9 nM to 65.9 ± 14.8 nM (p = 0.03).

4.5 Discussion

4.5.1 FSCV: A Powerful Tool for Simultaneous, Real-time Serotonin and Histamine Measurements

FSCV at CFMs is a powerful tool for neurotransmitter analysis because of FSCV's rapid, sensitive and selective analysis capabilities in addition to the minimally invasive dimensions of CFMs. A traditional drawback of FSCV is its limited *in vivo* analytical scope (measuring primarily dopamine) [26-28], which has been systematically challenged in recent years via advances to measure serotonin [10], adenosine [29], H_2O_2 [30] and gonadotropin-releasing hormone [31]. We are primarily interested in deciphering the *in vivo* dynamics that regulate extracellular serotonin levels, and we were thus oriented towards histamine. There is a significant body of literature that suggests histamine inversely modulates serotonin in the brain [6,15]. Many of these studies propose that dysregulations in histamine underlie disorders that are primarily considered to be serotonin mediated (e.g. depression) [32-34]. In 2011 we described simultaneous histamine and serotonin measurements in the rat SNr [22]. However, the FSCV peaks utilized to quantify histamine occurred at the anodic switching potential. These so called 'switching peaks' occur when spontaneous adsorption of analytes changes the electrical bilayer, hence capacitative current on the CFM. While switching peaks can be used to quantify histamine in a well-controlled environment (i.e. *in vitro* or tissue slice preparations), they cannot be used *in*

vivo because other analytes that adsorb to the CFM provide identical, indistinguishable CVs [16].

In 2015 we addressed the issue of selective *in vivo* histamine analysis by developing a detection waveform that displayed a distinct Faradaic-like peak corresponding to histamine oxidation. We successfully applied this waveform *in vivo* to selectively quantify histamine [16]. In this study, we show that this novel waveform can simultaneously and selectively measure not only histamine, but also serotonin (*vide infra*), which greatly aids our interests in establishing how histamine modulates serotonin chemistry.

4.5.2 MFB Stimulation Rapidly, Potently Inhibits Ambient Serotonin in the PM

Figure 4.1 shows histamine release upon MFB stimulation in a hypothalamic region, the PM. We and others previously established this stimulation and measurement model to be robust and successful in evoking histamine [35,36] since the PM is home to a dense population of histamine cell bodies [36] and the region of the MFB that we stimulate contains histamine axons [37,38]. The PM region also contains serotonin terminals [5,17], therefore we postulated that the PM seemed a promising area to study histamine/serotonin modulation, particularly because our data imply that the electrical stimulation does not evoke serotonin. This finding is supported by the presence of fewer serotonin axons in the anterior area of the MFB (our stimulation location) [39,40]. Importantly, this model allows us to investigate histamine's effects on serotonin chemistry in the absence of stimulated serotonin release. This type of measurement can be greatly facilitated in the future with the development of optogenetic tools that selectively target histamine.

In accord with our postulation, in **Figure 4.1**, an event following the evoked histamine event by around 2 seconds is apparent. Via comparison of CVs collected *in vitro* and *in vivo* in the SNr (an area we have well established for serotonin FSCV) [21,41], we can electrochemically verify this second event to be caused by serotonin. The small deviation in the peak positions in **Figure 4.1cii** is typical when comparing *in vivo* and *in vitro* responses and is likely due to differences in ohmic drop between *in vitro* and *in vivo* preparations. Of great interest, our data indicate that the serotonin levels are *decreasing* in response to the stimulation. Because FSCV is a background subtracted method, ambient levels cannot be established therefore the conclusion of this data is that MFB stimulation inhibits ambient serotonin activity by around 40 nM. FSCV most commonly observes increased neurotransmitter activity, thus our experiment represents an exciting opportunity to study inhibition of ambient activity.

We next hypothesize that this inhibition is, at least partially, mediated by histamine based on prior histamine/serotonin modulation studies [6,15]. In the next sections we take experimental, mathematical and pharmacological approaches towards this hypothesis.

4.5.3 Histamine Mediates Serotonin Inhibition in the PM

i) Serotonin Inhibition is Concentration and Time Correlated to Histamine Release

To show that histamine, rather than another result of MFB stimulation inhibits serotonin in the PM, we systematically altered our stimulation parameters to change the profile of histamine release. **Figure 4.2** shows excellent agreement between the time course and amplitude of histamine release and serotonin inhibition. The raw data in **Figures 4.2 C,D and E** show that the profile of serotonin inhibition closely tracks

histamine release, and the **Figure 4.2B** highlights this correlation more formally by plotting maximum histamine release amplitude vs. maximum serotonin inhibition amplitude. The linear relationship between histamine and serotonin with all stimulation parameters is strong evidence for chemical rapport between these two molecules in the PM.

ii) Mathematical Modeling of Serotonin Inhibition Necessitates an Autoreceptor Function.

The power of interpreting experimental data through mathematical models is the ability to test a number of physiological hypotheses. Above, we hypothesized that serotonin inhibition is histamine mediated, we now test this notion mathematically. Our model necessitates ambient (basal) histamine and serotonin levels which we are not yet able to determine with FSCV. For histamine, a value of 1.5 μM was chosen, because our data show that after stimulation histamine levels fall 1 μM or more below baseline (**Figures 4.2, 3, 4**). Similarly, for the same reason we chose 65 nM as the basal concentration of serotonin in the extracellular space. We found that we could fit the data closely via simple manipulations of H_3 heteroreceptor and autoreceptor strengths in our model. H_3 heteroreceptors on serotonin terminals [15,42] have previously been postulated to inhibit serotonin [6]. Our model supports this hypothesis, particularly given that is unlikely that the serotonin inhibition we observe is attributable to other slower mechanisms such as synthesis inhibition. Thus, to probe this idea further, we took a pharmacological approach.

iii) H_3 receptor Mediation of Serotonin Inhibition

Given the results of our mathematical modeling and the large body of prior work implicating H_3 heteroreceptors as an inhibitory mechanism for serotonin [15,42] we decided to probe H_3 receptor mediation of serotonin. **Figure 4.4** shows the results of systemically administering varying doses of a potent H_3 receptor antagonist, thioperamide, to different mice. The low dose (2 mg kg^{-1}) increased the amplitude of histamine release (consistent with prior studies with dopamine and D2 autoreceptor antagonism) [43,44], but has no significant effect on serotonin. This phenomenon is not difficult to explain because the serotonin response is controlled by dual mechanisms of a) now increased histamine available to antagonize H_3 receptors and b) a larger percentage of H_3 receptors antagonized on serotonin neurons. The overall result is a manifestation of two opposing effects that cancel each other out.

The 20 mg kg^{-1} dose had effects on both histamine release and clearance (reuptake effects have been previously been seen with serotonin autoreceptor antagonism) (Wood *et al.* 2014). The effect on the magnitude of serotonin inhibition was not significant, however it seems that the prolonged histamine in the synapse is outcompeting thioperamide for H_3 receptors on serotonin neurons to create prolonged serotonin inhibition (> 60 seconds).

H_3 heteroreceptors are likely more localized in the synapse, because of their position on serotonin terminals [45] than are H_3 autoreceptors on presynaptic histamine neurons. Autoreceptors are generally found outside of the direct synaptic space, asserting inhibition when a concentration threshold is reached [46]. The inhibition constant (K_i) of thioperamide is smaller than the Michaelis Menten constant (K_m) of histamine towards

H_3 receptors [47,48]. However, after stimulation histamine concentrations are very high in the direct synaptic space (likely reaching mMs based on prior dopamine models) [49] and fall off exponentially with distance. Because the thioperamide concentration is assumed to be homogenous throughout this brain region, the histamine most certainly outcompetes thioperamide for H_3 heteroreceptors on serotonin neurons. This notion is made apparent by the largest dose (50 mg kg^{-1}) of thioperamide which created significant and long lasting serotonin inhibition.

In sum, we showcased the power of FSCV for simultaneous measurements of histamine and serotonin the PM. We showed that MFB stimulation released histamine but created a potent inhibition of serotonin. Voltammetrically, mathematically and pharmacologically we showed serotonin inhibition was dependent on histamine release, via an H_3 receptor mediated mechanism. Our approach signals a powerful advancement in FSCV technology that will facilitate the systematic study of histamine and serotonin dynamics in the variety of different brain processes involving these two molecules.

4.6 References

(1) Haas, H. L.; Sergeeva, O. A.; Selbach, O. *Physiological reviews* **2008**, *88*, 1183.

(2) Brown, R. E.; Stevens, D. R.; Haas, H. L. *Progress in neurobiology* **2001**, *63*, 637.

(3) Chase, T. N.; Murphy, D. L. *Annual review of pharmacology* **1973**, *13*, 181.

(4) Russell, W. L.; Henry, D. P.; Phebus, L. A.; Clemens, J. A. *Brain Res* **1990**, *512*, 95.

(5) Moore, R. Y.; Halaris, A. E.; Jones, B. E. *J Comp Neurol* **1978**, *180*, 417.

(6) Threlfell, S.; Cragg, S. J.; Kallo, I.; Turi, G. F.; Coen, C. W.; Greenfield, S. A. *J Neurosci* **2004**, *24*, 8704.

(7) Laitinen, K. S. M.; Tuomisto, L.; Laitinen, J. T. *European Journal of Pharmacology* **1995**, *285*, 159.

(8) Portas, C. M.; Bjorvatn, B.; Ursin, R. *Progress in neurobiology* **2000**, *60*, 13.

(9) Cowen, P.; Sherwood, A. C. *Journal of psychopharmacology (Oxford, England)* **2013**, *27*, 575.

(10) Hashemi, P.; Dankoski, E. C.; Petrovic, J.; Keithley, R. B.; Wightman, R. M. *Analytical Chemistry* **2009**, *81*, 9462.

(11) Wood, K. M.; Cepeda, D.; Hashemi, P. *Compendium of in Vivo Monitoring in Real-Time Molecular Neuroscience, Vol 1: Fundamentals and Applications* **2015**, 269.

(12) Wood, K. M.; Zeqja, A.; Nijhout, H. F.; Reed, M. C.; Best, J.; Hashemi, P. *J Neurochem* **2014**, *130*, 351.

(13) Fink, K.; Schlicker, E.; Neise, A.; Gothert, M. *Naunyn Schmiedebergs Arch Pharmacol* **1990**, *342*, 513.

(14) Hough, L. B. *Prog Neurobiol* **1988**, *30*, 469.

(15) Schlicker, E.; Betz, R.; Gothert, M. *Naunyn Schmiedebergs Arch Pharmacol* **1988**, *337*, 588.

(16) Samaranayake, S.; Abdalla, A.; Robke, R.; Wood, K. M.; Zeqja, A.; Hashemi, P. *Analyst* **2015**, *140*, 3759.

(17) Marvin, E.; Scrogin, K.; Dudas, B. *J Chem Neuroanat* **2010**, *39*, 235.

(18) Michael, D. J.; Joseph, J. D.; Kilpatrick, M. R.; Travis, E. R.; Wightman, R. M. *Analytical Chemistry* **1999**, *71*, 3941.

(19) Jones, S. R.; Mickelson, G. E.; Collins, L. B.; Kawagoe, K. T.; Wightman, R. M. *Journal of neuroscience methods* **1994**, *52*, 1.

(20) Takmakov, P.; Zachek, M. K.; Keithley, R. B.; Bucher, E. S.; McCarty, G. S.; Wightman, R. M. *Anal Chem* **2010**, *82*, 9892.

(21) Hashemi, P.; Dankoski, E. C.; Lama, R.; Wood, K. M.; Takmakov, P.; Wightman, R. M. *Proceedings of the National Academy of Sciences of the United States of America* **2012**, *109*, 11510.

(22) Hashemi, P.; Dankoski, E. C.; Wood, K. M.; Ambrose, R. E.; Wightman, R. M. *Journal of Neurochemistry* **2011**, *118*, 749.

(23) Bernaerts, P.; Lamberty, Y.; Tirelli, E. *Behavioural brain research* **2004**, *154*, 211.

(24) Akhtar, M.; Pillai, K. K.; Vohora, D. *Basic & Clinical Pharmacology & Toxicology* **2005**, *97*, 218.

(25) Bordi, F.; Mor, M.; Plazzi, P. V.; Silva, C.; Caretta, A.; Morini, G. *Farmaco (Societa chimica italiana : 1989)* **1992**, *47*, 1095.

(26) Millar, J.; Stamford, J. A.; Kruk, Z. L.; Wightman, R. M. *European Journal of Pharmacology* **1985**, *109*, 341.

(27) Zhou, F. M.; Liang, Y.; Dani, J. A. *Nature neuroscience* **2001**, *4*, 1224.

(28) Montague, P. R.; McClure, S. M.; Baldwin, P. R.; Phillips, P. E.; Budygin, E. A.; Stuber, G. D.; Kilpatrick, M. R.; Wightman, R. M. *The Journal of neuroscience : the official journal of the Society for Neuroscience* **2004**, *24*, 1754.

(29) Swamy, B. E.; Venton, B. J. *Anal Chem* **2007**, *79*, 744.

(30) Sanford, A. L.; Morton, S. W.; Whitehouse, K. L.; Oara, H. M.; Lugo-Morales, L. Z.; Roberts, J. G.; Sombers, L. A. *Analytical chemistry* **2010**, *82*, 5205.

(31) Glanowska, K. M.; Venton, B. J.; Moenter, S. M. *The Journal of neuroscience : the official journal of the Society for Neuroscience* **2012**, *32*, 14664.

(32) Schneider, C.; Risser, D.; Kirchner, L.; Kitzmuller, E.; Cairns, N.; Prast, H.; Singewald, N.; Lubec, G. *Neuroscience letters* **1997**, *222*, 183.

(33) Muller, C. P.; Carey, R. J.; Huston, J. P.; De Souza Silva, M. A. *Progress in neurobiology* **2007**, *81*, 133.

(34) Barbeau, A. *Canadian Medical Association Journal* **1962**, *87*, 802.

(35) Rozov, S. V.; Zant, J. C.; Karlstedt, K.; Porkka-Heiskanen, T.; Panula, P. *The European journal of neuroscience* **2014**, *39*, 218.

(36) Panula, P.; Yang, H. Y.; Costa, E. *Proceedings of the National Academy of Sciences of the United States of America* **1984**, *81*, 2572.

(37) Garbarg, M.; Barbin, G.; Feger, J.; Schwartz, J. C. *Science (New York, N.Y.)* **1974**, *186*, 833.

(38) Auvinen, S.; Panula, P. *The Journal of comparative neurology* **1988**, *276*, 289.

(39) Veening, J. G.; Swanson, L. W.; Cowan, W. M.; Nieuwenhuys, R.; Geeraedts, L. M. *The Journal of comparative neurology* **1982**, *206*, 82.

(40) Nieuwenhuys, R.; Geeraedts, L. M.; Veening, J. G. *The Journal of comparative neurology* **1982**, *206*, 49.

(41) Dankoski, E. C.; Wightman, R. M. *Frontiers in Integrative Neuroscience* **2013**, *7*, 44.

(42) Esbenshade, T. A.; Browman, K. E.; Bitner, R. S.; Strakhova, M.; Cowart, M. D.; Brioni, J. D. *Br J Pharmacol* **2008**, *154*, 1166.

(43) Clark, D.; Exner, M.; Furmidge, L. J.; Svensson, K.; Sonesson, C. *Eur J Pharmacol* **1995**, *275*, 67.

(44) Kita, J. M.; Parker, L. E.; Phillips, P. E.; Garris, P. A.; Wightman, R. M. *J Neurochem* **2007**, *102*, 1115.

(45) Carlsson, A.; Carlsson, M. L. *Dialogues in clinical neuroscience* **2006**, *8*, 137.

(46) Langer, S. Z.; Galzin, A. M.; Costentin, J. *Presynaptic Receptors and Neuronal Transporters: Official Satellite Symposium to the IUPHAR 1990 Congress Held in Rouen, France, on 26–29 June 1990*; Elsevier Science, 2013.

(47) Liedtke, S.; Flau, K.; Kathmann, M.; Schlicker, E.; Stark, H.; Meier, G.; Schunack, W. *Naunyn Schmiedebergs Arch Pharmacol* **2003**, *367*, 43.

(48) Chen, J.; Liu, C.; Lovenberg, T. W. *Eur J Pharmacol* **2003**, *467*, 57.

(49) Garris, P. A.; Ciolkowski, E. L.; Pastore, P.; Wightman, R. M. *The Journal of neuroscience : the official journal of the Society for Neuroscience* **1994**, *14*, 6084.

CHAPTER 5

SELECTIVE SEROTONIN REUPTAKE INHIBITORS BLOCK HISTAMINE REUPTAKE VIA MONOAMINE TRANSPORTERS; A FAST-SCAN CYCLIC VOLTAMMETRIC STUDY

5.1 Introduction

Histamine plays many important roles in the brain and irregularities in this messenger have been implicated in many disorders[1-5]. Despite this association, the few central nervous system (CNS) histamine targeting therapeutics show inadequate efficacy[1-3]. This is primarily because little is known about histamine's roles as a neuromodulator, other than controlling monoamines via H_3 receptors[6-8]. The relationship between histamine and serotonin is of particular interest to our lab since we chiefly study *in vivo* serotonin regulation mechanisms.

Histamine is released into the synapse via exocytosis and thought to be primarily enzymatically degraded by histamine *N*-methyltransferase (HNMT)[9-12]. While there is evidence for partial histamine reuptake into synaptosomes[13,14] and astrocytes[15,16], a transporter for histamine has not been identified[17,18]. Given that HNMT has been found to be exclusively intracellular,[19,20] it seems incongruent that there would not exist an active histamine reuptake mechanism. We therefore sought to clarify this inconsistency.

We recently described a fast-scan cyclic voltammetry (FSCV) technique that can simultaneously measure *in vivo* histamine and serotonin with sub-second temporal resolution at carbon fiber microelectrodes (CFMs). In this paper we investigated histamine reuptake by dopamine transporters (DATs), serotonin transporters (SERTs), norepinephrine transporters (NETs) and organic cation transporters (OCTs). The rationale here originated from our prior work where we mathematically modeled histamine responses and found that the clearance curve could be fit with first order Michaelis-Menten kinetics,[14,6] commonly seen for dopamine[21] and serotonin[22,23] active reuptake. Additionally, Lyn Daws previously reviewed evidence for 'promiscuous' reuptake of

dopamine, serotonin and norepinephrine between monoamine transporters[24]. Taken together, these findings provide a compelling platform for monoamine transporters in synaptic histamine removal.

By electrically stimulating histamine release in the mouse posterior hypothalamus (PH) we observe the effects of pharmacological manipulations on the DAT, NET, SERT and OCTs on histamine reuptake. First, we show the lesion left by the CFM in histological section for all the experiments, attesting to the high accuracy of our surgical procedure. Second, the *in vivo* histamine response is highly reproducible between groups of animals. Third, vehicle injections do not substantially change control responses. Fourth, the histamine clearance profile is not altered by DAT inhibition. Fifth, desipramine-mediated NET inhibition and SERT inhibition via 3 different SSRIs exert varying degrees of reuptake inhibition on histamine. Despite the heterogeneous response to these agents, one commonality between them is that they all have the capacity to inhibit OCTs. Thus, OCTs are blocked, generating the most dramatic decrease in the rate of histamine reuptake. Collectively, our results suggest an active reuptake mechanism for histamine, likely primarily via the OCTs. This information is important for improving development and efficacy of neuropharmaceuticals for histamine during pathophysiology.

5.2 Materials and Methods

5.2.1 Pharmacological Agents

Escitalopram oxalate, citalopram hydrobromide, sertraline hydrochloride, GBR 12909 dihydrochloride, desipramine hydrochloride, decynium-22 iodide were ordered

from Sigma-Aldrich, MO, USA. All drugs were dissolved in 9% sterile saline solutions and administered via *i.p* injection at 0.1 20 mL/g except for sertraline and decynium-22, which were dissolved in DMSO at 5% concentration in sterile saline.

5.2.2 Carbon-Fiber Microelectrodes (CFMs)

Carbon-fibers (Goodfellow Corporation, PA, USA) of 7 µm diameter were aspirated into glass capillaries (0.6 mm external diameter, 0.4 mm internal diameter, A-M Systems, Inc., Sequim, WA) to fabricate the CFMs. A carbon-glass seal was formed using vertical micropipette puller (Narishige Group, Tokyo, Japan). The exposed length of the carbon-fiber was trimmed to 150 µm under an optical microscope. CFMs were electroplated with Nafion.

5.2.3 Data Collection

A commercially available potentiostat (Dagan Corporation, Minneapolis, MN) and custom build hardware interfacing a PCIe-6341 DAC/ADC card (National Instruments, Austin, TX) were used for waveform generation, data acquisition, and signal processing. Custom built software, written in-house using LabVIEW 2009, was used to drive the hardware and perform data analysis including background subtraction, signal averaging and digital filtering (Knowmad Technologies LLC, Tucson, AZ). All potentials were measured with respect to Ag/AgCl reference electrode. The reference electrode was fabricated via electrodeposition of Cl- by holding a silver wire at 5.0 V for 5 s in 1 M HCl. All the error bars represent the standard error of the mean (SEM).

5.2.4 Data Analysis

All current vs. time curves and cyclic voltammograms (CVs) were collected with software made in-house. Current was converted to concentration by using standard calibration factors, for histamine = 2.82 μM/nA and serotonin = 11 nM/nA. One-tailed Student's *t*-tests on paired data set were used to determine statistical significance ($p < 0.05$ was taken as significantly different).

5.2.5 Animal Surgeries

Handling and surgery on male C57BL/6J mice weighing 20−25 g (Jackson Laboratory, Bar Harbor, ME) was in agreement with the University of South Carolina's Guide for the Care and Use of Laboratory Animals, approved by the Institutional Animal Care and Use. Urethane (25% dissolved in 0.9% sterile saline solution, Hospira, Lake Forest, IL) was injected *i.p* and once deep anesthesia was confirmed, animals were secured into a stereotaxic instrument (David Kopf Instruments, Tujunga, CA) and stereotaxic surgery was performed. A heating pad was used to sustain mouse body temperature around 37 °C (Braintree Scientific, Braintree, MA). Stereotaxic coordinates were taken in reference to bregma. A Nafion plated CFM was placed in the PH (AP: −2.45, ML: +0.50, DV: −5.45 to −5.55.). A stainless-steel stimulating electrode (diameter: 0.2 mm, Plastics One, Roanoke, VA) was positioned into the MFB (AP: -1.07, ML: +1.10, DV: −5.00). Biphasic pulse trains were applied through a linear constant current stimulus isolator (NL800A, Neurolog, Medical Systems Corp., Great Neck, NY) to provoke histamine efflux. The 60 Hz trains were 360 μA each phase, 2 ms in width, and the stimulation was 2 s in length. All potentials were measured with respect to a

Ag/AgCl reference electrode (constructed by plating Cl^- ions onto an Ag wire) which was implanted into the opposite brain hemisphere.

5.2.6 Histology

To verify the placement of the CFMs *in vivo*, after experimentation the CFM was used to create a small lesion in the recording site by applying a constant potential (20 V for 10 s)[25]. Following experiments, mice were sacrificed and brains were removed from the skull and stored in 10% paraformaldehyde solution in phosphate buffered saline (PBS). The brains were then stored in 15% sucrose until they sank. Brains were then flash-frozen, sectioned into 20 µm slices using a cryostat (Cryotome FSE, Thermo Scientific, Kalamazoo, MI) and mounted on glass slides. Finally, brain slices were stained with 0.2% crystal violet and photographed under an optical microscope.

5.3 Results and Discussion

5.3.1 Histology

Figure 5.1 shows a representative image showing the lesion of the CFM (A) and the stimulating electrodes (B) circled in blue. In **Figure 5.1C**, the location of all the electrodes utilized in this study (one electrode per mouse) are shown in slices between Bregma -2.30 to -2.92.

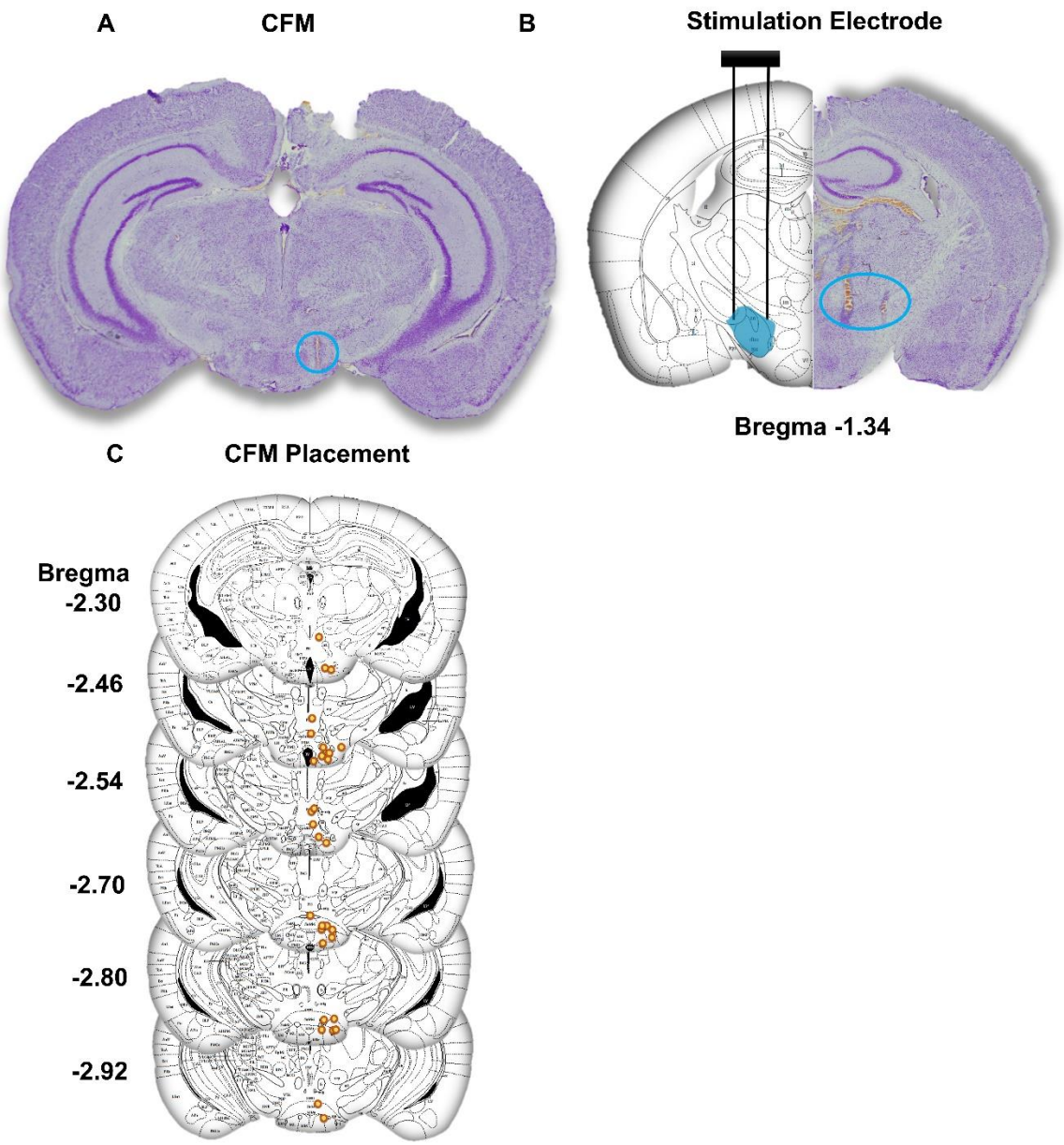

Figure 5.1. CFMs and stimulating electrode placements in PH and MFB respectively. **(A)** CFM lesion which is denoted by a blue circle. **(B)** Left hemisphere is a diagram illustrating intended placement of MFB, and right hemisphere shows the actual placement of the electrode. **(C)** CFMs placement in PH.

5.3.2 Selective sub-second neurochemical detection of histamine

Upon electrical stimulation of the MFB, histamine was evoked in the PH and this was verified with FSCV recording, as visualized in the color plot in **Figure 5.2. Figure 5.2A-F** shows representative color plots, cyclic voltammograms (CVs) and averaged [histamine] vs. time responses in groups of animals that served as controls for subsequent pharmacology experiments (animal groups A to F). The interpretation of color plots is described elsewhere in detail[6,26]. Briefly, background subtracted cyclic voltammograms collected at 10 Hz for 30 seconds are displayed as voltage (y-axis) vs. time (x-axis) and current (false color scale). The green bar directly underneath the color plot denotes the occurrence and duration of the electrical stimulation. Upon electrical stimulation, there are several non- faradaic events, due to other electroactive species, pH changes and ionic fluxes[27,28] which occur at the switching potentials. Distinct histamine oxidation occurs at 0.3 V, denoted by the horizontal dashed line.

CVs for histamine detection for each drug were extracted from each color plot at the vertical dashed line through the event, which is represented by a yellow star, and illustrated in middle column of the **Figure 5.2** (Cyclic Voltammograms). The oxidation peak at 0.3 V (blue bar named as histamine) proves the selective histamine detection. **Figure 5.2** right column shows the electrically evoked average histamine responses, which are extracted from horizontal dashed line named HA from each color plot. This data shows the high reproducibility between control histamine responses.

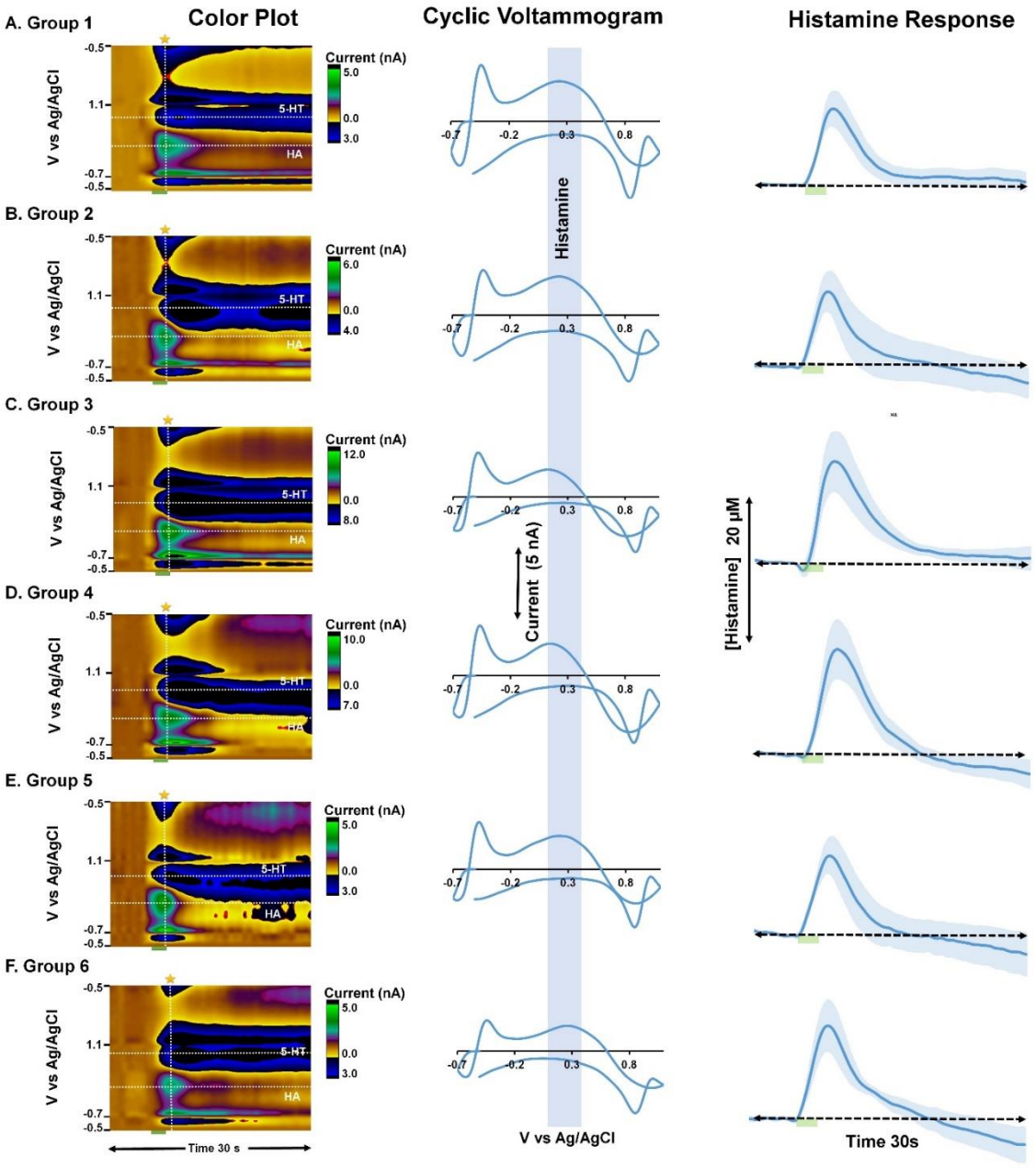

Figure 5.2. The representative color plots, cyclic voltammograms (CVs) and evoked histamine traces for control experiments in different sets of animal groups 1 to 6. Left column shows color plots. The middle column illustrates CVs that were extracted from each color plot at the vertical dashed line (denoted by the yellow star). Right column shows the average control [histamine] vs time traces for each drug category (n=5 ± SEM). Shaded region around the trace represents the SEM. Green bars underneath each color plot and each trace in the right column represent the stimulation. Blue vertical bars in the middle column highlights the histamine oxidation peak.

5.3.3 Effect of Vehicle

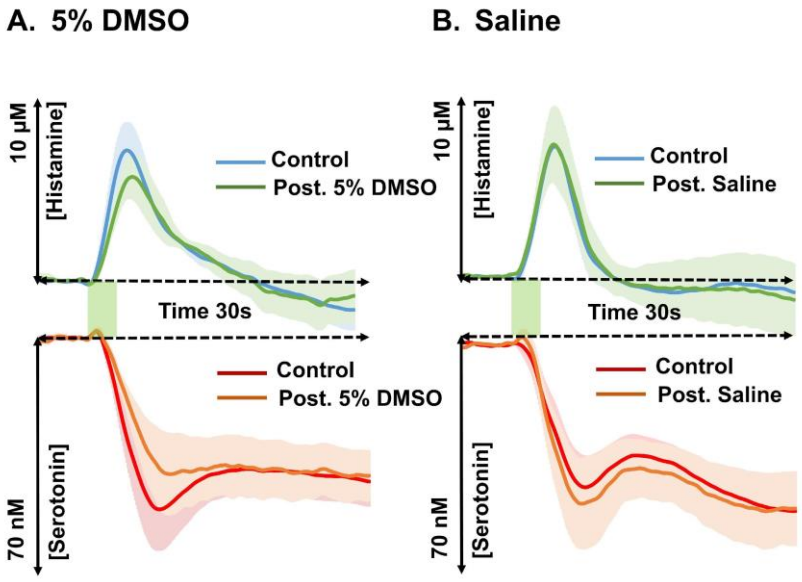

Figure 5.3. Top panel - [histamine] vs. time traces are shown in blue and green for pre and post-vehicle administration respectively. Bottom panel - [serotonin] vs. time traces are shown in red and orange for before and after the vehicle respectively. Error bars showing SEM (n=5 ± SEM) are lighter versions of these respective colors. (A) 5% DMSO and (B) Saline

In the proceeding pharmacological manipulations, either 5% DMSO or sterile saline were used to dissolve active agents. Therefore, DMSO and saline were administered to different groups of mice to test the effects of vehicle on the signal. **Figure 5.3A** shows the average concentration vs. time traces of histamine (top panel), we also measured serotonin (bottom panel). This inverse serotonin response illustrates the reduction of ambient serotonin concentration via H_3 receptor activation by evoked histamine, as we previously showed. Histamine and serotonin responses after 50 minutes of 5% DMSO administration (*i.p.*) are presented in green and orange traces respectively and have negligible effects on the signal.

5.3.4 OCT-mediated histamine uptake: pharmacological evidence

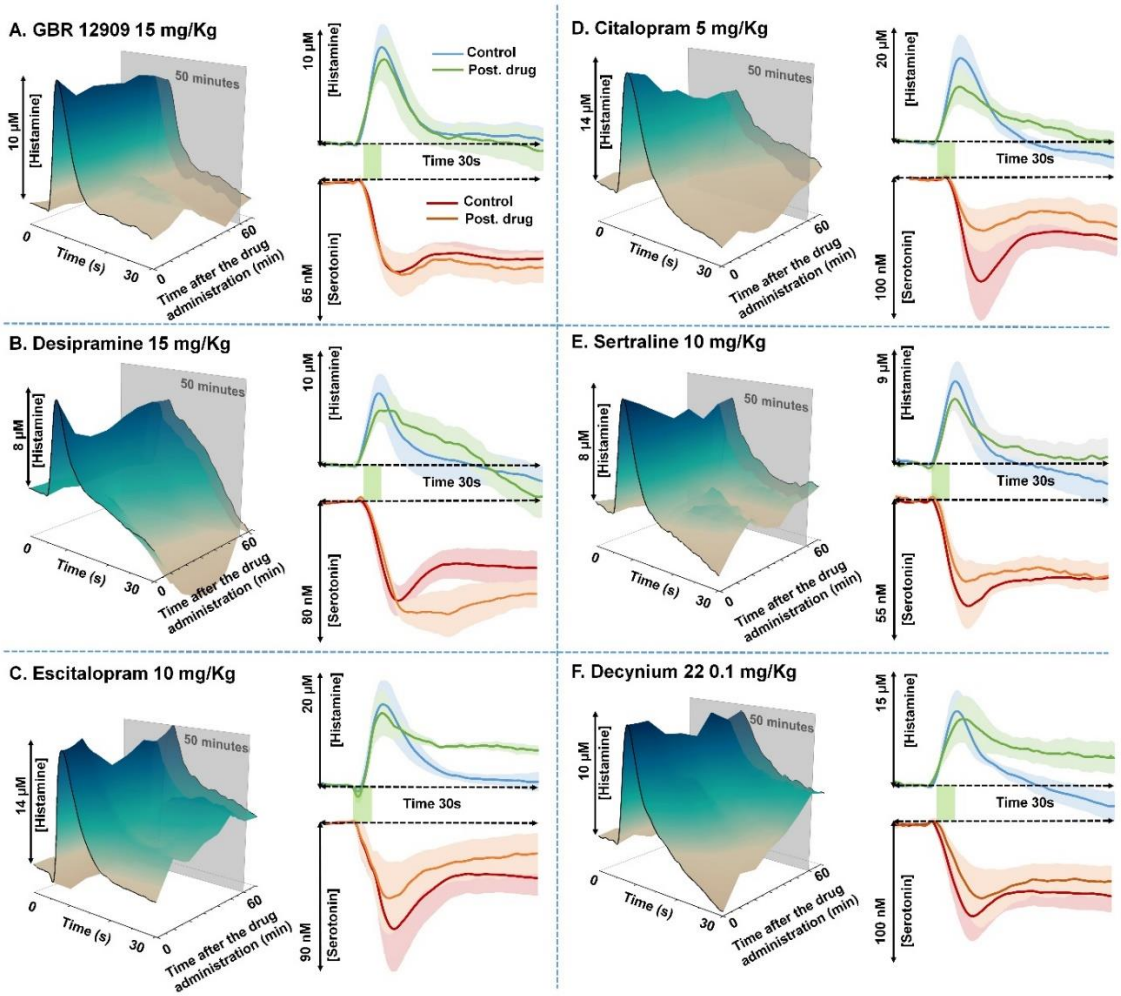

Figure 5.4. Comparison of histamine and serotonin responses after monoamine transporter inhibitors. (**A**) GBR 12902 (15 mg/kg) (**B**) desipramine (15 mg/kg) (**C**) escitalopram (10 mg/kg) (**D**) citalopram (5 mg/kg) I sertraline (10 mg/kg). (**F**) decynium-22 (0.1 mg/kg). In each drug category, average histamine vs. time traces collected every 10 minutes for 60 minutes are shown in 3D plots (left panel). The right panel shows the [histamine] vs. time traces for control in blue and 50 minutes post-drug in green. [serotonin] vs. time traces are shown in red and orange for control and post-drug respectively. Stimulation period is represented by a green bar between histamine and serotonin responses. Error bars represents the SEM (n=5 ± SEM) in lighter versions of these respective colors.

Next, we investigated histamine reuptake via 4 monoamine transporter proteins. Six different transporter inhibitor drugs, GBR 12902 (15 mg/kg), desipramine (15 mg/kg), escitalopram (10 mg/kg), citalopram (5 mg/kg), sertraline (10 mg/kg) and decynium-22 (0.1 mg/kg), were injected (*i.p.*) into different mice. Histamine and serotonin responses were measured every 10 minutes, for 60 minutes, after drug administration. **Figure 5.4A-left** shows a 2D representation of a 3D plot of histamine responses upon stimulation with time after drug. The first solid black trace in the 3D plot represents the pre-drug [histamine] response. [Histamine] responses collected every 10 minutes after drug administration, for 60 minutes, are stacked next to one another and given a false color. The x-axis represents 30 seconds for an individual file, y-axis represents 60 minutes after the drug administration and z-axis represents [histamine]. This 2D plot allows for visualization of the effects of the time course of an agent's effects on histamine reuptake. The right panel in **Figure 4A** shows averaged histamine traces before drug (blue) and 50 minutes after the drug (green) and averaged serotonin traces before drug in red and after drug in orange between animals (n=5 ± SEM). **Figure 4B, C, D, E,** and **F** demonstrate the effects of desipramine (15 mg/kg), escitalopram (10 mg/kg), citalopram (5 mg/kg), sertraline (10 mg/kg) and decynium-22 (0.1 mg/kg) respectively.

DATs

High levels of histamine decarboxylase have been found in dopamine-rich regions such as the striatum[29]. In addition, histamine receptors are heavily expressed in the nucleus accumbens[18,30], an area extensively studied for dopamine transmission[31,32]. There is also evidence for histaminergic modulation of dopamine transmission in the striatum and nucleus accumbens[33,34]. Given the abundance of physiological evidence for co-

actions of dopamine and histamine, we first tested whether DATs mediate histamine reuptake. A potent DAT inhibitor, GBR 12909[35], did not lead to significant changes in histamine reuptake as shown in **Figure 4A**. This observation suggested that there is no involvement of DAT in histamine reuptake in the PH.

NETs

Recent studies have shown the existence of NETs in rat posterior and anterior hypothalamic[36,37] area as well as the regulation of norepinephrine via H_3 receptors[38]. Together this evidence suggests possible comodulation of norepinephrine and histamine. In comparison to DAT, the NET inhibitor, desipramine, slightly decelerated the reuptake of histamine when compared to control animals (**Figure 4B**). An interesting finding is that NET blockage enhanced histamine-mediated serotonin firing inhibition. The antidepressant-like effects of this tricyclic antidepressant drug suggest the regulation of serotonergic system through SERTs[24,39,40]. Extracellular histamine also plays a significant role in regulating the serotonin release via H_3 receptors. Hence, resulting in greater inverse regulation of serotonin via H_3 activation.

SERTs

We and others have shown that histamine modulates serotonin transmission[8,41]. Serotonin is reuptaken with high efficiency by SERTs [42]. SERTs are localized in some of the highest numbers in the PH[43,44]. Given the close modulatory relationship between histamine and serotonin, we next decided to study whether SERT inhibition exerts an effect on histamine clearance. Escitalopram[45] and citalopram[46] (selective serotonin reuptake inhibitors (SSRIs)) substantially slowed histamine reuptake and lead to a decrease in histamine-mediated serotonin inhibition compared to control responses as

shown in **Figure 5.4D** & **E**. However, sertraline[47], also an SSRI, had minimal effects on the histamine signal. Thus, the discrepancy between the three SSRIs proposes that SERT may not be the primary reuptake mechanism for histamine. Like desipramine, escitalopram and citalopram both have high affinity for the OCT but sertraline does not[48,49]. We thus turned to the OCTs.

A point to note is that SERT inhibitors (escitalopram and citalopram) exhibit slightly less inhibition of serotonin with respect to controls (**Figure 5.4 D** & **E**). The enhanced release of serotonin by SERT inhibitors[45] overcomes the inhibition of serotonin via H_3 receptors[6] and makes the inverse modulation of serotonin less but insignificant in the post-drug condition.

OCTs

We inhibited the OCT reuptake mechanism via decynium-22[49] in a final set of mice. Decynium-22 demonstrated the most significant effect on histamine clearance, as shown in **Figure 4F,** suggesting OCT mediated histamine reuptake. Furthermore, post-drug inverse modulation of serotonin illustrated insignificant inhibition when compared to the control response (**Figure 4F**). This may be due to the bidirectional effects of elevated extracellular serotonin by inhibiting the OCT-mediated serotonin uptake[48-50] and the serotonin inhibition via histamine[6].

Conclusion

Histamine is a vital monoamine neurotransmitter which plays a significant role in the brain, but histamine's reuptake mechanism is less studied. This electrochemical and pharmacological study demonstrated the implications of monoamine transporters towards

histamine's reuptake mechanism. The histamine clearance profile was not affected by DAT inhibition. Whereas, NET and SERT inhibition demonstrated an inconsistency in reuptake inhibition on this messenger. Because of the NETs and SERTs inhibitory agents' ability to inhibit OCTs, we finally, blocked the OCTs, which in turn showed the largest decrease in the histamine reuptake rate. Collectively, this work suggests an OCT mediated histamine reuptake mechanism in the brain. These novel discoveries illustrate the actions of monoamine transporters on histamine neurodynamics and offer new insight into histamine targeting therapeutic strategies.

5.4 References

(1) Panula, P.; Yang, H. Y.; Costa, E. *Proceedings of the National Academy of Sciences of the United States of America* **1984**, *81*, 2572.

(2) Panula, P.; Rinne, J.; Kuokkanen, K.; Eriksson, K. S.; Sallmen, T.; Kalimo, H.; Relja, M. *Neuroscience* **1998**, *82*, 993.

(3) Panula, P.; Nuutinen, S. *Nature reviews. Neuroscience* **2013**, *14*, 472.

(4) Haas, H. L.; Sergeeva, O. A.; Selbach, O. *Physiological reviews* **2008**, *88*, 1183.

(5) Rinne, J. O.; Anichtchik, O. V.; Eriksson, K. S.; Kaslin, J.; Tuomisto, L.; Kalimo, H.; Röyttä, M.; Panula, P. *Journal of Neurochemistry* **2002**, *81*, 954.

(6) Samaranayake, S.; Abdalla, A.; Robke, R.; Nijhout, H. F.; Reed, M. C.; Best, J.; Hashemi, P. *J Neurochem* **2016**, *138*, 374.

(7) Schlicker, E.; Betz, R.; Göthert, M. *Naunyn-Schmiedeberg's Arch Pharmacol* **1988**, *337*, 588.

(8) Threlfell, S.; Cragg, S. J.; Kallo, I.; Turi, G. F.; Coen, C. W.; Greenfield, S. A. *The Journal of neuroscience : the official journal of the Society for Neuroscience* **2004**, *24*, 8704.

(9) White, T. *The Journal of physiology* **1960**, *152*, 299.

(10) Schayer, R. W.; Reilly, M. A. *The Journal of pharmacology and experimental therapeutics* **1973**, *184*, 33.

(11) Pollard, H.; Bischoff, S.; Schwartz, J. C. *The Journal of pharmacology and experimental therapeutics* **1974**, *190*, 88.

(12) Takemura, M.; Imamura, I.; Mizuguchi, H.; Fukui, H.; Yamatodani, A. *Life sciences* **1994**, *54*, 1059.

(13) Barnes, W. G.; Hough, L. B. *J Neurochem* **2002**, *82*, 1262.

(14) Sakurai, E.; Sakurai, E.; Oreland, L.; Nishiyama, S.; Kato, M.; Watanabe, T.; Yanai, K. *Pharmacology* **2006**, *78*, 72.

(15) Huszti, Z. *Inflammation research : official journal of the European Histamine Research Society ... [et al.]* **2003**, *52 Suppl 1*, S03.

(16) Huszti, Z.; Prast, H.; Tran, M. H.; Fischer, H.; Philippu, A. *Naunyn Schmiedebergs Arch Pharmacol* **1998**, *357*, 49.

(17) Hough, L. B. *Progress in neurobiology* **1988**, *30*, 469.

(18) Brown, R. E.; Stevens, D. R.; Haas, H. L. *Progress in neurobiology* **2001**, *63*, 637.

(19) Nishibori, M.; Tahara, A.; Sawada, K.; Sakiyama, J.; Nakaya, N.; Saeki, K. *The European journal of neuroscience* **2000**, *12*, 415.

(20) Maintz, L.; Novak, N. *The American journal of clinical nutrition* **2007**, *85*, 1185.

(21) Walters, S. H.; Robbins, E. M.; Michael, A. C. *ACS Chem Neurosci* **2015**, *6*, 1468.

(22) Wood, K. M.; Zeqja, A.; Nijhout, H. F.; Reed, M. C.; Best, J.; Hashemi, P. *Journal of Neurochemistry* **2014**, *130*, 351.

(23) Jones, S.; John, C. In *Electrochemical Methods for Neuroscience*; CRC Press: 2006, p 49.

(24) Gould, G. G.; Hensler, J. G.; Burke, T. F.; Benno, R. H.; Onaivi, E. S.; Daws, L. C. *J Neurochem* **2011**, *116*, 291.

(25) Park, J.; Kile, B. M.; Wightman, R. M. *The European journal of neuroscience* **2009**, *30*, 2121.

(26) Michael, D. J.; Joseph, J. D.; Kilpatrick, M. R.; Travis, E. R.; Wightman, R. M. *Analytical Chemistry* **1999**, *71*, 3941.

(27) Jones, S. R.; Mickelson, G. E.; Collins, L. B.; Kawagoe, K. T.; Wightman, R. M. *Journal of neuroscience methods* **1994**, *52*, 1.

(28) Takmakov, P.; Zachek, M. K.; Keithley, R. B.; Bucher, E. S.; McCarty, G. S.; Wightman, R. M. *Anal Chem* **2010**, *82*, 9892.

(29) Krusong, K.; Ercan-Sencicek, A. G.; Xu, M.; Ohtsu, H.; Anderson, G. M.; State, M. W.; Pittenger, C. *Neuroscience letters* **2011**, *495*, 110.

(30) Pillot, C.; Heron, A.; Cochois, V.; Tardivel-Lacombe, J.; Ligneau, X.; Schwartz, J. C.; Arrang, J. M. *Neuroscience* **2002**, *114*, 173.

(31) Jones, S. R.; Garris, P. A.; Wightman, R. M. *The Journal of pharmacology and experimental therapeutics* **1995**, *274*, 396.

(32) Cheer, J. F.; Heien, M. L. A. V.; Garris, P. A.; Carelli, R. M.; Wightman, R. M. *Proceedings of the National Academy of Sciences of the United States of America* **2005**, *102*, 19150.

(33) Schlicker, E.; Fink, K.; Detzner, M.; Göthert, M. *Journal of Neural Transmission / General Section JNT* **1993**, *93*, 1.

(34) Galosi, R.; Lenard, L.; Knoche, A.; Haas, H.; Huston, J. P.; Schwarting, R. K. *Neuropharmacology* **2001**, *40*, 624.

(35) John, C. E.; Jones, S. R. *Neuropharmacology* **2007**, *52*, 1596.

(36) Pau, K. Y.; Lee, C. J.; Cowles, A.; Yang, S. P.; Hess, D. L.; Spies, H. G. *Journal of neuroendocrinology* **1998**, *10*, 21.

(37) Hope, S. I.; Schmipp, J.; Rossi, A. H.; Bianciotti, L. G.; Vatta, M. S. *Neurochemistry international* **2008**, *53*, 207.

(38) Flik, G.; Folgering, J. H.; Cremers, T. I.; Westerink, B. H.; Dremencov, E. *Journal of molecular neuroscience : MN* **2015**, *56*, 320.

(39) Charney, D. S.; Heninger, G. R.; Sternberg, D. E. *Archives of general psychiatry* **1984**, *41*, 359.

(40) Zhao, Z.; Zhang, H.-T.; Bootzin, E.; Millan, M. J.; O'Donnell, J. M. *Neuropsychopharmacology : official publication of the American College of Neuropsychopharmacology* **2009**, *34*, 1467.

(41) Hashemi, P.; Dankoski, E. C.; Wood, K. M.; Ambrose, R. E.; Wightman, R. M. *Journal of Neurochemistry* **2011**, *118*, 749.

(42) Lin, K. J.; Yen, T. C.; Wey, S. P.; Hwang, J. J.; Ye, X. X.; Tzen, K. Y.; Fu, Y. K.; Chen, J. C. *Journal of nuclear medicine : official publication, Society of Nuclear Medicine* **2004**, *45*, 673.

(43) Borgers, A. J.; Alkemade, A.; Van de Giessen, E. M.; Drent, M. L.; Booij, J.; Bisschop, P. H.; Fliers, E. *EJNMMI Research* **2013**, *3*, 34.

(44) Borgers, A. J.; Koopman, K. E.; Bisschop, P. H.; Serlie, M. J.; Swaab, D. F.; Fliers, E.; la Fleur, S. E.; Alkemade, A. *Frontiers in Neuroscience* **2014**, *8*, 106.

(45) Wood, K. M.; Hashemi, P. *ACS Chemical Neuroscience* **2013**, *4*, 715.

(46) Dankoski, E. C.; Carroll, S.; Wightman, R. M. *Journal of Neurochemistry* **2016**, *136*, 1131.

(47) Pyakurel, P.; Privman Champaloux, E.; Venton, B. J. *ACS Chemical Neuroscience* **2016**, *7*, 1112.

(48) Wang, K.; Sun, S.; Li, L.; Tu, M.; Jiang, H. *Progress in neuro-psychopharmacology & biological psychiatry* **2014**, *53*, 90.

(49) Zhu, H. J.; Appel, D. I.; Grundemann, D.; Richelson, E.; Markowitz, J. S. *Pharmacological research* **2012**, *65*, 491.

(50) Horton, R. E.; Apple, D. M.; Owens, W. A.; Baganz, N. L.; Cano, S.; Mitchell, N. C.; Vitela, M.; Gould, G. G.; Koek, W.; Daws, L. C. *The Journal of neuroscience : the official journal of the Society for Neuroscience* **2013**, *33*, 10534.

CHAPTER 6

HISTAMINERGIC MODULATION OF SEROTONIN DURING DISEASE; THE HIV-1 TG MODEL

6.1 Introduction

Neuroinflammation is garnering increasing interest for its potential role in the pathology of many diseases and is commonly marked by increases in biomarkers such as proinflammatory cytokines[1-3]. In addition, recent studies have shown elevated brain histamine levels during neuroinflammation[2,4]. Neuroinflammation can originate from infections, brain injuries, viruses like human immune deficiency virus (HIV-1) and many other neurological disorders. Histamine is a monoamine neurotransmitter that regulates important brain functions and modulates other neurotransmitters like serotonin[5-10]. These monoamine neurotransmitters, including histamine and serotonin, are frequently implicated in the neurological disorders which are comorbid with neuroinflammation[10-12]. The lack of knowledge on the actions of the brain's chemical messengers during inflammation seen with certain brain disorders makes the pathology difficult to properly elucidate.

Neuroinflammation is an important symptom in HIV and in the rat HIV-1 Tg disease model. Recent studies have shown that HIV-1 Tg rats exhibit elevated levels of proinflammatory cytokines (INF-γ, TNF-α, and IL-1β), which are key biomarkers of inflammation[13]. In addition, the viral protein glycoprotein gp120 binds to the chemokine receptor, which exists in many of the cells present in the central nervous system, including neurons[14,15]. The neurotoxic effects of gp120 include induction of apoptosis and neural injury[16] and can result in neuroinflammation during the adolescent period of the HIV-1 Tg rat's life. Therefore, HIV-1 Tg is an excellent animal model to study neurotransmitter dynamics that accompany low-grade, chronic neuroinflammation.

This disease model has shown a trend toward increased anxiety-like behavior[17,18] as shown by open-field, general locomotor activity, and motivated behavior tests. Additionally, social interaction, novel stimulus and forced swim tests have revealed that HIV-1 Tg rats exhibit elevated depressive-like behaviors[18]. These observations are of particular interest as serotonin is the transmitter primarily implicated in depression and anxiety[19,20]. Given that histamine release is associated with local peripheral inflammation, and given we find that histamine inversely regulates serotonin in the brain, an important question follows: Is histamine involved in neuroinflammation and if so, how do alterations in histamine affect serotonin? We will ask these questions in the HIV-1 Tg rat.

In this study, we employed our dual histamine/serotonin measurement strategy to investigate histaminergic regulation of serotonin in HIV-1Tg rats. To accomplish this task, we positioned the carbon fiber microelectrodes (CFMs) in the rat posterior hypothalamus (PH) and the stimulation electrode in the medial forebrain bundle (MFB). We found that histamine release was elevated in the disease model resulting in increased serotonin inhibition. We hypothesized that this elevated histamine would suppress evoked serotonin release. To test this hypothesis, we positioned another CFM in the prefrontal cortex (PFC) to investigate the stimulated release of serotonin. HIV-1 Tg rats were shown to have attenuated serotonin release with respect to control animals. Our results imply that histamine may play an important role in this regard. Collectively, this study works toward characterizing the importance of histamine's role in controlling the serotonin release during disease states marked by neuroinflammation.

6.2 Methods

6.2.1 Animals

Male and female F344 rats (n=17) and HIV-1 Tg rats (n=17) (Harlan Laboratories, Indianapolis, Indiana) were commercially ovariectomized and pair-housed by genotype. Food and water were provided *ad libitum* throughout the experiment. Animals were kept in an AALAC-accredited facility at 21 +/- 2 C, 50% +/- 10% relative humidity, in a 12-hr light-dark cycle with lights on at 07:00h. All experiments were performed according to the National Institute of Health guidelines for AAALAC accredited facilities. All behavioral testing was conducted during the animal's light cycle. The research protocol was approved by the Institutional Animal Care and Use Committee (IACUC) of the University of South Carolina, Columbia, SC, under animal assurance number A3049-01.

6.2.2 Carbon fiber microelectrodes (CFMs)

CFMs were fabricated according to Samaranayake *et. al.*,[21]. In brief, 7 um-diameter carbon fibers (Goodfellow Inc, Coraopolis, PA) were aspirated into glass capillary tubes (OD 0.6 mm, ID 0.4 mm, A-M Systems INC, Sequim, WA). A vertical pipette puller was used to seal the carbon fiber to the capillary tube (Narishige Group, Tokyo, Japan). The carbon fiber was then trimmed to 150 µm under a low-power light microscope. All microelectrodes were nafion-coated as per Hashemi *et al.*, 2009[22].

6.2.3 Animal Surgery

Before surgery, animals were anesthetized using 2-3% sevoflurane inhalant (Abbot Laboratories, North Chicago, IL). Once the animal was fully anesthetized, it was placed in the stereotaxic apparatus, and the head was leveled with respect to bregma (David Kopf Instruments, Tujunga, CA). A heating pad (37 ^{0}C) was placed under the animal throughout the course of the experiment. CFMs were placed to PFC (AP: +2.6, ML: +0.6, DV: -4.7) and PH (AP: -3.96, ML: +1.8, DV: -8.0 to -8.5) to detect serotonin and histaminergic regulation of serotonin respectively. A stainless-steel stimulating electrode (diameter: 0.2 mm, Plastics One, Roanoke, VA) was positioned into the MFB (for histamine, AP: -1.8, ML: +1.8, DV: −8.0 and for serotonin, AP: -2.40, ML: +1.8, DV: -8.0). Biphasic pulse trains were applied through a linear constant current stimulus isolator (NL800A, Neurolog, Medical Systems Corp., Great Neck, NY) to provoked histamine efflux. The 60 Hz trains were 360 μA each phase, 2 ms in width, and 2 s in length. All potentials were measured with respect to a Ag/AgCl reference electrode (constructed by plating Cl^- ions onto a Ag wire) which was implanted into the brain's opposite hemisphere.

6.2.4 Data Collection

A commercially available potentiostat (Dagan Corporation, Minneapolis, MN) and a custom built hardware interfacing a PCIe-6341 DAC/ADC card (National Instruments, Austin, TX) were used to attain waveform generation, data acquisition, and signal processing. Custom built software, written in-house using LabVIEW 2009, was used to drive the hardware and perform data analysis including background subtraction,

signal averaging and digital filtering (Knowmad Technologies LLC, Tucson, AZ). All the error bars represent the standard error of the mean (SEM).

6.3 Results

6.3.1 Histaminergic Regulation of Serotonin

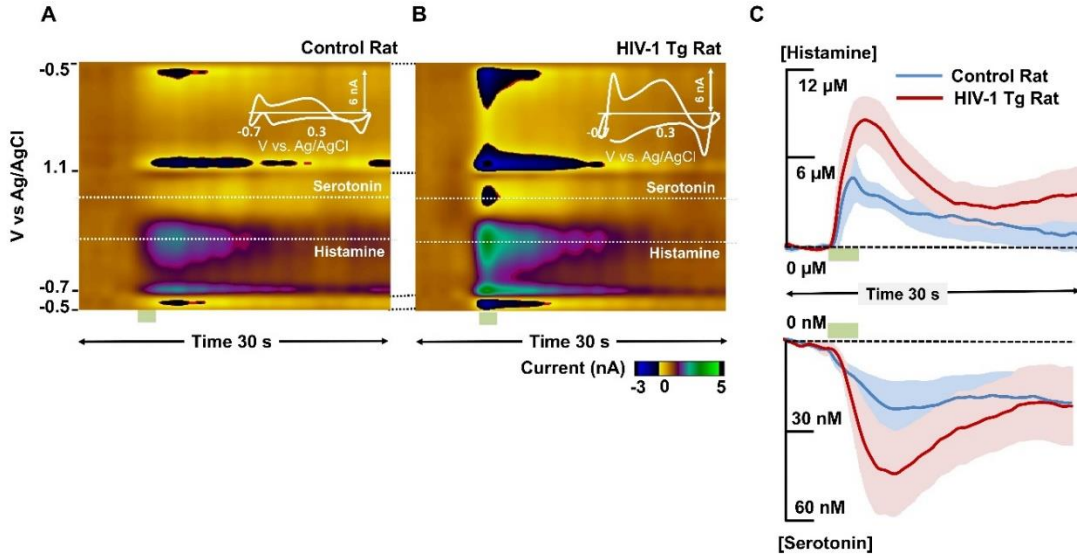

Figure 7.2. (A & B) Representative color plots of simultaneous detection of evoked histamine and ambient serotonin in the posterior hypothalamus of control (F344) and HIV-1 Tg rats respectively. Inset in each color plot (white trace) are CVs taken from the vertical dashed lines. (C) Top panel - [Histamine] vs. time plots for the control rats (solid blue trace) and HIV-1 Tg rats (solid red trace). Bottom panel - [Serotonin] vs. time plots comparing control animal (solid blue trace) and HIV-1 Tg (solid red trace). Shaded regions in each trace show the standard error of the mean (SEM) for n=7 animals. Green bars underneath the color plots denote occurrence and duration of the electrical stimulation (2 s)

In this experiment, we simultaneously detected *in vivo* histamine and serotonin in HIV-1 Tg rats. **Figure 7.2** illustrates histaminergic regulation of serotonin in the rat PH. **Figure 7.2A** & **B** show representative color plots of simultaneous detection of histamine and serotonin for control and HIV-1 Tg rats, respectively. Stimulated release of histamine is enhanced in HIV-1 Tg rats (red) with respect to control animal (blue) as shown in

Figure 7.2C- top panel. Similarly, inverse regulation of serotonin is also increased in HIV-1 Tg rats (red) when compared to the control (blue) as shown in **Figure 7.2C**.

6.3.2 Serotonin

We then positioned the CFM in the prefrontal cortex to detect the stimulated release of serotonin. **Figure 7.2 A** & **B** illustrate representative color plots of evoked serotonin for control and HIV-1 Tg rats, respectively. Stimulated release of serotonin was significantly attenuated in HIV-1 Tg rats (red) in comparison to control animals (blue) as shown in **Figure 7.2 C**.

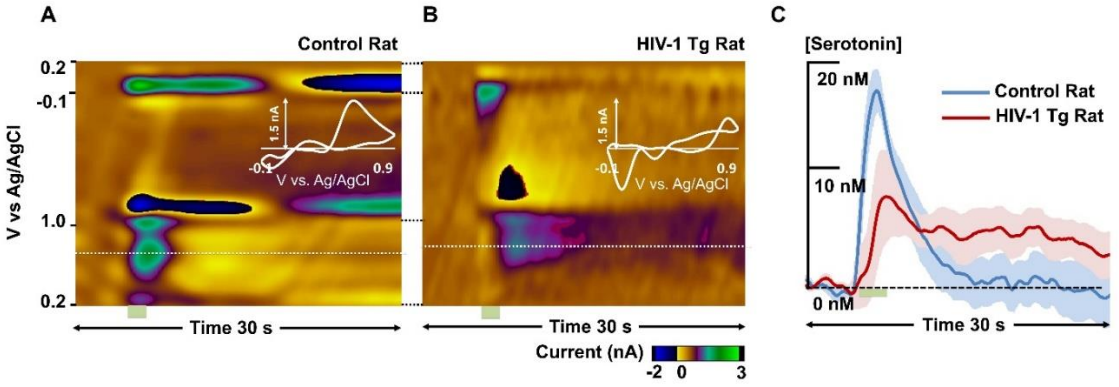

Figure 7.3. (A & B) Representative color plots of the stimulated release of serotonin in the prefrontal cortex of control and HIV-1 Tg rats, respectively. Inset in each color plot (white trace) shows the typical cyclic voltammogram for serotonin, extracted from the vertical dashed line along the event. (C) [Serotonin] vs. time plot comparing control (solid blue trace) and HIV-1 Tg rats (solid red trace). Shaded regions in each trace show the standard error of the mean (SEM) for n=10 animals. Green bars underneath the color plots denote the occurrence and duration of the electrical stimulation (2s)

6.4 Discussion

This animal model (HIV-1 Tg rats) expresses seven of the nine genes produced by the HIV-1 virus in humans and displays the same symptoms occurring after infection in patients receiving combination antiretroviral therapies[23]. Replication of the HIV virion is

dependent on the Pol protein which is not expressed in the HIV-1 Tg rat. Therefore, while the presence of the virus is maintained in the blood, the virus cannot replicate. These transgenic rats have been shown to express neurological disorders that mirror HIV in humans[24,25]. In addition, this disease model develops cognitive, motor and behavioral anomalies which may be linked to elevated immune activation[26-28]. Thus, we can safely use this model of disease to investigate the histamine and serotonin chemistry underlying neuroinflammation.

Recent studies of HIV in humans proved that the virus enters the central nervous system in early stages of the infection through infected macrophages and monocytes[29]. Various HIV-1 glycoprotein gp120 isolates interact with the α- or β-chemokine receptors that exist on macrophages/microglia, astrocytes, and neurons[15]. These infected cells secrete THF-α, IL-1β, nitric oxide and quinolinone which are inflammatory markers[30]. These inflammatory mediators are neurotoxic and can potentially lead to neuroinflammation. Therefore, apoptosis could occur through direct interaction between gp120 and neurons or through the release of neurotoxic factors like inflammatory mediators[15].

Microglial cells, the immune cells in the brain, protect the brain from injuries, viruses and infections. These immune cells migrate to the infected sites and release inflammatory mediators[31]. Recent studies have shown that histamine modulates microglial migration and the release of inflammatory mediators like cytokines[32] and nitric oxide[2]. Mast cells also contribute to the innate immune system in both central nervous system and peripheral system[33]. Mast cells can be found in the brain and these cells interact with astrocytes, neurons, and microglial cells[34,35]. The number of mast cells

present is considerably lower in healthy organisms than in inflammation states. With inflammation, mast cells migrate through BBB[36] and release more inflammatory mediators like histamine and cytokines[37] again suggesting histamine may have a significant role in brain diseases which are associated with neuroinflammation. Our results also support the hypothesis, as elevated histamine release was observed in HIV-1 Tg rats when compared to the control animals (**Figure 7.1**). The recruiting of more mast cells into the brain during neuroinflammation and the release of more histamine to regulate microglial cells may possibly result in the elevated stimulated release of histamine in HIV-1 Tg rats.

Our own and other studies have shown that H_3 receptors regulate serotonin release[7,9,38]. Therefore, it follows that histamine release during neuroinflammation would result in enhanced serotonin inhibition. Accordingly, HIV-1 Tg rats demonstrated greater inhibition of serotonin (**Figure 7.1**). This observation was also reflected in the stimulated release of serotonin in PFC (**Figure 7.2**). Moreover, impaired serotonin levels have been implicated in many brain disorders like depression and neurodegeneration, which are also comorbid with neuroinflammation[39-42]. Collectively, histamine may have a significant impact in controlling the serotonin release during brain diseases that also exhibit increased neuroinflammation.

In summary, we have illustrated that our novel electrochemical method can be used to investigate real-time *in vivo* histaminergic regulation of serotonin in disease or pathophysiological states. The fundamental neurochemical information gained from this study will be vital to revealing histamine's true role in neurological disorders. More

pharmacological, animal model, and behavior experiments are necessary to further establish this hypothesis.

6.5 References

(1) Cacabelos, R.; Torrellas, C.; Fern; ndez-Novoa, L.; pez-Mu; oz, F. *Mediators of Inflammation* **2016**, *2016*, 10.

(2) Rocha, S. M.; Pires, J.; Esteves, M.; Graça, B.; Bernardino, L. *Frontiers in Cellular Neuroscience* **2014**, *8*.

(3) Passani, M. B.; Ballerini, C. *Frontiers in Systems Neuroscience* **2012**, *6*, 32.

(4) Rosa, A. C.; Fantozzi, R. *British Journal of Pharmacology* **2013**, *170*, 38.

(5) Haas, H.; Panula, P. *Nature reviews. Neuroscience* **2003**, *4*, 121.

(6) Haas, H. L.; Sergeeva, O. A.; Selbach, O. *Physiological reviews* **2008**, *88*, 1183.

(7) Samaranayake, S.; Abdalla, A.; Robke, R.; Nijhout, H. F.; Reed, M. C.; Best, J.; Hashemi, P. *J Neurochem* **2016**, *138*, 374.

(8) Flik, G.; Folgering, J. H.; Cremers, T. I.; Westerink, B. H.; Dremencov, E. *Journal of molecular neuroscience : MN* **2015**, *56*, 320.

(9) Threlfell, S.; Cragg, S. J.; Kallo, I.; Turi, G. F.; Coen, C. W.; Greenfield, S. A. *The Journal of neuroscience : the official journal of the Society for Neuroscience* **2004**, *24*, 8704.

(10) Panula, P.; Nuutinen, S. *Nature reviews. Neuroscience* **2013**, *14*, 472.

(11) Miller, A. H.; Raison, C. L. *Nat Rev Immunol* **2016**, *16*, 22.

(12) Najjar, S.; Pearlman, D. M.; Alper, K.; Najjar, A.; Devinsky, O. *Journal of Neuroinflammation* **2013**, *10*, 43.

(13) Royal, W., 3rd; Zhang, L.; Guo, M.; Jones, O.; Davis, H.; Bryant, J. L. *Journal of neuroimmunology* **2012**, *247*, 16.

(14) Tran, P. B.; Miller, R. J. *Nature reviews. Neuroscience* **2003**, *4*, 444.

(15) Kaul, M.; Lipton, S. A. *Proceedings of the National Academy of Sciences of the United States of America* **1999**, *96*, 8212.

(16) Lannuzel, A.; Lledo, P. M.; Lamghitnia, H. O.; Vincent, J. D.; Tardieu, M. *The European journal of neuroscience* **1995**, *7*, 2285.

(17) Moran, L. M.; Booze, R. M.; Webb, K. M.; Mactutus, C. F. *Experimental neurology* **2013**, *239*, 139.

(18) Nemeth, C. L.; Glasper, E. R.; Harrell, C. S.; Malviya, S. A.; Otis, J. S.; Neigh, G. N. *PLOS ONE* **2014**, *9*, e108399.

(19) Owens, M. J.; Nemeroff, C. B. *Clinical chemistry* **1994**, *40*, 288.

(20) Delgado, P. L.; Charney, D. S.; Price, L. H.; Aghajanian, G. K.; Landis, H.; Heninger, G. R. *Archives of general psychiatry* **1990**, *47*, 411.

(21) Samaranayake, S.; Abdalla, A.; Robke, R.; Wood, K. M.; Zeqja, A.; Hashemi, P. *Analyst* **2015**, *140*, 3759.

(22) Hashemi, P.; Dankoski, E. C.; Petrovic, J.; Keithley, R. B.; Wightman, R. M. *Analytical Chemistry* **2009**, *81*, 9462.

(23) Vigorito, M.; Connaghan, K. P.; Chang, S. L. *Brain, Behavior, and Immunity* **2015**, *48*, 336.

(24) Reid, W.; Sadowska, M.; Denaro, F.; Rao, S.; Foulke, J.; Hayes, N.; Jones, O.; Doodnauth, D.; Davis, H.; Sill, A.; O'Driscoll, P.; Huso, D.; Fouts, T.; Lewis, G.; Hill,

M.; Kamin-Lewis, R.; Wei, C.; Ray, P.; Gallo, R. C.; Reitz, M.; Bryant, J. *Proceedings of the National Academy of Sciences* **2001**, *98*, 9271.

(25) Peng, J.; Vigorito, M.; Liu, X.; Zhou, D.; Wu, X.; Chang, S. L. *Journal of neuroimmunology* **2010**, *218*, 94.

(26) Mazzucchelli, R.; Amadio, M.; Curreli, S.; Denaro, F.; Bemis, K.; Reid, W.; Bryant, J.; Riva, A.; Galli, M.; Zella, D. *Molecular immunology* **2004**, *41*, 979.

(27) June, H. L.; Yang, A. R. S. T.; Bryant, J. L.; Jones, O.; Royal, W. *Journal of neurovirology* **2009**, *15*, 380.

(28) Royal, W.; Iii; Wang, H.; Jones, O.; Tran, H.; Bryant, J. L. *Journal of neuroimmunology* **2007**, *185*, 29.

(29) Braathen, L. R.; Ramirez, G.; Kunze, R. O. F.; Gelderblom, H. *The Lancet* **1987**, *330*, 1094.

(30) Meltzer, M. S.; Skillman, D. R.; Gomatos, P. J.; Kalter, D. C.; Gendelman, H. E. *Annual review of immunology* **1990**, *8*, 169.

(31) Polazzi, E.; Monti, B. *Progress in neurobiology* **2010**, *92*, 293.

(32) Ferreira, R.; Santos, T.; Goncalves, J.; Baltazar, G.; Ferreira, L.; Agasse, F.; Bernardino, L. *J Neuroinflammation* **2012**, *9*, 90.

(33) Gilfillan, A. M.; Austin, S. J.; Metcalfe, D. D. *Advances in experimental medicine and biology* **2011**, *716*, 2.

(34) Khalil, M.; Ronda, J.; Weintraub, M.; Jain, K.; Silver, R.; Silverman, A.-J. *Brain research* **2007**, *1171*, 18.

(35) Florenzano, F.; Bentivoglio, M. *The Journal of comparative neurology* **2000**, *424*, 651.

(36) Silverman, A. J.; Sutherland, A. K.; Wilhelm, M.; Silver, R. *The Journal of neuroscience : the official journal of the Society for Neuroscience* **2000**, *20*, 401.

(37) Dong, H.; Zhang, X.; Qian, Y. *Medical Science Monitor Basic Research* **2014**, *20*, 200.

(38) Schlicker, E.; Betz, R.; Gothert, M. *Naunyn Schmiedebergs Arch Pharmacol* **1988**, *337*, 588.

(39) Brites, D.; Fernandes, A. *Frontiers in Cellular Neuroscience* **2015**, *9*, 476.

(40) Morgan, D. G.; May, P. C.; Finch, C. E. *Journal of the American Geriatrics Society* **1987**, *35*, 334.

(41) Gardner, A.; Boles, R. G. *Progress in neuro-psychopharmacology & biological psychiatry* **2011**, *35*, 730.

(42) Hurley, L. L.; Tizabi, Y. *Neurotoxicity research* **2013**, *23*, 131.

CHAPTER 7

CONCLUSIONS AND PROSPECTS

Histamine and serotonin are important biogenic amines that regulate a variety of brain functions. These two chemical messengers are thought to modulate each other, but their fundamental neuromodulation mechanisms are not well understood, making such brain disorders difficult to diagnose and treat. However, studying the underlying neurochemistry of histamine and serotonin has been challenging due to the absence of suitable analytical techniques. This dissertation introduced a systematic approach to overcome this challenge.

In this dissertation, I first used Cu(II) metal analysis to understand the adsorption driven FSCV response. We described that adsorption of Cu(II) onto CFMs follows a monolayer Langmuir adsorption isotherm. I then used the adsorption phenomenon to established a novel FSCV method to selectively and sensitively monitor histamine neurotransmission in the mouse PH. In this method, electrically evoked histamine was measured in the PH upon stimulation in the MFB. This work was extended to simultaneously monitor *in vivo* histamine and serotonin in real time. This work revealed that histamine potently inhibits serotonin in a concentration dependent manner, highlighting histamine's roles in regulating serotonin release in the brain. Additionally, pharmacological and mathematical models proved that this inhibitory mechanism is mediated by the H_3 receptors. Following that, I utilized our novel method to study

histamine's reuptake mechanism via monoamine transporter proteins by pharmacological manipulations. I demonstrated that the histamine uptake mechanism is mediated by OCT. Interestingly, the histamine reuptake mechanism was also inhibited by escitalopram and citalopram which are commercially available antidepressant drugs. Transporter inhibitory drugs elevate extracellular serotonin, which is in turn inhibited by increased histamine via H_3 receptors. Finally, I utilized FSCV to measure serotonin and histamine neurotransmissions in HIV-1 Tg rats, which display neuroinflammation, to investigate neurochemical changes in the disease state. In this study, both stimulated release of histamine and inverse regulation of serotonin were enhanced in HIV-1 Tg rats when compared to the control animals.

Future studies will be required for the in-depth understanding of fundamental neurochemical changes that happen during neuroinflammation. The preliminary observations that we obtained with HIV-1 Tg rats (chapter 6) suggest that histamine plays a vital role in inversely regulating serotonin release in the brain during neuroinflammation. Since neuroinflammation is comorbid with various brain disorders like depression, more pharmacological, animal model, and behavior experiments are necessary to establish the histamine hypothesis.

In chapter 4, we illustrated the simplest version of the mathematical model, which explains the FSCV response related to fundamental physiological functions for histamine and serotonin. More experiments are required to expand this original mathematical model with the ultimate goal of applying the model in brain diseases. This goal can be achieved by pharmacological manipulations of histamine and serotonin neurochemistry. This mathematical model will then provide essential information about impaired

neurochemistry during any disease state, and this information can be subsequently used to develop more effective therapies and drugs for histamine and serotonin related brain disorders.

Collectively, this dissertation showcased a novel, powerful FSCV method for simultaneous detection of *in vivo* histamine and serotonin in real time. The advancement of this approach facilitates the systematic study of the histaminergic modulation of serotonin in a variety of neurochemical processes and brain diseases, stressing the potential role of histamine.

APPENDIX A

PERMISSION OBTAINED FROM THE ROYAL SOCIETY OF CHEMISTRY TO REPRINT THE ARTICLE IN CHAPTER 2

Fast voltammetry of metals at carbon-fiber microelectrodes: copper adsorption onto activated carbon aids rapid electrochemical analysis

P. Pathirathna, S. Samaranayake, C. W. Atcherley, K. L. Parent, M. L. Heien, S. P. McElmurry and P. Hashemi,*Analyst*, 2014, **139**, 4673

DOI: 10.1039/C4AN00937A

If you are not the author of this article and you wish to reproduce material from it in a third party non-RSC publication you must formally request permission using RightsLink. Go to our Instructions for using RightsLink page for details.

Authors contributing to RSC publications (journal articles, books or book chapters) do not need to formally request permission to reproduce material contained in this article provided that the correct acknowledgement is given with the reproduced material.

Reproduced material should be attributed as follows:

- For reproduction of material from NJC:
  Reproduced from Ref. XX with permission from the Centre National de la Recherche Scientifique (CNRS) and The Royal Society of Chemistry.
- For reproduction of material from PCCP:
  Reproduced from Ref. XX with permission from the PCCP Owner Societies.
- For reproduction of material from PPS:
  Reproduced from Ref. XX with permission from the European Society for Photobiology, the European Photochemistry Association, and The Royal Society of Chemistry.
- For reproduction of material from all other RSC journals and books:
  Reproduced from Ref. XX with permission from The Royal Society of Chemistry.

If the material has been adapted instead of reproduced from the original RSC publication "Reproduced from" can be substituted with "Adapted from".

In all cases the Ref. XX is the XXth reference in the list of references.

If you are the author of this article you do not need to formally request permission to reproduce figures, diagrams etc. contained in this article in third party publications or in a thesis or dissertation provided that the correct acknowledgement is given with the reproduced material.

Reproduced material should be attributed as follows:

- For reproduction of material from NJC:
  [Original citation] - Reproduced by permission of The Royal Society of Chemistry (RSC) on behalf of the Centre National de la Recherche Scientifique (CNRS) and the RSC
- For reproduction of material from PCCP:
  [Original citation] - Reproduced by permission of the PCCP Owner Societies
- For reproduction of material from PPS:
  [Original citation] - Reproduced by permission of The Royal Society of Chemistry (RSC) on behalf of the European Society for Photobiology, the European Photochemistry Association, and RSC
- For reproduction of material from all other RSC journals:
  [Original citation] - Reproduced by permission of The Royal Society of Chemistry

If you are the author of this article you still need to obtain permission to reproduce the whole article in a third party publication with the exception of reproduction of the whole article in a thesis or dissertation.

Information about reproducing material from RSC articles with different licences is available on our Permission Requests page.

APPENDIX B

PERMISSION OBTAINED FROM THE ROYAL SOCIETY OF CHEMISTRY TO REPRINT THE ARTICLE IN CHAPTER 3

In vivo histamine voltammetry in the mouse premammillary nucleus

S. Samaranayake, A. Abdalla, R. Robke, K. M. Wood, A. Zeqja and P. Hashemi, *Analyst*, 2015, **140**, 3759

DOI: 10.1039/C5AN00313J

If you are not the author of this article and you wish to reproduce material from it in a third party non-RSC publication you must formally request permission using RightsLink. Go to our Instructions for using RightsLink page for details.

Authors contributing to RSC publications (journal articles, books or book chapters) do not need to formally request permission to reproduce material contained in this article provided that the correct acknowledgement is given with the reproduced material.

Reproduced material should be attributed as follows:

- For reproduction of material from NJC:
  Reproduced from Ref. XX with permission from the Centre National de la Recherche Scientifique (CNRS) and The Royal Society of Chemistry.
- For reproduction of material from PCCP:
  Reproduced from Ref. XX with permission from the PCCP Owner Societies.
- For reproduction of material from PPS:
  Reproduced from Ref. XX with permission from the European Society for Photobiology, the European Photochemistry Association, and The Royal Society of Chemistry.
- For reproduction of material from all other RSC journals and books:
  Reproduced from Ref. XX with permission from The Royal Society of Chemistry.

If the material has been adapted instead of reproduced from the original RSC publication "Reproduced from" can be substituted with "Adapted from".

In all cases the Ref. XX is the XXth reference in the list of references.

If you are the author of this article you do not need to formally request permission to reproduce figures, diagrams etc. contained in this article in third party publications or in a thesis or dissertation provided that the correct acknowledgement is given with the reproduced material.

Reproduced material should be attributed as follows:

- For reproduction of material from NJC:
  [Original citation] - Reproduced by permission of The Royal Society of Chemistry (RSC) on behalf of the Centre National de la Recherche Scientifique (CNRS) and the RSC
- For reproduction of material from PCCP:
  [Original citation] - Reproduced by permission of the PCCP Owner Societies
- For reproduction of material from PPS:
  [Original citation] - Reproduced by permission of The Royal Society of Chemistry (RSC) on behalf of the European Society for Photobiology, the European Photochemistry Association, and RSC
- For reproduction of material from all other RSC journals:
  [Original citation] - Reproduced by permission of The Royal Society of Chemistry

If you are the author of this article you still need to obtain permission to reproduce the whole article in a third party publication with the exception of reproduction of the whole article in a thesis or dissertation.

Information about reproducing material from RSC articles with different licences is available on our Permission Requests page.

APPENDIX C

PERMISSION OBTAINED FROM JOURNAL OF NEUROCHEMISTRY TO REPRINT THE ARTICLE IN CHAPTER 4

Title: A voltammetric and mathematical analysis of histaminergic modulation of serotonin in the mouse hypothalamus

Author: Srimal Samaranayake,Aya Abdalla,Rhiannon Robke,H. Frederik Nijhout,Michael C. Reed,Janet Best,Parastoo Hashemi

Publication: Journal of Neurochemistry

Publisher: John Wiley and Sons

Date: Jun 27, 2016

Order Completed

Thank you for your order.

This Agreement between University of South Carolina -- Srimal Samaranayake ("You") and John Wiley and Sons ("John Wiley and Sons") consists of your license details and the terms and conditions provided by John Wiley and Sons and Copyright Clearance Center.

Your confirmation email will contain your order number for future reference.

Printable details.

License Number	4132150390381
License date	Jun 18, 2017
Licensed Content Publisher	John Wiley and Sons
Licensed Content Publication	Journal of Neurochemistry
Licensed Content Title	A voltammetric and mathematical analysis of histaminergic modulation of serotonin in the mouse hypothalamus
Licensed Content Author	Srimal Samaranayake,Aya Abdalla,Rhiannon Robke,H. Frederik Nijhout,Michael C. Reed,Janet Best,Parastoo Hashemi
Licensed Content Date	Jun 27, 2016
Licensed Content Pages	10

Type of use	Dissertation/Thesis
Requestor type	Author of this Wiley article
Format	Electronic
Portion	Full article
Will you be translating?	No
Title of your thesis / dissertation	DEVELOPMENT OF A NOVEL ELECTROCHEMICAL METHOD TO STUDY REAL-TIME IN VIVO NEUROTRANSMITTER MODULATION
Expected completion date	Jun 2017
Expected size (number of pages)	120
Requestor Location	University of South Carolina 631 Sumter St COLUMBIA, SC 29208 United States Attn: University of South Carolina
Publisher Tax ID	EU826007151
Billing Type	Invoice
Billing address	University of South Carolina 631 Sumter St

COLUMBIA, SC 29208
United States
Attn: University of South Carolina

Total	0.00 USD

TERMS AND CONDITIONS